NASA CONTRACTOR REPORT

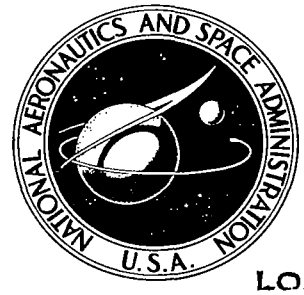

NASA CR-325

NASA CR-2576

FLIGHT EFFECTS ON NOISE GENERATED BY THE JT8D-17 ENGINE IN A QUIET NACELLE AND A CONVENTIONAL NACELLE AS MEASURED IN THE NASA-AMES 40- BY 80-FOOT WIND TUNNEL

Summary Report

Frank G. Strout

Prepared by
BOEING COMMERCIAL AIRPLANE COMPANY
Seattle, Wash. 98124
for Ames Research Center

NATIONAL AERONAUTICS AND SPACE ADMINISTRATION • WASHINGTON, D. C. • JUNE 1976

1. Report No.	2. Government Accession No.	3. Recipient's Catalog No.
CR-2576		

4. Title and Subtitle	5. Report Date
Flight Effects on Noise Generated by the JT8D-17 Engine in a Quiet Nacelle and a Conventional Nacelle as Measured in the NASA-Ames 40- by 80-Foot Wind Tunnel—Summary Report	June 1976
	6. Performing Organization Code

7. Author(s)	8. Performing Organization Report No.
Frank G. Strout	D6-42813-1
	10. Work Unit No.

9. Performing Organization Name and Address	11. Contract or Grant No.
Boeing Commercial Airplane Company P.O. Box 3707 Seattle, Washington 98124	NAS 2-8213
	13. Type of Report and Period Covered
12. Sponsoring Agency Name and Address National Aeronautics and Space Administration Ames Research Center Moffett Field, California 94035	Contract Report
	14. Sponsoring Agency Code

15. Supplementary Notes

NASA Project Manager, Adolph Atencio, Jr.

16 Abstract

A JT8D-17 turbofan engine was tested in the NASA-Ames 40- by 80-Foot Wind Tunnel to determine flight effects on jet and fan noise. Baseline, quiet nacelle with 20-lobe ejector/suppressor, and internal mixer configurations were tested over a range of engine power settings and tunnel velocities. Flight effects derived from the 40- by 80-Foot Wind Tunnel test are compared with 727/JT8D flight test data and with model data obtained in a smaller wind tunnel. Procedures are defined for measuring noise data in a wind tunnel relatively near the sources and analyzing the results to obtain far-field flight effects. Wind tunnel and 727 flight test noise results compare favorably for both the baseline and quiet nacelle configurations. Two reports are provided, including a comprehensive version with extensive test results and analysis and the subject summary version that emphasizes data analysis and program findings.

17. Key Words (Suggested by Author(s))	18. Distribution Statement
Jet noise Fan noise Flight effects Suppresor nozzle Wind tunnel	Unclassified—Unlimited STAR Category 07

19. Security Classif. (of this report)	20. Security Classif. (of this page)	21. No. of Pages	22. Price*
Unclassified	Unclassified	95	$4.00

For sale by the National Technical Information Service, Springfield, Virginia 22161

CONTENTS

FIGURES

FIGURES (Continued)

FIGURES (Concluded)

FLIGHT EFFECTS ON NOISE GENERATED BY THE JT8D-17 ENGINE IN A QUIET NACELLE AND A CONVENTIONAL NACELLE AS MEASURED IN THE NASA-AMES 40- BY 80-FOOT WIND TUNNEL-- SUMMARY REPORT

by Frank G. Strout
Boeing Commercial Airplane Company

1.0 SUMMARY

A test was conducted in the NASA Ames Research Center (ARC) 40- by 80-Foot Wind Tunnel to study the flight noise characteristics of the JT8D engine. The objectives of the program were to:

- Determine the feasibility and potential of wind tunnel tests for studying flight effects on engine noise
- Establish specific jet and fan noise flight effects for the JT8D engine configured as a baseline, 20-lobe ejector/suppressor, and internal mixer
- Compare 40- by 80-Foot Wind Tunnel derived flight effects with available 727/JT8D flight test results and Boeing 9- by 9-wind tunnel model test results

The analysis emphasizes data acquired by a pair of traversing microphones mounted at engine centerline height on a 3-m (10-ft) sideline. The relatively near-field measuring station was selected to minimize 40- by 80-Foot Wind Tunnel reverberant field effects. Special analysis techniques were developed in order to properly interpret the near-field noise data in terms of far-field flight effects. Tunnel-off and tunnel-on noise tests were conducted over a range of nozzle pressure ratios (NPR) from 1.2 to 2.1. Tunnel velocities ranged up to 105 m/s and primary jet velocities up to 570 m/s.

It is concluded that wind tunnel noise testing of engines or models to determine flight effects is feasible. Noise data taken relatively close to the sources can be properly interpreted to provide meaningful far-field flight noise characteristics.

Good agreement is shown between wind tunnel and 727/JT8D flight test results for the baseline and quiet nacelle configurations. Model results obtained in a small wind tunnel facility compare favorably with the full-scale results.

The study shows the importance of testing suppressor concepts for flight noise. The 20-lobe ejector/suppressor experiences a significant loss of suppression during flight, while the internal mixer nozzle indicates a slight gain in suppression.

Engine core noise is identified at low engine power and restricts the amount of low frequency noise reduction due to forward velocity.

Forward quadrant noise was measured in the wind tunnel to evaluate forward speed effects on fan noise. Analysis indicates that at approach power (6200 rpm) the first stage fundamental fan tone was reduced in power level by 8 dB. Power level reductions of 3 dB and 1.5 dB were experienced by the second and third harmonic fan tones, respectively.

Two reports are provided to describe the test, test results, and analysis. They include a comprehensive report with extensive test results and analysis (CR 137797) and this summary report that emphasizes data analysis and program findings.

2.0 INTRODUCTION

There is currently an industry-wide interest in understanding and defining the influence of flight on aircraft engine noise. The most direct method of obtaining this knowledge is to compare static and flight test data that have been corrected to a common base. There are, however, limitations and concerns that are inherent to this approach. Flight testing is costly, in particular, where unique engine hardware is being evaluated. The accuracy of flight effects analysis may be compromised by differences in static and flight noise measurement details, installation effects, source-to-microphone propagation variations, flight data integration time limitations, and possibly airframe noise contributions to the measured flight spectra. Accordingly, several alternate methods for studying engine noise flight effects are being investigated by industry, including the use of wind tunnels, rotary devices, and ground vehicles.

A wind tunnel flight effects test can be conducted with nonflightworthy hardware at a significant cost saving relative to flight test. Further, the wind tunnel is potentially more accurate because of improved experiment control and longer data samples. Detailed flow field measurements may be made to relate changes in noise characteristics with appropriate source mechanisms. The subject program was conducted to establish the feasibility of full-scale engine noise tests in the NASA Ames Research Center (ARC) 40- by 80-Foot Wind Tunnel (40 x 80) and to determine specific flight effects on important engine noise sources. An advanced Pratt & Whitney (P&WA) JT8D-17 turbofan engine was selected for the test. The engine was configured as a baseline with production conical nozzle, a 12-lobe internal mixer, and a quiet nacelle 20-lobe ejector/suppressor. The quiet nacelle test hardware was provided by the FAA. The study emphasizes aft quadrant jet noise; however, data pertinent to inlet fan noise were also acquired.

Noise measurements are made relatively near the engine sources and require special analysis techniques to define far-field flight effects. These techniques were developed as part of a Boeing wind tunnel program using model-scale hardware and are described in this report.

The engine noise flight effects measured in the 40 x 80 are compared with 727/JT8D flight test data for the baseline and quiet nacelle configurations. Comparisons are also made with available model results obtained in the Boeing 9 x 9 wind tunnel. The total data base available for this program provides a unique collection of information needed to establish the feasibility and potential of wind tunnels for studying engine noise flight effects. The resulting experimental and analytical techniques will be of considerable value to future model studies in small wind tunnel facilities and engines in larger facilities such as the NASA-ARC 40- by 80-Foot Wind Tunnel. The major payoff will be engine cycles and suppression systems that are efficiently designed to meet flight noise objectives in a cost-effective manner.

3.0 ABBREVIATIONS AND SYMBOLS

A	cross-sectional flow area, m^2
A_i	incremental area, m^2
alt	altitude, m
ARC	Ames Research Center
BPR	bypass ratio
BPT	blade passage tone
cm	centimeter
dB	decibel
deg	degree
EJ	ejector
EJ/SUPP	ejector/suppressor
EPNL	effective perceived noise level, EPNdB
EPR	engine pressure ratio–P_{T7}/P_{T2}
f; ft	feet
FAA	Federal Aviation Administration
fig.	figure
ft/s	feet per second
Hz	Hertz
IGV	inlet guide vane
kn	knot
kN	kilonewton
lb	pound
m	meter

MIC	microphone
m/s	meter per second
M_∞	freestream Mach number
n	velocity index
N	Newton
N_1	low pressure compressor rpm
NPR	nozzle pressure ratio–P_{T7}/P_{SA}
OASPL	overall sound pressure level, dB
OB	octave band
P&WA	Pratt & Whitney Aircraft
PNdB	unit of perceived noise
PNL	perceived noise level, PNdB
P_T	total pressure, N/m^2
P_{T2}	engine inlet total pressure, N/m^2
P_{T7}	exhaust nozzle total pressure, N/m^2
PWL	power level, dB
QN	quiet nacelle
ref.	reference
rms	root mean square
rpm	revolutions per minute
s, sec	second
SPL	sound pressure level, dB
SPL_i	sound pressure level at angle i, dB
suppr	suppression

ΔSPL	difference in sound pressure level, dB
T	temperature, C
T/R	thrust reverser
TRV-L	lower traverse microphone
TRV; TRAV	traverse
V	velocity, m/s
V_{EJ}	ejector exit velocity, m/s
VG	vortex generator
V_j	jet velocity, m/s
V_{mix}	jet velocity of mixed fan and primary flows, m/s
V_{Pint}	ejector internal primary velocity, m/s
V_{pri}	engine primary jet velocity, m/s
V_R	relative jet velocity = $V - V_\infty$, m/s
V_{sec}	velocity of entrained ejector air, m/s
V_T	nominal tunnel test velocity, kn
V_∞	aircraft or tunnel velocity, m/s
40 x 80	NASA Ames 40- by 80-Foot Wind Tunnel
9 x 9	Boeing 9- by 9-ft wind tunnel
Δ	delta
θ	angle
∞	ambient
%	percent

4.0 TEST DESCRIPTION

The test was conducted in the NASA-ARC 40- by 80-Foot Wind Tunnel (12.2 x 24.4 m). The test engine was a JT8D-17 turbofan engine on loan from P&WA. The engine develops a thrust of approximately 71 kN (16 000 lb) at an engine pressure ratio (EPR) of 2.2 and has a bypass ratio (BPR) of 1.1.

Six nacelle configurations were tested and are shown schematically in figure 1. The configurations included: the Boeing/FAA quiet nacelle (QN) with two-ring inlet and 20-lobe ejector/suppressor; internal mixer with inner wall acoustic treatment; internal mixer without inner wall acoustic treatment (hardwall); internal mixer (hardwall) with external vortex generators (VG); baseline with two-ring inlet; and baseline with production inlet.

Quiet nacelle and baseline installations are shown in figures 2 and 3. Noise measurements were made by a fixed array of microphones and a pair of beam-mounted traversing microphones (fig. 3). The traversing microphones were used to record acoustic data in steady state mode at discrete angles and in sweep mode. The microphones were located on a 3-m (10-ft) sideline and covered aft quadrant angles from 90^{o} to 165^{o}. During the inlet fan noise test, the traverse was moved to the forward quadrant to record data at angles from 20^{o} to 110^{o}. Engine, nozzle, and facility parameters were measured and recorded in order to monitor engine operation and performance (thrust and jet velocities), ejector performance, and tunnel velocity. Tunnel-off and tunnel-on noise tests were conducted over a range of nozzle pressure ratios (1.2 to 2.1), primary jet velocities (275 to 550 m/s), and tunnel velocities up to 105 m/s. Acoustic data were recorded on 14-track analog tape. Data reduction provided tabulated and plotted 1/3-octave band (OB) spectra for the aft quadrant measurements and narrow band spectra for the forward quadrant measurements.

A more detailed description of the 40 x 80 test is provided in references 1 and 2.

5.0 TEST RESULTS

Engine performance and acoustic test results are contained in reference 1. Acoustic results are provided for the reverberation test, noise floor test, aft quadrant jet noise tests, and forward quadrant fan noise test. Aft quadrant noise data are presented in the form of 1/3-OB spectra plots where tunnel-off and tunnel-on spectra are compared at equal primary jet velocities and noise emission angles. The tunnel-on data were corrected for noise floor and for convection of noise in a moving stream. Forward quadrant data are provided in the form of narrow band spectra (20 Hz) in order to isolate fan tone noise characteristics.

6.0 ANALYSIS OF ACOUSTIC RESULTS

6.1 WIND TUNNEL DATA ANALYSIS TECHNIQUE

The noise measurements in the 40 x 80 were made relatively close to the engine noise sources. The sideline distance was selected to minimize reverberant field effects while at the same time avoiding dominant near-field effects. Ideally, measurements would be taken in the acoustic far field where noise source locations are relatively unimportant to data analysis. At the test measuring station of 3 m, however, noise source location and directivity are very important to a proper evaluation of the acoustic data.

For noise sources that originate at or very near the engine inlet or exit planes (fan noise, core noise, suppressor premerged mixing noise), the near- (3 m) and far-field signals are common and will differ in level primarily because of propagation distance and atmospheric absorption. Wind tunnel flight effects analysis of this data is based on near-field tunnel-off to tunnel-on noise increments being equal to far-field noise increments at equal angles referenced to the engine inlet or exit.

Noise generated by the jet as it mixes with surrounding ambient air presents a more difficult problem. The proximity of the near-field microphones to the sources requires that source location and directivity be known for each frequency of interest if accurate far-field flight effects are to be identified. A method of defining source location and directivities has been devised involving the use of multiple sideline data recording. The analysis is based on the premise that spherical divergence and atmospheric absorption account for the level differences observed for a given signal as it passes from a source location through a given near-field location to the far-field location.

Correlations of near- and far-field angles are established in reference 1 as a function of frequency and power setting for each nozzle configuration. Similar correlations are established that relate near- and far-field angles for OASPL and PNL rather than discrete frequencies. The measured change in noise at a given near-field angle, due to tunnel flow, is equated to the far-field noise change at an angle defined by the appropriate correlation (SPL, OASPL, PNL). An example of each type of correlation is provided in figures 4 and 5 for the baseline configuration operating at cutback power. A complete set of correlations is included in reference 1 together with additional details concerning application.

During tunnel-on operation, engine noise is convected downstream by the moving medium. A correction must be applied so that tunnel-off and tunnel-on noise data are compared at equal emission angles. For the 40 x 80 test the traverse microphone tunnel-on position was moved downstream relative to the tunnel-off position in order to compensate for convection. The adjustment is correct for sources that originated from the nozzle exit (ejector premerged mixing noise, core noise, aft fan noise) or the inlet (fan noise). For jet mixing noise that originates downstream of the nozzle exit, the adjustment is approximately correct, and a slight angle correction was applied to the tunnel-on data during the analysis.

The analysis of wind tunnel results that follows is based primarily on data acquired with the lower traverse microphone operating in steady state mode. Steady state data from the upper traverse microphone and sweep mode data from the lower traverse microphone were used as a backup source of information.

6.2 20-LOBE EJECTOR/SUPPRESSOR

The 20-lobe ejector/suppressor test results are evaluated in this section. The analysis includes: a review of 40 x 80 near-field tunnel-off data comparisons with near and far free field data, an evaluation of 40 x 80 flight effects, comparisons of 40 x 80 and 727 flight test results, and comparisons of 40 x 80 and Boeing 9 x 9 wind tunnel model test results.

6.2.1 COMPARISONS WITH FREE FIELD DATA

Comparisons of 40 x 80 tunnel-off noise data are made with near- and far-field data acquired at the Boeing Boardman and NASA-ARC static test facilities (ref. 1). The comparisons show that the reverberant field noise level in the 40 x 80 does not significantly influence the direct signal of the 20-lobe ejector/suppressor. The reverberant field correction for OASPL is negligible over the range of near-field angles from 90° to 165°. For PNL, the correction is negligible through 140° and is about 2 PNdB at the higher angles. These results generally are consistent with reverberation test data obtained in the 40 x 80 prior to the engine test (ref. 1).

6.2.2 40 X 80 FLIGHT EFFECTS

The signal received by a given microphone during tunnel-on operation is representative of changes in noise source strength due to tunnel flow. During an aircraft flyover, an observer will experience the effect of source strength changes and a Doppler frequency shift. Therefore, to properly define the flight effect of an engine in motion past an observer, it is necessary to apply a Doppler frequency shift to the wind tunnel data. The Doppler frequency shift is dependent upon noise emission angle and freestream Mach number. This results in a frequency reduction in the aft quadrant and a frequency increase in the forward quadrant relative to the measured tunnel-on data.

Tunnel-off and tunnel-on spectra are compared in figure 6 for cutback power and angles of 90° and 120° (peak noise). The angles are near field but are representative of far-field angles. This is caused by the dominance of ejector premerged mixing noise (200 to 3150 Hz) that radiates to the near and far field much like a point source. The 90° spectra do not require a Doppler frequency shift, and tunnel-on spectra reflect the as-measured frequencies. The tunnel-on spectra at 120° have been corrected for the Doppler effect by reducing the measured frequencies by 40% of a one-third octave band.

The noise reduction due to flight is the difference between the tunnel-off and tunnel-on spectra. A reference spectrum is included for each angle that represents tunnel-off data at a primary velocity equal to tunnel-on primary relative velocity ($V_{pri} - V_{\infty}$). Static data at flight relative velocity is one method of estimating the flight noise of a given engine/nozzle system. The reference level predicts the low frequency noise reasonably well; however, the moderate-to-high frequencies experience less reduction than predicted by primary relative velocity. The Doppler frequency shift at 120° influences the amount of noise reduction caused by flight. The flight noise reduction becomes less

in the frequency range from 200 to 500 Hz but increases in the frequency range from 800 to 3150 Hz. In regions where the spectra are relatively flat (50 to 100 Hz and 4000 to 10 000 Hz), little change occurs because of the Doppler frequency shift.

The spectra at angles from 90° to 120° (peak noise) are dominated by the ejector premerged mixing noise. This noise is generated by the mixing process between the discrete primary jets and the entrained ejector air. Ejector flow parameters measured during the 40 x 80 test show that the internal relative velocity (V_{pint} - V_{sec}) decreases only slightly with tunnel velocity. Thus, the premerged mixing noise undergoes a correspondingly small reduction in level caused by tunnel flow.

The low frequency noise is generated by the mixing process between the ejector efflux and the freestream (postmerged mixing noise). This noise component undergoes a more substantial reduction due to tunnel-flow with the amount of reduction increasing as the jet axis is approached.

Tunnel-off and tunnel-on OASPL and PNL directivities are compared in figure 7 for cutback power. The tunnel-on data have been corrected for Doppler frequency shift and are considered to be representative of flight. A reference noise level is included that represents tunnel-off data at a primary jet velocity equal to the tunnel-on primary relative velocity ($V_{pri} - V_{\infty}$). Application of Doppler frequency shift to the tunnel-on data results in a slight reduction in PNL but does not change the OASPL. Both OASPL and PNL comparisons indicate relatively small reductions of noise due to flight at low angles through peak noise (90° to 120°) with increasing reduction at angles near the jet axis. Since the amount of noise reduction is greater at higher angles, there is a natural tendency for the in-flight peak noise to shift toward the inlet axis. However, for this power setting the change in peak noise location due to flight is slight.

The small reduction of OASPL and PNL at low angles is the result of premerged mixing noise dominance in this region. The premerged noise, generated within the ejector, undergoes a small reduction due to flight; consequently, both OASPL and PNL are reduced by a small amount. At angles near the jet axis, the postmerged mixing noise is more dominant. This component undergoes a relative velocity reduction with forward velocity; thus, OASPL and PNL are substantially reduced.

The reference relative velocity noise level overpredicts the amount of low and peak angle noise reduction and underpredicts the reduction at angles near the jet axis. The reference level is based on the relative velocity of the primary jet. This does not fit the noise generating mechanism of either the premerged or postmerged mixing process and results in a poor prediction of in-flight noise at most angles.

Analysis provided in reference 1 shows that the premerged mixing noise correlates well with the ejector internal relative velocity ($V_{pint} - V_{sec}$). That is, the measured change in the internal relative velocity with tunnel velocity is consistent with the measured change in premerged mixing noise. Thus, predicted flight noise for the important premerged noise component should be based on the internal relative velocity parameter rather than the more conventional primary relative velocity ($V_{pri} - V_{\infty}$). Similar analysis shows that the postmerged mixing noise correlates reasonably well with the

relative velocity of the ejector exit flow ($V_{ej} - V_{\infty}$). The predicted flight noise for this component must be based on the ejector exit flow parameter rather than primary relative velocity.

6.2.3 FLIGHT EFFECTS ESTIMATES USING 40 X 80 RESULTS

One of the desirable outputs of the 40 x 80 test is to establish a method for predicting flight noise levels using far-field static noise data. The previous analysis indicates that the two major sources of jet mixing noise are governed by different flow parameters. The premerged mixing noise, dominant at low angles and at peak, tends to follow the primary internal relative velocity. This noise is generated within the ejector and changes only slightly with flight. The postmerged mixing noise is generated downstream of the ejector exit and is governed by the relative velocity between the well mixed ejector exhaust flow and the freestream. This noise becomes more dominant at angles near the jet axis and undergoes a significant reduction in level during flight.

The recommended approach is to separate the far-field static spectra into postmerged and premerged components. Flight effects are then applied to each component using the proper flow correlating parameter; the components are recombined to define the flight spectra. The flight spectra estimate is made in the following manner and is illustrated in figure 8. The upper half of the figure shows measured far-field static spectra for the 20-lobe suppressor and JT8D-9 engine at 120°. The components are separated by estimating the spectra level and shape for the postmerged jet. Ejector calculations define the exit velocity and the approximate gas conditions. An available jet noise prediction program (ref. 3) was used to calculate the postmerged spectra for each angle. For the example shown in figure 8, the calculated level and shape match the low frequency portion of the static spectra quite well through 200 Hz and then depart from the total spectra as indicated. The premerged spectra are defined by subtracting the postmerged spectra from the total spectra (315 Hz and above). The premerged spectra level below 200 Hz cannot be defined by subtraction but may be estimated by using a typical Strouhal spectra shaping correlation (ref. 4).

The lower half of figure 8 shows the estimated flight noise level for each component and the recombined flight spectra. The postmerged noise level is defined by interpolating static data at the ejector exit relative velocity. Again, a postmerged predicted spectrum is defined at the flight relative velocity to be matched with the low frequency portion of the interpolated spectra. The calculated spectrum matched the low frequency level and shape well and is plotted as shown. The premerged noise level is reduced in accordance with correlations defined in reference 1 as a function of primary internal relative velocity. The reduction in premerged noise level is about 1 to 2 dB. It is noted that aft fan noise appears in the spectra at frequencies above 3150 Hz where a 1-dB reduction in noise level is assumed due to flight. The recombined spectra are dominated by premerged mixing noise, indicating that design improvements to reduce flight noise must concentrate on this component.

Flight spectra estimates were made for angles of 90° to 150° in this manner and are provided in reference 1. The technique can be programmed and may be used for similar multielement suppressor concepts where the total spectra includes premerged and postmerged components.

6.2.4 COMPARISON WITH 727/JT8D FLIGHT DATA

Comparisons are made between 727/JT8D flight test data and 40 x 80 results using two different methods. The first approach, referred to as the noise increment technique, is to subtract tunnel-off to tunnel-on noise changes from static far-field noise levels that have been corrected to the flight conditions. The second approach is to compare absolute noise levels measured in the wind tunnel, that are extrapolated to the flight condition.

Wind tunnel and static test data that are extrapolated to the flight conditions are corrected for slight differences in engine power settings, three engine operation (+4.8 dB or PNdB), and angle of attack (6^0). The correction for angle of attack accounts for the difference in propagation distance between a sideline parallel to the jet centerline and one that is inclined at 6^0. Noise source location is also considered in extrapolating either near-field or 30.5-m sideline data to the flight altitude.

6.2.4.1 Noise Increment Technique

Flight test and wind tunnel spectra and directivities are provided in figures 9 through 13, where comparisons are based on static-to-flight noise increments.

6.2.4.1.1 Spectra Comparisons.–The spectra comparisons reflect cutback power and include 727 flight data, measured 40 x 80 data, and predicted spectra based on 40 x 80 derived flight effects as described in section 6.2.3. Flight test spectra for the 727 with JT8D-9 engines and the 20-lobe ejector/suppressor quiet nacelle are shown in figure 9. The spectra reflect the peak noise angle (120^0) and a representative angle near the jet axis (150^0). A reference static spectra level is also shown that represents Boardman far-field static data extrapolated to the flight condition in the manner previously described. The difference in level between the extrapolated static spectra and the measured flight spectra represents the flight effect on engine noise plus installation effects, if any.

Measured 40 x 80 tunnel-off and tunnel-on spectra are provided in figure 10 for near-field angles of 120^0 and 150^0. The wind tunnel spectra are similar to flight test at 120^0 in terms of basic spectra shape and relative flight effect. This is caused by the dominance of the premerged mixing noise that radiates to the near and far field much like a point source. The flight test spectra indicate a greater reduction of peak premerged mixing noise than the wind tunnel by about 1.5 dB. The wind tunnel 150^0 spectra have a much different shape than the flight test spectra. The difference is caused by a combination of near-field source location effects on the postmerged mixing noise and reverberation effects on the premerged mixing noise. The net result is that the wind tunnel low frequency noise level is low (source location effect) and the moderate-to-high frequency noise level is high (reverberation effect). The flight effects are more representative of a far-field angle of approximately 140^0 based on the near/far field correlation of reference 1.

The spectra shown in figure 11 are based on far-field static spectra and flight effects criteria defined by the 40 x 80 test results. The spectra shape and the static-to-flight changes in noise level are comparable to the flight test spectra of figure 9.

6.2.4.1.2 Directivity Comparisons.–Wind tunnel and flight test OASPL and PNL directivities are compared in figures 12 and 13. Each comparison includes a reference static noise level established by extrapolating far-field static data to the flight condition. When compared with flight test data, the static level indicates the static-to-flight noise reduction at each angle. The wind tunnel flight noise levels of figure 12 are defined by subtracting measured tunnel-off to tunnel-on noise increments from the reference static noise level. The near/far field correlations of reference 1 are used to relate the measured near-field noise increments to the proper far-field angles. For the 20-lobe suppressor, the near- and far-field angles are considered to be equivalent through 120° for evaluating either OASPL or PNL flight effects. At higher angles, the static-to-flight noise increment for a given far-field angle is obtained at a near-field angle that is larger by 10°. The resulting noise levels compare reasonably well with flight test. The best comparison is obtained for OASPL where wind tunnel and flight test noise levels fall within 1 dB.

The wind tunnel PNL values show greater variance with flight test values than OASPL. As previously mentioned, the wind tunnel indicates less reduction of peak premerged mixing noise than flight test (figs. 9 and 10). This accounts for the higher wind tunnel peak PNL and OASPL. The flight data show less reduction of far aft quadrant PNL than the wind tunnel. This is caused by a significant in-flight noise level increase in the high frequency range at high angles (see fig. 9). This frequency (3150 to 4000 Hz) has a strong influence on PNL and, therefore, restricts the amount of reduction in PNL due to flight. There is no confirmed reason for this apparent flight noise anomaly; however, it may be the result of an installation effect that influences high frequency noise generation or propagation.

The wind tunnel noise levels shown in figure 13 are based on spectra established in the manner described for figure 8. Static and flight OASPL and PNL values are calculated for each far-field angle. The resulting static-to-flight OASPL and PNL increments are then subtracted from the reference static levels of figure 13 to define the flight noise level. This technique results in a slightly better comparison with flight test data than the measured noise increment technique. The largest deviation from flight test data occurs at peak noise where the wind tunnel OASPL is higher by 1 dB and PNL is higher by 1.5 PNdB. It is noted that the accuracy of the noise increment technique in predicting flight noise is dependent upon the correctness of the wind tunnel static-to-flight noise difference and the precision in relating the extrapolated static data to the desired flight conditions. Considering the number of test variables involved with the static, flight, and wind tunnel data bases, the resulting comparisons of figures 12 and 13 appear to be within reasonable tolerances.

Comparisons of flight test and 40 x 80 SPL directivities are provided in reference 1 for a range of frequencies from 50 to 1000 Hz. The wind tunnel flight noise levels are established by applying measured tunnel-off to tunnel-on increments to the reference static noise levels in accordance with near/far field correlations. On the whole, the wind tunnel noise levels compare favorably with the flight test results.

6.2.4.2 Absolute Noise Level Technique

Extrapolation of absolute tunnel-on noise levels to the equivalent flight operating conditions represents an alternate procedure to the noise increment technique for

estimating flight noise. In the case of the 40 x 80 test, this represents an extrapolation from a 3-m sideline to a 122-m altitude. The extrapolation was made using near/far field correlations for OASPL and PNL and standard atmospheric conditions. Level adjustments are made to account for three engines, angle of attack, and for slight differences in engine power setting. The results are shown in figures 14 and 15 where absolute 40 x 80 and 727 flight test OASPL and PNL directivities are compared at takeoff and cutback power. A further adjustment of the high angle data points is noted in the figures to account for reverberation effects on the absolute wind tunnel PNL.

At takeoff power (fig. 14), the extrapolated 40 x 80 OASPL and PNL compare favorably with flight test data. The peak OASPL values are approximately equal, while offpeak levels tend to be slightly low but within 1 dB of flight test. The wind tunnel PNL values fall within 0.5 PNdB of flight noise levels from low angles through 130°. The higher angles fall below flight test by about 1.5 PNdB.

The comparison at cutback power (fig. 15) indicates good agreement of peak OASPL and PNL but more variance in offpeak noise levels than at takeoff power. The higher flight test PNL at high angles is largely the result of the high frequency anomaly previously discussed (see fig. 9). In general, the two basic methods of defining flight noise levels from wind tunnel data result in reasonable estimates. The absolute noise level technique appears to provide the best estimate for peak flight OASPL and PNL. Offpeak noise estimates are quite comparable for each procedure.

The noise increment technique results in a higher peak noise level than flight test or conversely indicates less reduction of peak noise due to flight. This technique is dependent upon the accuracy of the measured tunnel-off to tunnel-on noise increments and the accuracy of the static data extrapolated to the flight condition. It is believed that the peak noise reduction measured in the wind tunnel is relatively accurate because of favorable experiment control, good angular resolution in the vicinity of peak noise, and relatively long data samples. The discrepancy with flight data may be caused by tolerances associated with the peak noise of the extrapolated static data or flight test data. The 20-lobe ejector/suppressor has a relatively sharp noise peak (near 120°) that varied up to 2 dB or PNdB during repeat far-field static runs. This characteristic undoubtedly contributes to a more sizable tolerance band for the static and flight test peak noise levels. The absolute noise level technique will likely provide the best estimate for configurations similar to the ejector/suppressor where dominant noise sources are located at the nozzle exit.

6.2.5 COMPARISON WITH BOEING 9 X 9 WIND TUNNEL RESULTS

A one-fifth scale model of the 20-lobe ejector/suppressor was tested in the Boeing 9 x 9 wind tunnel prior to the 40 x 80 full-scale test. The facility uses a traversing microphone similar to the 40 x 80 test. Since dual flow was not available at the time the test was run, a uniform flow was used at the JT8D primary gas conditions. Tunnel-off and tunnel-on OASPL and PNL directivity comparisons are provided in figure 16. The model data shows essentially no reduction at low angles, about 1 dB or PNdB at peak, and more substantial reduction at angles near the jet axis. The 40 x 80 and flight data show somewhat greater reductions at all angles than the 9 x 9 results; however, the trends with angle are the same.

6.3 BASELINE

The baseline test results are evaluated in this section with emphasis on jet noise. Inlet fan noise results for the baseline configuration are evaluated in section 6.5, while core noise is evaluated in section 6.6. The jet noise analysis includes: comparisons of 40 x 80 near-field tunnel-off data with free field data measured in the near field, an evaluation of flight effects as measured in the 40 x 80, comparisons of 40 x 80 and 727 flight test results, a comparison of baseline and 20-lobe ejector/suppressor results, and a comparison of 40 x 80 and Boeing 9 x 9 wind tunnel model test results.

6.3.1 COMPARISONS WITH FREE FIELD DATA

Spectra and directivity comparisons are made between the 40 x 80 tunnel-off data and static data acquired at the Boeing Boardman test site (ref. 1). The comparisons show that the 40 x 80 noise levels are substantially higher than the Boardman free field values at low frequencies and low angles. The problem is illustrated in figure 17 where takeoff power spectra are compared at angles of 90^0 and 110^0. The high level of 40 x 80 low frequency noise is not consistent with results for the 20-lobe ejector/suppressor and the reverberation test conducted prior to the engine test. The low frequency anomaly is sensitive to the engine power setting being relatively severe at high power and less severe at low power.

A number of possible causes of the low frequency level problem are considered and discussed in reference 1. A likely explanation is that the 40 x 80 is limited in the amount of noise reduction than can occur between the peak noise at a given frequency and the reverberant field level. Where large differences in low angle (90^0) to peak free field SPL are present (baseline at high power), a reverberation problem results. Where the SPL difference is small (baseline at low power, ejector/suppressor at all power conditions), the low angle reverberation problem is minimal. The important finding is that the low angle reverberation correction is dependent upon the source directivity characteristics that in turn are dependent upon nozzle configuration, engine power condition, and frequency.

Having a reverberation characteristic that is a function of the noise level being generated has a significant influence on the determination of low angle jet noise reduction due to tunnel flow. For example, the tunnel-off reverberation correction will be higher than the tunnel-on correction because of a larger reduction of peak noise than low angle noise with tunnel velocity. The corrected flight noise reduction will be less than measured, differing by the increment in reverberation correction (tunnel-off minus tunnel-on reverberation correction).

Reverberation corrections are defined in reference 1 for OASPL, PNL, and SPL as a function of test nozzle pressure ratio, tunnel operating condition, and measurement station. The corrections are based on the assumption that the reverberation correction is dependent on the level of noise being generated and that noise level is a function of primary jet relative velocity. The accuracy of these assumptions is not known at this time. Since the difference in reverberation correction between tunnel-off and tunnel-on

operation is relatively small, the potential error in flight effect is likely to be small (0.5 dB or less). The reverberation corrections were established by plotting 40 x 80 tunnel-off noise (OASPL, PNL, and SPL) and Boardman free field noise as a function of primary velocity for each test angle.

6.3.2 40 X 80 FLIGHT EFFECTS

As previously mentioned, the wind tunnel results require a Doppler frequency shift in order to approximate the total flight effect of an engine in motion past an observer. Doppler shifted spectra are provided in figure 18 for a nozzle pressure ratio of 2.1. It is noted that both tunnel-on and tunnel-off spectra have been corrected for reverberation. The near-field angles shown (110° and 155°) are approximately equivalent to far-field angles of 90° and 140° (peak noise) based on the near/far field correlation of reference 1. Thus, the 110° spectra have no Doppler frequency shift while the 155° spectra frequencies are reduced by about 80% of a one-third octave band relative to the recorded frequencies. The effect of the Doppler frequency shift at the 155° position is to increase the static-to-flight noise increment at frequencies above 200 Hz and decrease it at frequencies below 200 Hz. For this case, the noise increment changes up to 1.5 dB depending upon the shape characteristics of the spectra (flat spectra shows little change).

A reference noise level is included in figure 18 that represents interpolated tunnel-off data at the tunnel-on primary relative velocity. As indicated, the peak noise tunnel-on spectra compare reasonably well with the reference spectra. This indicates that a good estimate of peak flight noise at high power can be made by interpolating static data at flight primary relative velocity. The low angle (110°) tunnel-on spectra compare well with the relative velocity level at low frequency but show less reduction at intermediate and high frequencies. Thus, the use of primary relative velocity to predict flight noise at low angles will result in a lower OASPL or PNL than measured in the wind tunnel.

Tunnel-off and tunnel-on OASPL and PNL directivities are compared in figure 19 for the takeoff power condition. The PNL comparison includes a tunnel-on noise level that has been corrected for Doppler frequency shift. Reference OASPL and PNL curves are also included that represent interpolated tunnel-off data at tunnel-on primary relative velocity. The comparisons show that the largest reduction of noise due to tunnel flow occurs at or near the peak noise location. The low angle reduction is significantly less, while the higher angles show slightly less reduction than at peak. The OASPL peak noise location is approximately the same for both tunnel-off and tunnel-on, while the peak PNL tends to shift toward a lower angle.

The Doppler frequency shift adjustment for tunnel-on PNL reflects noise emission angle based on near/far field correlations and the test wind tunnel Mach number. The resulting correction lowers the flight noise by up to 1 PNdB at angles near the jet axis.

The tunnel-on (flight) OASPL's are closely approximated by the reference relative velocity noise level at angles of 130° and higher. Lower angles show less flight noise reduction than predicted by relative velocity. Note that these are near-field angles

where the 155° peak noise location is equivalent to a far-field angle of about 140°, while 110° is equivalent to a far-field angle of about 90°.

The tunnel-on (flight) perceived noise level with Doppler frequency shift is approximately equal to the relative velocity reference level at angles above 130°. Lower angles undergo less flight noise reduction than the relative velocity estimate, similar to the trend shown for OASPL.

Tunnel-off and tunnel-on OASPL and PNL are plotted as a function of primary relative velocity in figures 20 and 21 for several near-field angles. The plotted data points include all necessary corrections for noise floor, convection, and reverberation. The solid line is faired through the tunnel-off data and serves as a primary relative velocity reference level for the tunnel-on data. The dashed lines are estimated slope characteristics for the tunnel-on data referenced to the tunnel-off noise level. These slopes are used to define flight noise reduction velocity index values for later comparison with 727 flight data.

The OASPL data at 90° (fig. 20a) show tunnel-on slopes less than tunnel-off slope characteristics. As the near-field angle increases, the tunnel-on slopes approach tunnel-off until at 130° they are essentially equal. That is, tunnel-off and tunnel-on data all fall on the same line, and tunnel-on noise levels are correctly predicted by primary relative velocity. At higher angles (fig. 20b), the tunnel-on data continue to fall on or slightly below the tunnel-off line, indicating that relative velocity is an acceptable means of predicting tunnel-on OASPL over a wide range of angles (near-field angles of 130° to 165°). Doppler frequency shift does not influence OASPL; thus, the forward velocity effects on OASPL are representative of aircraft flight effects, where installation effects are negligible.

The 90° PNL data (fig. 21a) indicate tunnel-on slopes well below tunnel-off slope characteristics. As the angle increases, the tunnel-on slopes approach but do not quite reach the tunnel-off slope. It is noted that Doppler frequency effects are not included in the PNL curves. At the highest tunnel velocity and high emission angles (fig. 21b), this will lower the flight PNL about 1 PNdB causing the tunnel-on data to essentially fall on the tunnel-off curve. In general, the use of primary relative velocity will provide a reasonably accurate flight PNL estimate for near-field angles of 130° and higher.

6.3.3 FLIGHT EFFECTS ESTIMATES USING 40 X 80 RESULTS

Several methods of predicting flight noise levels from far-field static data and 40 x 80 results are discussed in this section. The easiest technique is to interpolate static data (OASPL or PNL) at flight primary relative velocity ($V_{pri} - V_\infty$). As previously discussed in section 6.3.2, this will provide a good estimate of the measured flight levels at near-field angles of about 130° or higher, or equivalent far-field angles of 110° or higher. At far field angles below 110°, the estimated flight noise will be lower than measured but may be adjusted to a higher level if low angle noise is important to the study. This technique should be limited to cases where jet noise is dominant (high power).

Another approach is to define velocity index values as a function of power setting and angle. The velocity index is defined as follows and may be applied to OASPL, PNL, or SPL:

$$n = \frac{OASPL_{static} - OASPL_{flight}}{10 \log \frac{V_{pri}}{V_R}} \quad (1)$$

Curves similar to figures 20 and 21 were used to define the near- and far-field velocity index curves provided in figures 22 through 24. The upper part of figure 22 is a fairing through the calculated velocity index values for pressure ratios of 1.6, 1.8, and 2.1. For a given angle, the slopes for these pressure ratios are approximately the same; thus, a single line is satisfactory for the range of primary velocities indicated. The far-field velocity index curve shown in the lower half of figure 22 was determined from the near-field curve and the near/far field correlation data provided in reference 1. The far-field curve also represents a fairing through the points that result from the near/far field OASPL correlation for pressure ratios of 1.6, 1.8, and 2.1. This procedure was followed to define the PNL velocity index curves of figure 23. In this case the slopes vary enough with pressure ratio to justify multiple fairings as indicated. The far-field curves of figure 23 do not include the effect of Doppler frequency shift. Velocity index curves with Doppler frequency shift are provided in figure 24 and are believed to be the most accurate for flight PNL predictions.

The OASPL and PNL velocity index curves may be used to predict flight noise levels from static test data. The static-to-flight noise difference at a given far-field angle is equal to:

$$n\left(10 \log \frac{V_{pri}}{V_R}\right) \quad (2)$$

The noise increment is then subtracted from the static noise level to establish a predicted flight OASPL or PNL. This technique will provide fairly accurate flight noise estimates over the range of primary jet velocities or pressure ratios indicated in figures 22 and 24 for OASPL and PNL, respectively.

A third and more detailed technique is to estimate flight spectra at each angle using far-field static data and tunnel-off to tunnel-on noise increments as measured in the 40 x 80. An example of this technique is provided in reference 1 for cutback power that includes far-field angles of 70° to 150°. The estimate requires working plots of tunnel-off and tunnel-on sound pressure level versus measurement axial location for each 24 one-third octave band. A typical plot is shown in figure 25 for a frequency of 200 Hz. Far-field static spectra for the JT8D-17 engine are plotted for the desired angles (see fig. 26). For a given far-field angle, the corresponding near-field angle is determined from the near/far field correlation curves for each frequency. The SPL directivity curves are interpolated at the appropriate near-field angle and desired flight velocity to define the far-field noise reduction. This noise increment is applied to the static spectra and shifted in frequency to account for Doppler effects. This procedure is repeated for each frequency and each far-field angle to obtain the desired flight spectra typified by figure 26. OASPL and PNL values are then calculated to define static and predicted flight

noise or static-to-flight noise increments. It is noted that reverberation corrections were not applied to the SPL directivity curves. A correction was applied to the calculated OASPL and PNL static-to-flight increments using correction curves defined in reference 1. The resulting flight noise characteristics are compared with flight test data in the following section.

6.3.4 COMPARISON WITH 727/JT8D FLIGHT DATA

Measured 727/JT8D flight test results for the baseline configuration are compared with 40 x 80 results in this section. Two techniques are used for the comparisons: one based on static-to-flight noise increments, the other based on absolute noise levels. Wind tunnel and static test data that are extrapolated to the flight conditions are corrected for slight differences in engine power, three engine operation, angle of attack, and noise source location.

6.3.4.1 Noise Increment Technique

Flight test OASPL and PNL directivities are compared with 40 x 80 data based on measured differential noise in figure 27 for cutback power. The flight test data reflect JT8D-9 engines as opposed to the wind tunnel JT8D-17 configuration. The primary difference in noise signature will be aft fan noise that has a relatively small impact on OASPL but a more significant effect on perceived noise level, in particular, at low angles. The reference static level was established by extrapolating far-field JT8D-9 engine data to the flight condition in the manner previously described.

The wind tunnel test condition of NPR = 1.8 and 150 kn was selected as being most representative of the flight test cutback power condition. The match is good in terms of NPR, N_1, primary jet velocity, and absolute airplane velocity. Because of entrained tunnel velocity during tunnel-off operation, the wind tunnel effective flight velocity (tunnel-on V_∞ minus tunnel-off V_∞) is less than the flight test V_∞ of 82 m/s. The tunnel-off OASPL and PNL values are, therefore, increased slightly (by interpolation) so that tunnel-off to tunnel-on noise increments are representative of all flight test conditions, including V_∞. The near- to far-field correlation of figure 5 was used to relate the adjusted tunnel-off to tunnel-on noise increments to the proper far-field angles. The resulting OASPL and PNL differential values are subtracted from the reference static noise levels to define the wind tunnel flight noise levels shown in figure 27.

The resulting comparison of wind tunnel and flight test data is considered to be relatively good considering the tolerances involved in the flight data (±1 dB or PNdB), the static data extrapolated to the flight condition (±1 dB or PNdB), the different engine configurations, and possible installation effects (more apt to influence PNL).

A similar comparison for cutback power is shown in figure 28 where calculated OASPL and PNL static-to-flight increments are applied to the static data extrapolated to the flight condition. These noise differences were obtained from spectra similar to those in figure 26 where flight spectra were established from far-field static spectra and measured 40 x 80 tunnel-off to tunnel-on SPL noise reductions. The resulting comparison with flight test data is very similar to that obtained using the measured OASPL and PNL increment technique (fig. 27).

Comparisons of flight test and 40 x 80 discrete frequency noise reductions are provided in reference 1 for the cutback power condition. The resulting noise increments compare reasonably well in terms of trends with acoustic angle. The 40 x 80 noise reduction tends to be relatively close to flight test at angles near the jet axis but generally higher at low angles. Considering the larger data scatter associated with discrete frequencies, the overall comparison of flight test and 40 x 80 data (within ±2 dB) is considered to be fairly good.

A comparison of flight test and 40 x 80 OASPL and PNL directivity is provided in figure 29 for takeoff power. The 40 x 80 results are based on measured tunnel-off to tunnel-on noise changes similar to figure 27. In this case the 185-kn test condition provides an approximately correct match for the flight condition. The OASPL and PNL noise reductions were obtained from figure 19 using the near/far field correlation for NPR = 2.1 provided in reference 1. The PNL static-to-flight differential values include the added increment of figure 19 to account for Doppler frequency shift. The resulting comparison of figure 29 shows good agreement for both OASPL and PNL in terms of flight noise directivity and absolute level.

Another means of evaluating static-to-flight noise changes is to compare wind tunnel and flight test velocity index values. This comparison is provided in figures 30 and 31 for cutback and takeoff power, respectively. The velocity index values were calculated in the manner described in section 6.3.3. The wind tunnel curves are taken from figures 22 and 24, while the flight test data points are calculated using the static-to-flight increments of figures 27 and 29. As indicated, the OASPL and PNL velocity index values compare well, in particular, at takeoff power where jet noise is quite dominant. The flight test values at cutback power appear to be somewhat erratic. This may be caused by the problem of extrapolating static data to the flight condition where aft fan noise is starting to become a factor. Fan tone levels are quite sensitive to atmospheric effects, measurement techniques (integration time, etc.), and installation effects (inlet flow and wake interference).

6.3.4.2 Absolute Noise Level Technique

Comparison of absolute wind tunnel noise levels with flight data is an alternate technique to the noise increment procedure. This comparison is provided in figures 32 and 33 for cutback and takeoff power, respectively. The cutback comparison used the 150-kn, NPR 1.8 data that closely matched the absolute flight condition. The 40 x 80-data were extrapolated to a 122-m altitude by applying spherical divergence and standard day atmospheric absorption to the proper noise emission angle. Level adjustments were made to both OASPL and PNL to account for three engines, angle of attack, and differences in static peak-to-peak near/far field noise at a common sideline (+1.0 dB or PNdB). Reverberation corrections defined in reference 1 are also applied to the absolute cutback power noise levels. The resulting corrected 40 x 80 OASPL and PNL values compare reasonably well with the flight test data as shown in figure 32. The largest discrepancy occurs for PNL at low angle where the 40 x 80 level exceeds the flight test by 2 PNdB. This difference is attributed to aft fan noise where the 40 x 80 spectra show a significantly higher noise level at frequencies of 3150 Hz and higher when compared with flight data. Again, this may be caused by atmospheric effects, installation effects, measurement technique, or engine differences.

A similar comparison is made in figure 33 for takeoff power. The 185-kn, NPR-2.1 data provide the closest match with flight data; however, a slight upward level correction was necessary to adjust to the flight relative velocity. Corrections for reverberation, near/far field peak-to-peak noise differences, and angle of attack were made in a similar manner to the cutback condition. The flight test and 40 x 80 OASPL's and PNL's compare reasonably well. The comparison is best at low angles through peak noise. At high angles, the wind tunnel levels fall below flight test by up to 1.5 dB for OASPL and 2 PNdB for PNL. Part of this difference is the result of flight test data at high angles that show a significant 160-Hz spike. (Two out of three flybys show the spike.) At this time there is no satisfactory explanation for this phenomenon. The low angle PNL comparison is better than cutback power, probably because aft fan noise is less of a factor at takeoff power.

The noise increment and absolute noise level techniques provide comparable flight noise estimates for the baseline configuration. In general, the noise increment technique is recommended where dominant downstream noise sources require a significant near-to far-field angular adjustment (baseline and internal mixer). The static to flight increment is less sensitive to the exactness of the near/far field correlation than the absolute level at off-peak noise locations.

6.3.5 COMPARISON OF BASELINE AND 20-LOBE EJECTOR/SUPPRESSOR RESULTS

The in-flight suppression characteristics of the 20-lobe ejector/suppressor nozzle are evaluated in this section. The evaluation includes wind tunnel and flight test results and is based on peak noise suppression at cutback and takeoff power. Peak noise suppression is defined as the difference in baseline and 20-lobe ejector/suppressor peak OASPL or PNL measured along a given sideline or altitude. Since the baseline experiences a larger noise reduction due to tunnel velocity (or flight) than does the suppressor, a loss of suppression occurs relative to static operation. The OASPL and PNL suppression characteristics are summarized in figure 34 which shows a static suppression, flight suppression, and loss of suppression due to flight. The flight test static suppression is the difference in far-field (122-m) peak noise of the baseline and suppressor operating at flight ideal jet velocity. The flight suppression is the difference of flyover peak noise levels for the designated power setting. The suppression loss is the difference between the two suppression values. Wind tunnel suppression values are provided in figure 34 for comparison with flight test results. The wind tunnel static suppression is arbitrarily set equal to far-field values. The comparisons are, therefore, meaningful only for suppression loss and flight suppression. The wind tunnel suppression loss values were obtained by subtracting the measured 20-lobe ejector/suppressor tunnel-off to tunnel-on peak noise reduction from the corresponding baseline peak noise reduction. The resulting suppression losses reflect the appropriate flight test power conditions and aircraft velocities. The wind tunnel flight suppression is then determined by subtracting the suppression loss from the static suppression. In general, the 40 x 80 results predict the in-flight peak noise suppression of the 20-lobe ejector/suppressor quite well, falling within 1 dB or PNdB of flight test values.

6.3.6 COMPARISON WITH BOEING 9 X 9 WIND TUNNEL RESULTS

A one-seventh scale model of the JT8D baseline was tested in the Boeing 9 x 9 wind tunnel. The model was supplied with heated dual flow at conditions equivalent to the JT8D-17 cycle. Test results provided in reference 1 include tunnel-off and tunnel-on

spectra, OASPL and PNL directivity, and an OASPL/relative velocity correlation. Tunnel-off and tunnel-on OASPL and PNL directivities are provided in figure 35 for takeoff power. The 9 x 9 flight effects are similar to the 40 x 80 results (fig. 19) in showing a flight noise reduction approximately equal to the relative velocity reference level at angles above 130° to 140°. The tendency for less reduction at low angles is also consistent with full-scale results. A cutback power directivity comparison is provided in reference 1 and shows that 9 x 9 and 40 x 80 flight effects are comparable for OASPL. The reduction of PNL with tunnel velocity is consistent in the region of peak noise and higher angles; however, the model data show more reduction at low angles (90° to 120°). The difference at low angles may be influenced by the presence of fan noise in the full-scale data that tend to restrict the amount of PNL reduction.

On the whole, the 9 x 9 wind tunnel results compare favorably with the 40 x 80 results. This indicates that model tests in small wind tunnel facilities can be used to study flight effects on engine jet noise with reasonable confidence when the engine is jet noise dominated.

6.4 INTERNAL MIXER

The internal mixer analysis emphasizes the configuration with acoustic lining downstream of the mixer. The influence of replacing the inner wall lining with a hardwall and adding external vortex generators is also evaluated.

6.4.1 LINED INTERNAL MIXER

The analysis for the lined internal mixer evaluates flight effects as measured in the 40 x 80 and compares these results with baseline and 20-lobe ejector/suppressor results. It is noted that the internal mixer has not been flight tested on the 727 airplane; thus, comparisons with flight data are not possible.

6.4.1.1 Comparisons With Free Field Data

Spectra comparisons between the 40 x 80 tunnel-off data and static data acquired at the Boeing Boardman test site indicate a low frequency reverberant field problem similar to the baseline. Reverberation corrections are defined for OASPL and PNL in reference 1.

6.4.1.2 40 x 80 Flight Effects

Tunnel-off and tunnel-on spectra are compared in figure 36 for takeoff power and near-field angles of 140° and 155°. As previously noted, the measured tunnel-on data does not include the effect of Doppler frequency shift. The tunnel-on spectra of figure 36 include a Doppler frequency shift defined as a function of noise emission angle and tunnel velocity. The near-field angles of 140° and 155° are approximately equivalent to far-field angles of 120° and 140° based on the near/far field correlation of reference 1. For the noted test conditions, the frequencies at 140° were reduced by 40% of a one-third octave band, while the frequencies at 155° were reduced by 60%. The influence of Doppler frequency shift is small for this configuration because of the relatively flat spectra shape characteristic. At 155° the static-to-flight noise increment increases by about 0.5 dB at frequencies above 160 Hz due to the Doppler frequency shift. At 100 to 160 Hz the change in noise increment is less than 0.5 dB, while at frequencies below 100 Hz the noise increment decreases by as much as 1.5 dB.

The fan and primary streams are reasonably well mixed by the 12-lobe internal mixer. The mixed jet velocity is calculated from measured test primary and fan gas conditions and serves as a correlating parameter for the flight effects analysis of the internal mixer configuration. Tunnel-off spectra at the tunnel-on mixed jet relative velocity are provided as a reference noise level in figure 36.

The tunnel-off pressure ratio 1.8 data were taken at a mixed relative velocity very close to the tunnel-on relative velocity of figure 36 and were used to define the reference noise level. At 155° the tunnel-on spectra compare very well with the reference tunnel-off level. At 140° the comparison is reasonably good, although the high frequency wind tunnel noise reduction is slightly less than predicted by the use of mixed jet relative velocity. For the angles shown, it appears that interpolating static data at the flight mixed jet relative velocity will provide a reasonably accurate flight noise estimate.

Tunnel-off and tunnel-on OASPL and PNL directivities are compared in figure 37 for an NPR = 2.1 and a tunnel velocity of 150 kn. Both tunnel-off and tunnel-on data have been corrected for reverberation, and tunnel-on data have been corrected for noise floor and for convection effects. The tunnel-off data at NPR = 1.8 match the tunnel-on mixed jet relative velocity ($V_{mix} - V_{\infty}$) and serve as a reference noise level.

The OASPL plot shows that the tunnel-on noise level is closely predicted by the tunnel-off data at equal mixed jet relative velocity over the indicated range of angles. Substantial reduction is shown at all angles with the largest reductions occuring near the region of peak noise. The location of peak OASPL is slightly changed due to tunnel velocity.

The PNL comparison indicates that tunnel-off data at equal mixed jet relative velocity slightly overpredicts the amount of reduction due to tunnel flow. At low angles (90° to 110°), the overprediction is as much as 1 PNdB while at peak noise and higher angles the difference is less than 0.5 PNdB. For the JT8D engine cycle, the internal mixer is basically a low frequency suppressor. The low frequency noise is generated well downstream of the nozzle exit and tends to follow a relative velocity reduction with tunnel flow. The OASPL is more sensitive to low frequency noise than PNL and, therefore, follows the relative velocity predicted level reasonably well. The high frequencies are dominated by noise generated nearer to the nozzle exit plane and are sensitive to exit velocity profile characteristics. The exit profile will have an influence on the amount of high frequency noise reduction that in turn will influence the amount of PNL reduction, in particular at low angles.

It is believed that the specific profile of the 40 x 80 mixer configuration would tend to limit the amount of high frequency noise reduction (relative to a flat profile). Thus, the PNL noise reduction with tunnel flow appears to be reasonable.

The location of peak PNL does not appear to change substantially due to tunnel flow. The static directivity is very flat over a range of angles in the peak noise region. Since the amount of PNL reduction is greater at angles near the jet axis, there is a natural tendency for the peak noise to move toward the inlet axis with tunnel flow. For the takeoff power condition shown in figure 37, a change in peak PNL location caused by tunnel flow is difficult to discern.

The influence of Doppler frequency shift on PNL is indicated in figure 37. The flight noise reduction is seen to increase by as much as 1 PNdB at angles near the jet axis.

Tunnel-off and tunnel-on OASPL and PNL are plotted as a function of mixed primary relative velocity in figures 38 and 39 for several near-field angles. The plotted data points have been corrected for noise floor, convection, and reverberation. The solid line is faired through the tunnel-of data and provides a relative velocity reference level for the tunnel-on data. The dashed lines are estimated slope characteristics for the tunnel-on data referenced to the tunnel-off noise level. These slopes are used to define flight noise reduction velocity index values for use in predicting mixer flight noise levels.

The OASPL tunnel-on data fall relatively close to the tunnel-off level for a range of angles from 90° to 165°. At low angles (90° to 130°), the tunnel-on data are slightly above the tunnel-off line (fig. 38a), while at higher angles the tunnel-on data fall on or slightly below the line (fig. 38b). This indicates that the use of mixed jet relative velocity will provide a good estimate of flight OASPL for the range of angles covered by the test.

The PNL tunnel-on data include the effect of Doppler frequency shift and show the low angle tunnel-on levels to be consistently above the tunnel-off level at equal relative velocity by about 1 PNdB (see fig. 39a). At angles of 150° and higher the tunnel-on data fall relatively close to the reference tunnel-off level (see fig. 39b).

6.4.1.3 Flight Effects Estimates Using 40 x 80 Results

Two approaches for estimating the flight noise level of the JT8D engine with internal mixer are suggested. The simplest is to apply the relative velocity principle where static data are interpolated at flight relative velocity. In this case, the OASPL will be closely approximated at all aft quadrant angles while PNL will be closely approximated at peak noise and higher angles. An alternate procedure for predicting low angle PNL would be to use primary (unmixed) relative velocity. This approach is illustrated in figure 40 for a near-field angle of 90° and indicates a good correlation between tunnel-on and tunnel-off PNL at equal primary relative velocity. The analysis in reference 1 shows that static PNL at primary relative velocity will provide a good estimate of flight PNL for far-field angles up to approximately 120°. Static PNL at mixed relative velocity is recommended for angles greater than 120° (based on near/far field correlations).

Velocity index values have been defined from the relative velocity correlations of reference 1 in a manner similar to that described for the baseline in section 6.3.3. The results are shown in figures 41 and 42 for OASPL and PNL, respectively. The mixed jet velocity is used for both the OASPL and PNL velocity index correlations.

The velocity index curves may be used to predict flight noise levels from static far-field data. The change in noise at a given far-field angle is equal to:

$$n\left(10 \log \frac{V_{mix}}{V_{mix} - V_{\infty}}\right) \qquad (3)$$

The resulting noise increment is then subtracted from the static noise level (at flight ideal mixed velocity) to establish a predicted flight OASPL or PNL.

6.4.1.4 Comparison of Baseline and Internal Mixer Results

The static and flight suppression characteristics of the lined internal mixer are evaluated in this section. The comparison is based on peak noise suppression of the internal mixer relative to the baseline at takeoff power. The results are summarized in figure 43 and include static and flight suppression as measured in the 40 x 80 and an alternate approach using far-field data plus 40 x 80 flight effects. The first method subtracts the peak internal mixer noise from the peak baseline noise for tunnel-off and tunnel-on operation. Slight adjustments in noise levels were made so that the comparison reflects equal engine and tunnel operating conditions. The flight OASPL suppression is greater than static suppression by 2.5 dB, while the flight PNL suppression increases by 0.5 PNdB. This is in contrast to the 20-lobe ejector/suppressor that experiences a loss of suppression due to flight (sec. 6.3.5, fig. 34). The mixer suppression gain is caused by the reduced velocity of the mixed jet relative to the baseline primary velcity. For a given velocity index and flight velocity, the lower velocity jet will experience a larger noise reduction (10 log V/V_R is larger). The increased noise reduction experience by the mixer is primarily in the low frequency regime; thus, the gain in OASPL suppression is greater than the gain in PNL suppression.

The second approach considered in figure 43 establishes the mixer static suppression from far-field noise data. It is interesting to note that the far-field static OASPL peak suppression is essentially equal to that measured in the 40 x 80. The far-field static PNL peak suppression is about 1 PNdB less than the 40 x 80. Considering the sensitivity of PNL to high frequency noise and the fact that the baseline configuration used in the far-field test incorporated tailpipe lining, this difference is reasonable. The flight OASPL and PNL suppression values were determined by applying the velocity index curves (figs. 22, 24, 41, and 42) to the far-field baseline and internal mixer noise data. The resulting flight peak noise levels were subtracted and resulted in the flight suppression shown in figure 43. The gain in OASPL and PNL suppression compares favorably with the 40 x 80 as measured values.

6.4.2 COMPARISON OF LINED AND HARDWALL INTERNAL MIXER RESULTS

Tunnel-off and tunnel-on spectra comparisons are made between the lined and hardwall internal mixer configurations in figures 44 and 45. The lining, located downstream of the mixer elements, was believed to have potential for absorbing internal noise generated by the fan/primary mixing process. Far-field static spectra comparisons indicated that this lining had little benefit other than absorbing some of the aft fan noise. The lined and hardwall configurations were tested in the 40 x 80 to see if this trend was also observed in flight where externally generated jet noise is reduced.

Tunnel-off spectra at cutback power are shown in figure 44 for the lined and hardwall configurations and confirm the far-field static results; i.e., little or no benefits result because of the lining with the exception of aft fan noise (observable at 100° and

frequencies above 2500 Hz). It is noted that the comparisons of figures 44 and 45 reflect slightly higher jet velocities for the hardwall. Part of the lined/hardwall noise difference may be attributed to this (about 0.5 dB).

During tunnel-on operation (fig. 45), the benefit of downstream lining tends to improve slightly at low angles and frequencies above 800 Hz. This benefit is probably associated with absorption of aft fan noise as opposed to absorbtion of an internal mixing noise. At 140^0 and higher angles, the lining influence on noise appears to be relatively small for both static and flight operation at all but the very high frequencies.

6.4.3 INFLUENCE OF EXTERNAL VORTEX GENERATORS

The hardwall internal mixer configuration was tested with and without external vortex generators. It was hoped that these devices might enhance the rate of mixing between the nozzle exhaust and the freestream and provide a modest reduction of in-flight noise. The spectra comparisons of figure 46 indicate that the vortex generators did not reduce the jet mixing noise at either low or high angles. If anything, the mixing noise increased slightly (about 1 dB) at the cutback power condition. Perhaps a different VG design (larger, greater number, different station) would prove to be more effective. Based on these results, this suppression device does not appear to be promising.

6.5 COMPARISON OF BASELINE AND SUPPRESSOR NOZZLE STATIC AND FLIGHT PNL

A comparison of static and flight PNL directivities is provided in figure 47 for the baseline, internal mixer, and 20-lobe ejector/suppressor configurations. The comparisons include cutback and takeoff power and reflect noise levels for a 727 aircraft during a level flyover at an altitude of 122 m (400 ft). It is assumed that each engine configuration is operating at the noted ideal primary jet velocity as opposed to equal net thrust. The static PNL estimates are based on Boardman far-field data that are extrapolated to the flight condition. The flight noise levels for the baseline and internal mixer were estimated by using the wind tunnel derived velocity index curves shown in figures 24 and 42. The PNL static-to-flight increments are calculated as described in section 6.3.3. The increments at each angle are subtracted from the reference static PNL values of figure 47 to establish the estimated flight PNL characteristics shown in the figure.

The flight noise level for the 20-lobe ejector/suppressor was estimated by subtracting measured tunnel-off to tunnel-on PNL increments from the reference static PNL values. This is the same procedure used to define the wind tunnel noise levels shown in figure 12 and is consistent with the technique used for the baseline and internal mixer configurations.

The PNL directivity comparisons of figure 47 emphasize the importance of flight effects to a proper evaluation of a suppressor concept. In going from static-to-flight operation, the noise characteristics of the internal mixer improve slightly relative to the baseline; i.e., the flight PNL suppression is greater than static suppression over the range of angles shown in figure 47. The 20-lobe ejector/suppressor experiences a significant loss

of PNL suppression during flight. Although the ejector/suppressor generates substantially less noise than the internal mixer under static conditions, the in-flight noise levels are much more comparable, in particular at low and peak noise angles. It is noted that the margin increases at angles near the jet axis and contributes to a further advantage for the ejector/suppressor in terms of effective perceived noise level (EPNL).

Factors other than noise must be considered in evaluating the effectiveness of a suppressor concept including; suppressor complexity, weight, propulsion efficiency, maintenance, cost, and overall aircraft performance penalties. The internal mixer is a much simpler suppressor concept than the 20-lobe ejector/suppressor and offers definite advantages in virtually all categories other than noise. The potential for improving the in-flight noise characteristics of the internal mixer is relatively small. The ejector/suppressor has potential for a substantially lower in-flight noise level than that demonstrated during flight test or the 40 x 80 test. The major problem area is premerged mixing noise that dominates the low angle and peak noise and is little reduced by forward velocity. There are a number of design variables that may be exercised to either generate less premerged mixing noise or absorb more of this component within the confines of the ejector. If successful, the improved in-flight noise levels would make the ejector/suppressor much more competitive with the internal mixer as a suppressor candidate.

6.6 BASELINE FAN NOISE

The major emphasis of the 40 x 80 program is the study of forward velocity effects on jet noise. During these tests, however, a limited quantity of data was taken in the forward quadrant to experimentally determine the effects of forward motion on JT8D engine fan noise. For modern high bypass engines, much evidence exists that shows large reductions in the fan fundamental tone from static to flight at approach power settings. These engines do not have inlet guide vanes (IGV), and the rotor/stator interaction is acoustically cut off. It is now generally believed that the observed tone noise reduction is caused by reduced inflow velocity variations in flight as compared to the static case (ref. 5).

Fan noise generation at subsonic rotor tip speeds is associated with component unsteady aerodynamics. For the rotor, the unsteadiness is attributed to asymmetric development of the inlet boundary layer and ambient disturbances ingested into the inlet. The latter disturbances consist of (1) fan inflow velocity distortion such as ground attached vortex, (2) fan inflow velocity distortion or turbulence resulting from total temperature distortion, and (3) eddies of atmospheric turbulence stretched in the inlet flow contraction. There is also the interaction between these possible disturbances. The stator noise from modern engines is attributed to the viscous wakes from the rotor interacting with the vanes. For the blade passage tone (BPT), this source is minimized by selecting a rotor blade/stator vane ratio that acoustically cuts this tone off. The rotor is then the primary source of the BPT.

The major known change from static to flight is a reduction in the velocity variations caused by ambient disturbances. In flight the large atmospheric eddies are not stretched with the associated angular momentum increase. For most modern aircraft in flight,

vortex ingestion is minimum. In addition, the flow unsteadyness caused by diffusion of the inlet flow at the rotor is reduced. The attitude of the inlet in flight can cause higher velocity variations than the static case but, based on observed tone noise reductions, it is believed to be secondary to the other inflow cleanup effects. These rotor inflow and related source noise changes are mainly caused by the forward motion of the engine from static to flight and can be simulated to a large degree in a wind tunnel. Flow contraction, absence of ground attached vortex, and effects of inlet diffusion are like that in flight. However, freestream velocity and temperature variations are not similar. It is not clear at this time how this deficiency effects the results.

In addition to the source noise changes from static to flight, changes in the flow field through which the noise propagates also affect the far-field noise. Statically the velocity gradients in the area of the inlet throat are significantly greater than in flight. From existing evidence, this is expected to result in a noise increase from static to flight. The wind tunnel accounts for this change.

For an engine with IGV's like the JT8D, this inlet cleanup effect on fan noise was believed to be of secondary importance. The IGV wakes interacting with the rotor, as well as the stator sources, produce propagating tone noise at all engine operating conditions. These sources were thought to dominate the noise caused by the other inflow velocity variations interacting with the rotor.

At this time there is little or no evidence that defines the relative magnitudes of these sources. An exception to this is that tests with very close IGV/rotor spacing (i.e., one half an IGV chord) indicate that the IGV wake interaction and respective potential field interactions were predominant. For the JT8D-17, this spacing is about 0.6. The reason that basic understanding of the relative importance of the different sources is so limited is that previous investigations were done statically and without controlled inflow so that all sources were involved in the results. Flyover data that are not contaminated by installation effects, like shielding and/or acoustic lining, are not available. Analytical models exist that predict the various sources but have not been experimentally substantiated.

The 40 x 80 test data when combined with static data taken at the Boeing Boardman test site offer the first opportunity to evaluate the significance of forward motion effects on an IGV fan. Within the qualifications previously discussed, this represents an evaluation of static-to-flight effects. Engine inflow at Boardman is expected to include not only atmospheric turbulence but also temperature distortion and ground vortex.

The objective of the effort reported here is to present the existing evidence that demonstrates the significance of forward motion effect on JT8D engine fan noise. This includes predicting the tone noise using state-of-the-art analytical models and comparing the wind tunnel data with static data taken at the Boardman test site. Due to the limited scope of this study, only fan tone noise at simulated approach power is discussed.

6.6.1 ANALYTICAL STUDY OF THE IGV/ROTOR AND INLET TURBULENCE/ ROTOR NOISE SOURCE MECHANISMS FOR THE JT8D ENGINE

In this study analytical models were used to estimate the importance of the inlet turbulence source compared to blade interaction sources associated with the first fan stage (BPT) of the JT8D engine. These estimates were made only at the approach power conditions. The analytical models used in these predictions are described in reference 6.

For the first fan stage, the power level (PWL) of the rotor/stator interaction was predicted to be 7 dB below the IGV/rotor source, neglecting attenuation from rotor blockage of the forward propagating rotor/stator noise. At approach power, the rotor/stator source is near cutoff. This means that the wave fronts of the propagating modes are nearly parallel to the duct axis; therefore, the propagating modes see considerable rotor blockage. Based on reference 7, it is estimated that the rotor/stator source PWL would be reduced approximately 10 dB due to these rotor blockage effects. This indicates that the rotor/stator source is insignificant compared to the IGV/rotor source.

Noise level versus fan speed curves is presented for the IGV/rotor and inlet turbulence/rotor sources in figure 48. Under static test conditions, the observed noise levels would correspond to the sum of these two sources. Since they have the same frequency, the root mean square (rms) value of this sum depends on the phase difference between them. The sum is maximum when they are in phase and minimum when they are 180^0 out of phase. Because of the randomness of the inlet turbulence, the sum would be expected to fluctuate between its maximum and minimum values. Therefore on the average, the phase difference between the two sources would most likely be near 90^0. In figure 48, both the maximum and average sums are shown.

Comparisons between the curves for the average sum and IGV/rotor source show that the absence of the inlet turbulence/rotor source could cause significant noise reductions for the JT8D engine at approach power.

6.6.2 STATIC REFERENCE DATA

A JT8D-17 turbofan engine was tested at the Boardman test facility prior to the NASA-ARC 40- by 80-Foot Wind Tunnel test. In anticipation of the wind tunnel tests, noise measurements were taken on a 3-m sideline at various angular stations duplicating those used in the tunnel tests; however, the engine inlet used in these tests was different than the inlet used in the wind tunnel tests.

The Boardman 3-m sideline test used a QN production inlet. This inlet is acoustically treated with 66.8 cm (26.3 in.) of polyimide lining, overall thickness 0.94 cm (0.37 in.). The lining was added specifically to reduce the noise levels of the fan tones. Except for the acoustic lining differences, the QN inlet used in the Boardman 3-m sideline test and the standard production inlet used in the NASA-Ames tests are the same. The standard production inlet is acoustically treated with a 15.2-cm (6-in.) strip of perforated aluminum sheet with aluminum twill backing set over an airspace 1.5-cm (0.6-in.) deep. This treatment has negligible noise reduction effectiveness.

Analysis is provided in reference 1 to determine lining attenuation corrections that account for differences in the Boardman and 40 x 80 inlet hardware.

For approach power the corrections to be applied to the 3-m fan tone PWL's are:

First fan stage BPT	3.5 dB
Second harmonic	2.5 dB
Third harmonic	1.5 dB

6.6.3 FAN TONE FLIGHT EFFECTS

The flight effects discussed herein are estimations obtained by comparing static and wind tunnel data. As discussed previously, the wind tunnel is only partially representative of actual flight conditions. In comparing static and tunnel data, atmospheric attenuation caused by humidity and temperature and other propagation effects such as velocity gradients between the noise source and microphone were neglected.

Static and tunnel-on PWL's are determined for the first stage fan BPT and related second and third harmonics in reference 1 for the approach power condition. Reverberation corrections were applied to the measured fan tone SPL's and were determined from the reverberation test conducted prior to the engine test. The corrections are small, being 2 dB or less at most angles for the BPT.

Power levels were calculated by extrapolating the 3-m sideline SPL's to a 3-m polar arc, assuming free field propagation and no ambient effects. The PWL's were then calculated on the basis of a semisphere with a radius of 3 m. The following equation was used:

$$PWL = 10 \log_{10} \Sigma A_i \, 10^{SPL_i/10}, \text{ ref. } 10^{-12} \text{ watts} \qquad (4)$$

PWL differences between the static and wind tunnel data (flight) are summarized in figures 49 and 50. The previously mentioned inlet lining attenuation PWL corrections are applied to the Boardman static PWL as indicated in each figure. The comparisons show the following tone noise reductions:

First fan stage BPT	8.0 dB
Second harmonic	3.0 dB
Third harmonic	1.5 dB

These reductions are attributed to the elimination of the ground vortex present in the static test and to decreased eddy stretching because of the tunnel mean flow. The above reductions were observed even at the lowest tunnel velocity of 15 m/s (49 ft/s) where the tunnel flow resulted only from the JT8D engine pumping action. (The tunnel fans were off.) Possible explanations for this result include:

1. Approach type forward velocity is not required to achieve the static-to-flight tone noise reductions.

2. The tunnel turbulence is less severe than that in the atmosphere.

3. The ground vortex is more of a significant contributor to the tone noise than the ingested turbulent eddies and is minimized with low forward speed.

4. Combination of any or all the above.

At this time, which of the above items is responsible remains an open question.

In the cutback power range, PWL static to wind tunnel comparisons were possible only at the highest tunnel velocity setting because of the limited tunnel data available. These comparisons indicate that static-to-flight reductions for the BPT are not as large at cutback as at approach (ref. 1).

6.6.4 SUMMARY OF FAN TONE FLIGHT EFFECTS

Static-to-flight effects on fan noise were discussed as well as the applicability of the wind tunnel to simulate them. It is hypothesized that the major static-to-flight effects on fan source noise are simulated and include elimination of ground vortex ingestion and reduced atmospheric eddy stretching. The major unknowns in using the wind tunnel are the differences in the velocity and temperature variations between those in the tunnel and in the atmosphere.

Analytical predictions for the first stage BPT at approach power showed the two major rotor sources compete with each other. These sources are (1) the rotor interacting with the IGV wakes and (2) inflow velocity variations caused by ingested atmospheric turbulence with no forward motion interacting with the rotor. Elimination of the latter is predicted to reduce the tone by 4 to 7 dB. It was argued that with forward motion—in flight or in the wind tunnel—the source due to atmospheric turbulence is minimized resulting in a tone noise decrease.

Comparisons of the first stage fan tone noise data from static and wind tunnel tests were presented. These results indicate that, at approach power, the BPT amplitude is reduced from the static case by about 8 dB. This reduction occurred for tunnel speed from 15 to 85 m/s (49 to 278 ft/s). The tone variations with time were also reduced. The second and third harmonics were reduced 3 dB and 1.5 dB, respectively.

The analytical predictions and experimental results support each other and imply a rotor/turbulence source change from static to flight similar to the non-IGV engines. The effect was surprising because the IGV wake/rotor interaction was expected to dominate the tone noise.

As previously mentioned, this investigation of fan noise was limited with the major emphasis on jet noise. The results do indicate that fans with IGV's experience a significant static-to-flight noise reduction similar to fans without IGV's. This identifies a static test problem for turbofan engines that include IGV's.

6.7 BASELINE CORE NOISE

Core noise is defined as noise that is generated within the engines as the result of combustion or gas flow, such as swirl. This component is relatively low for the JT8D-17 engine and is not considered to be an important noise source at normal aircraft operating power conditions. Evaluation of JT8D engine static data indicates that core noise is prominent at low power settings (NPR = 1.2 and below) and low angles (below 130°).

In order to demonstrate the potential influence of core noise on in-flight engine noise, tunnel-off and tunnel-on noise data were taken at an NPR = 1.2. The resulting data may have value for evaluating the flight effects of higher bypass engines that tend to include a significant core noise signal. The core noise analysis is based on a frequency of 315 Hz and angles of 100° and 120°. The frequency was selected as being representative of core noise, while the angles are in the region of peak noise radiation for this component.

An example of core noise influence on engine noise flight effect is provided in figure 51. The power setting of interest is NPR = 1.2 for both tunnel-off and tunnel-on operation. The presence of core noise is evidenced by the change in the noise/velocity slope of the tunnel-off data at the low power setting. The slope established by the higher power settings is likely dominated by jet noise. The change in slope at lower power is caused by the emergence of an additional noise source (core noise) that combines with the jet noise and results in the measured level. The level of core noise for static operation at NPR = 1.2 is estimated by subtracting the projected jet noise level from the measured total noise. In order to assess the influence of core noise on tunnel-on noise, the following assumptions are made:

1. Tunnel-on core noise level equals tunnel-off core noise. This appears to be a reasonable assumption since engine operating conditions are nearly equal. It is noted that a Doppler amplification effect is expected for core noise in going from static-to-flight conditions. The magnitude is equal to 10 n log $(1 - M_\infty \cos \theta)$ where n may be as high as 4. For this example taken at low tunnel velocity and angles near 90°, the reduction in core noise due to the Doppler amplification effect is relatively small (less than 1 dB) and is not included in the analysis.

2. Tunnel-on jet noise follows the projected slope of figure 51. This may provide a jet noise level that is slightly low, since the higher power tunnel-on noise levels generally fall above the tunnel-off data fairing.

If these assumptions are valid, then the resulting tunnel-on noise level at NPR = 1.2 is reasonably well accounted for; i.e., the tunnel-on jet noise plus the unchanged static core noise add to approximately equal the measured tunnel-on level. Although this analysis is by no means exact, it is clear that a prominent core noise signal will restrict the flight noise reduction of a given engine.

7.0 CONCLUSIONS

The following conclusions are made as a result of the JT8D engine noise test in the NASA-ARC 40-by 80-Foot Wind Tunnel. The major objectives of the test were to:

- Establish the feasibility of wind tunnel tests for studying flight effects on engine noise
- Establish specific flight effects for the engine configured as a baseline and jet noise suppressor
- Compare the results with available 727/JT8D flight test data

The results and analysis show that the wind tunnel derived flight effects compare favorable with 727/JT8D flight test data for both the baseline and quiet nacelle configurations. Specific conclusions regarding analysis techniques and engine noise flight effects are summarized in the following paragraphs.

1. Comparisons of 40 x 80 and 727/JT8D flight test data for the baseline and quiet nacelle configurations show good agreement for OASPL and PNL at takeoff and cutback power. Model results obtained in the Boeing 9 x 9 wind tunnel for these configurations compare favorably with full-scale wind tunnel results.

2. Flight test and wind tunnel data comparisons indicate that a wind tunnel is a viable method for studying flight effects on engine noise. This flight simulation technique offers great potential for cost savings and development of quiet engine systems that are effectively designed for the flight environment.

3. Measurement of engine noise relatively near to the sources will provide a satisfactory assessment of far-field flight effects when the correlations established herein are applied.

4. For the baseline configuration, significant reduction of jet noise occurs with tunnel velocity over the test range of near-field angles (90^0 to 165^0) and equivalent far-field angles (80^0 to 155^0). The largest reduction of jet noise is experienced in the region of peak noise and angles near the jet axis, with progressively less reduction at lower angles. In terms of velocity index, the OASPL noise reduction follows a primary velocity to the 8th to 9th power at peak noise and to the 4th power at a far-field angle of 90^0.

5. For the baseline configuration, interpolation of static data at flight primary relative velocity will provide a reasonably good estimate of flight OASPL and PNL in the region of peak noise and higher angles (above 120^0), but will underpredict low angle flight noise (below 120^0). The use of wind tunnel derived velocity index curves is the favored method of estimating flight OASPL or PNL for the baseline nozzle.

6. For the 20-lobe ejector/suppressor configuration, the peak (120°) and low angle OASPL and PNL are dominated by premerged mixing noise and undergo relatively small reductions due to flight. The OASPL and PNL at angles near the jet axis are more dominated by postmerged mixing noise and experience a significant reduction due to flight.

7. Extrapolation of absolute noise levels is recommended for predicting the flight noise level of the 20-lobe and similar suppressor types where wind tunnel data are available. Flight noise levels can best be predicted by correcting static noise spectra in accordance with noise-generating mechanisms where wind tunnel data are not available.

8. The wind tunnel tests show that the 20-lobe ejector/suppressor experiences a loss of suppression due to flight. At takeoff power the flight OASPL peak noise suppression is lower by 5 dB, while PNL peak noise suppression is reduced by 4 PNdB. At cutback power the suppression losses are 4 dB and 2 PNdB, respectively.

9. The flight noise reduction of the internal mixer is greater than that of the baseline configuration. The increased noise reduction is experienced by the low-to-moderate frequencies and is caused by the reduced primary jet velocity of the mixed jet.

10. Interpolation of static data at flight mixed primary relative velocity will provide a good estimate of internal mixer flight OASPL. This technique will closely approximate peak (130°) and high angle PNL but slightly underpredict low angle PNL. Flight noise may also be estimated by use of velocity index curves that are provided.

11. At takeoff power, the peak OASPL suppression of the internal mixer increases in flight by 2.5 dB while peak PNL suppression increases by 0.5 PNdB.

12. The presence of acoustic lining downstream of the mixer elements has little or no influence on the internal mixer flight effects.

13. External vortex generators are not effective in reducing the flight mixing noise of the internal mixer configuration.

14. At approach power, the first stage fan tone power levels are reduced by tunnel velocity. The average reductions relative to static operation are 8 dB for the fan blade passage tone, 3 dB for the second harmonic, and 1.5 dB for the third harmonic. The fan tone reductions are attributed to the inlet turbulence/rotor source mechanism. Analytical predictions show that the static-to-flight change in inlet turbulence can account for the observed reduction in first stage fundamental fan tone power level.

15. Core noise for the JT8D-17 engine is significant only at very low power settings (NPR = 1.2) and is not an important noise source for normal aircraft operations. At the pressure ratio 1.2 power condition, the presence of core noise restricts the amount of engine noise reduction due to forward velocity.

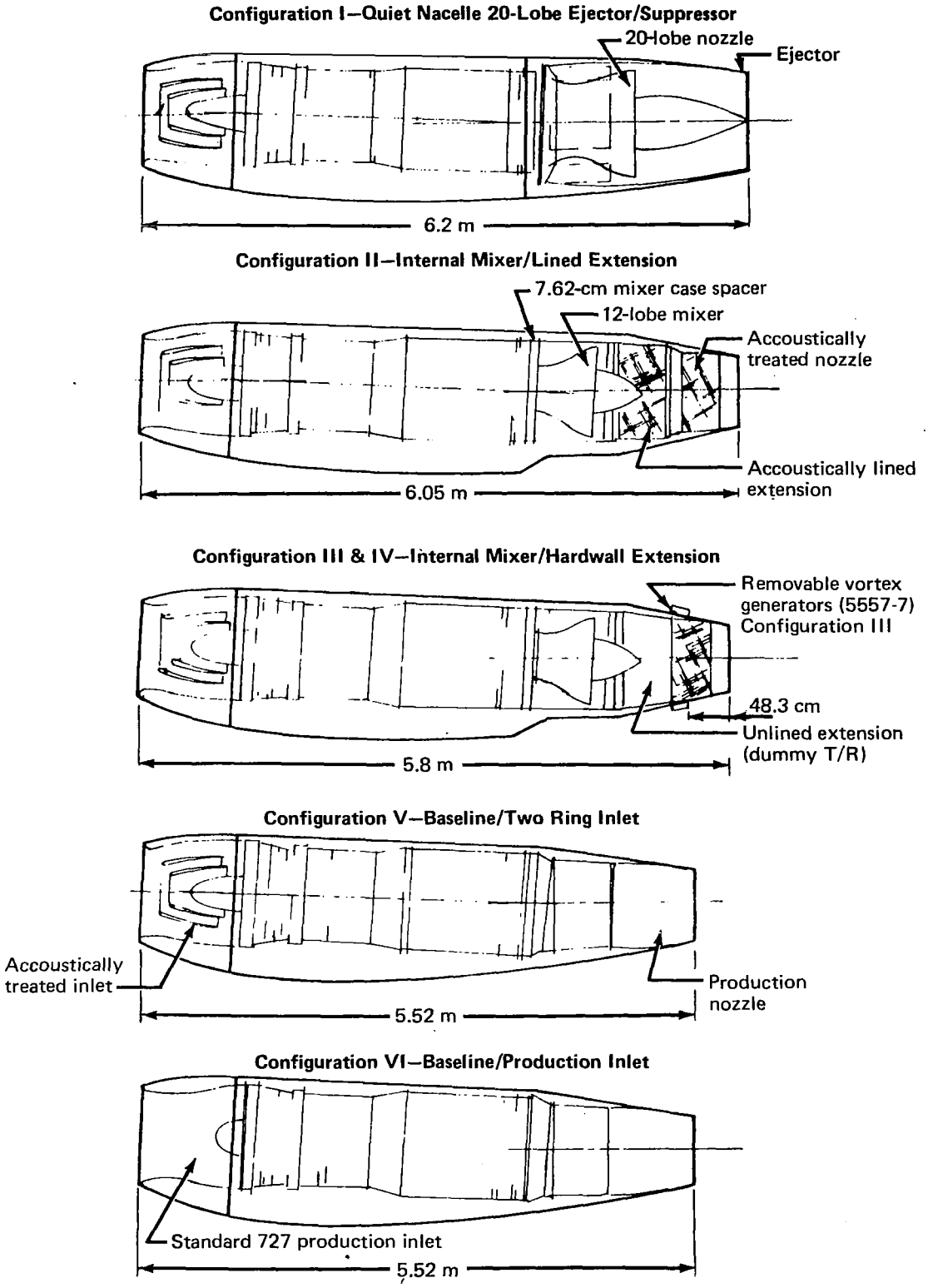

Figure 1.—Schematics of Test Configurations

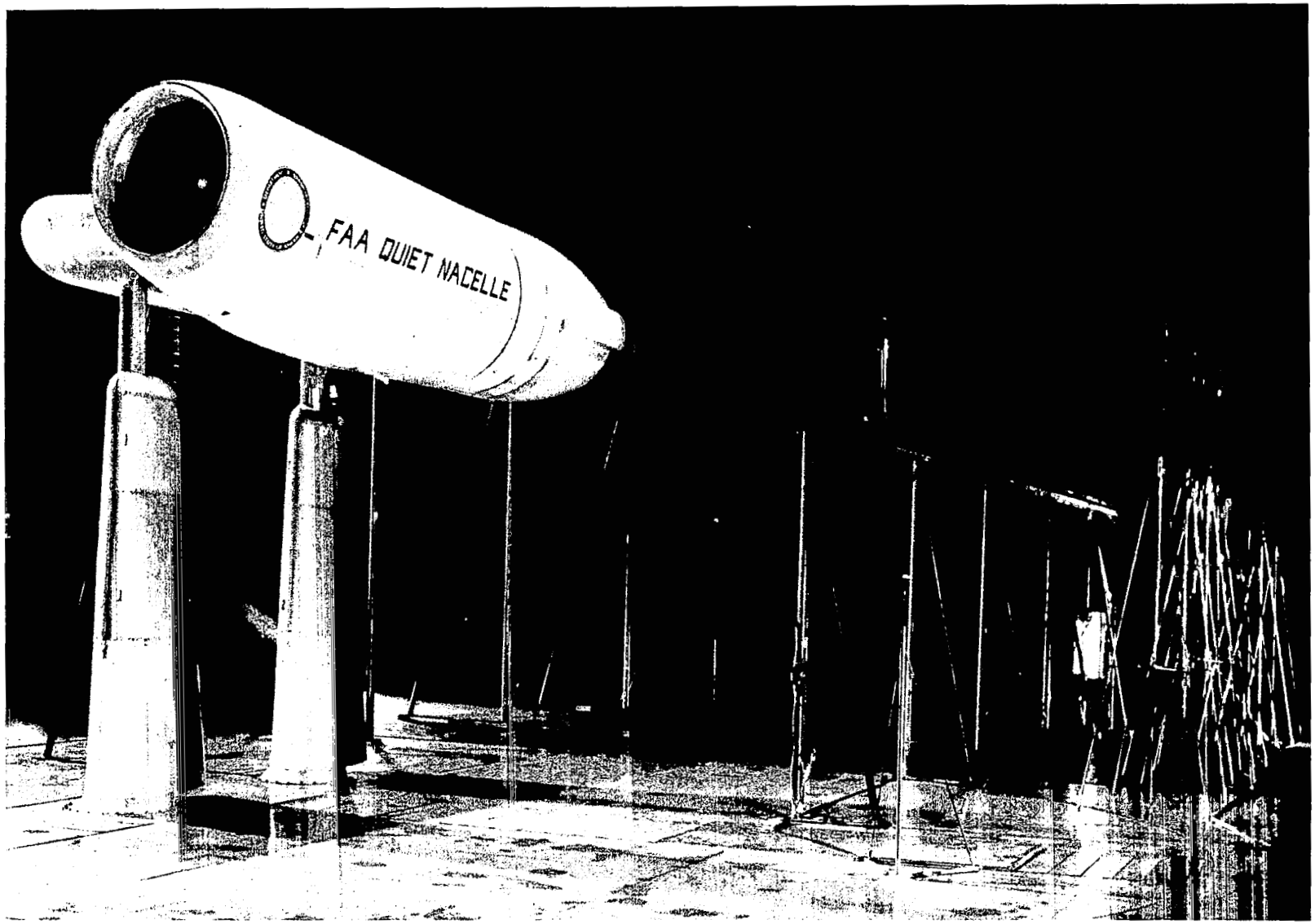

Figure 2.—Configuration I, Quiet Nacelle 20-Lobe Ejector/Suppressor, Front View

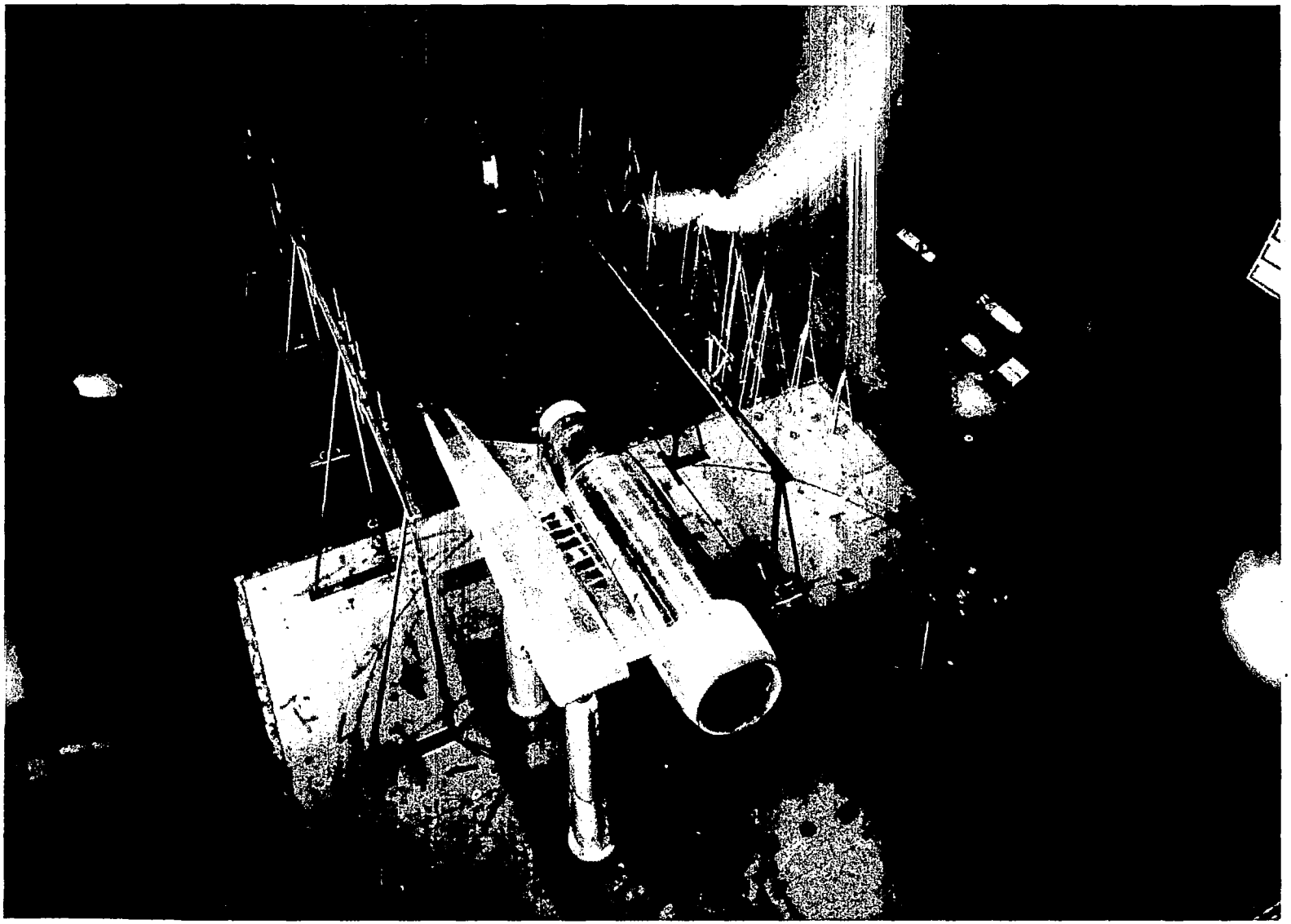

Figure 3.—Test Installation, JT8D-17 in NASA-ARC 40 x 80 Wind Tunnel

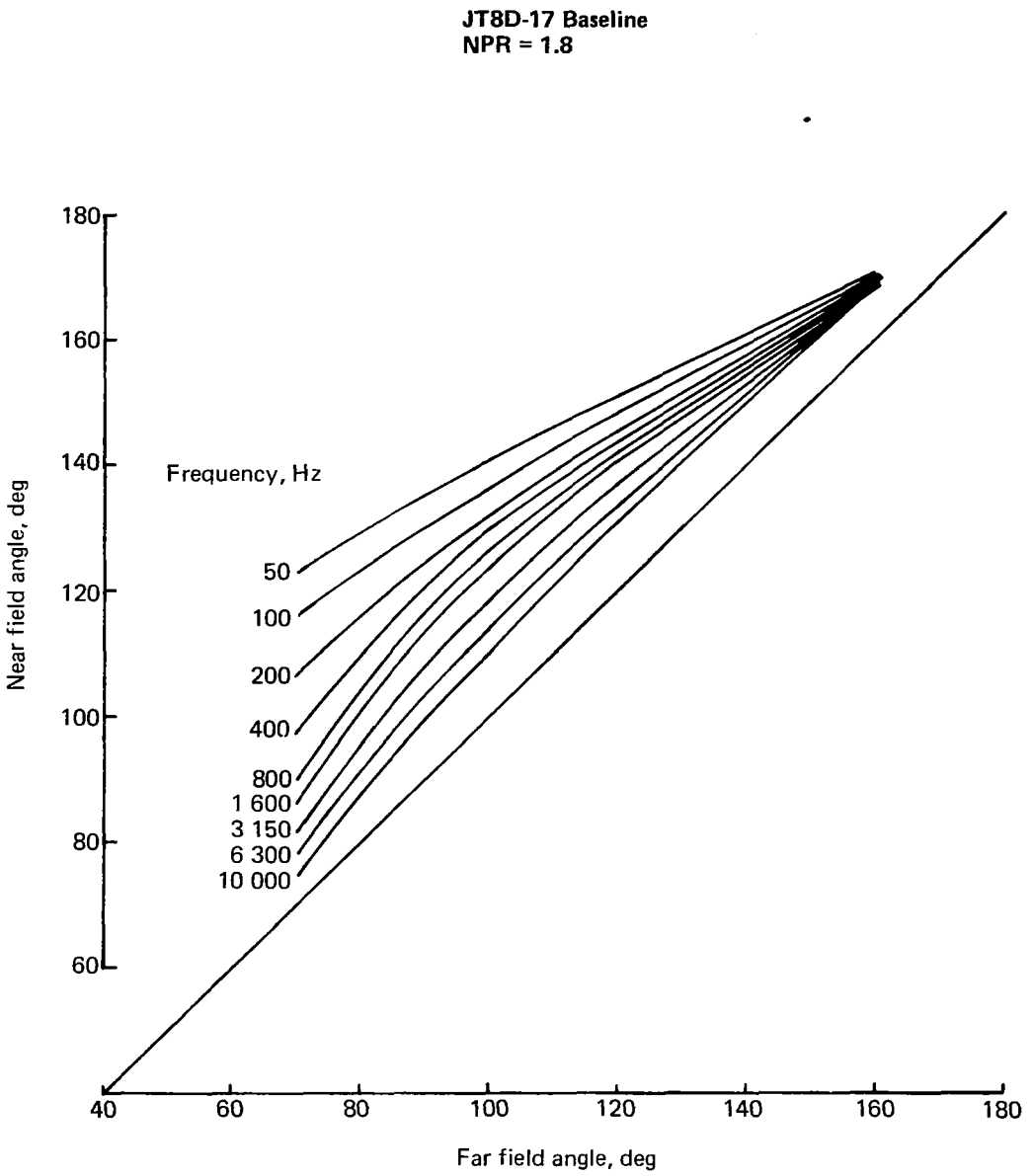

Figure 4.—Near/Far Field Correlation Frequencies

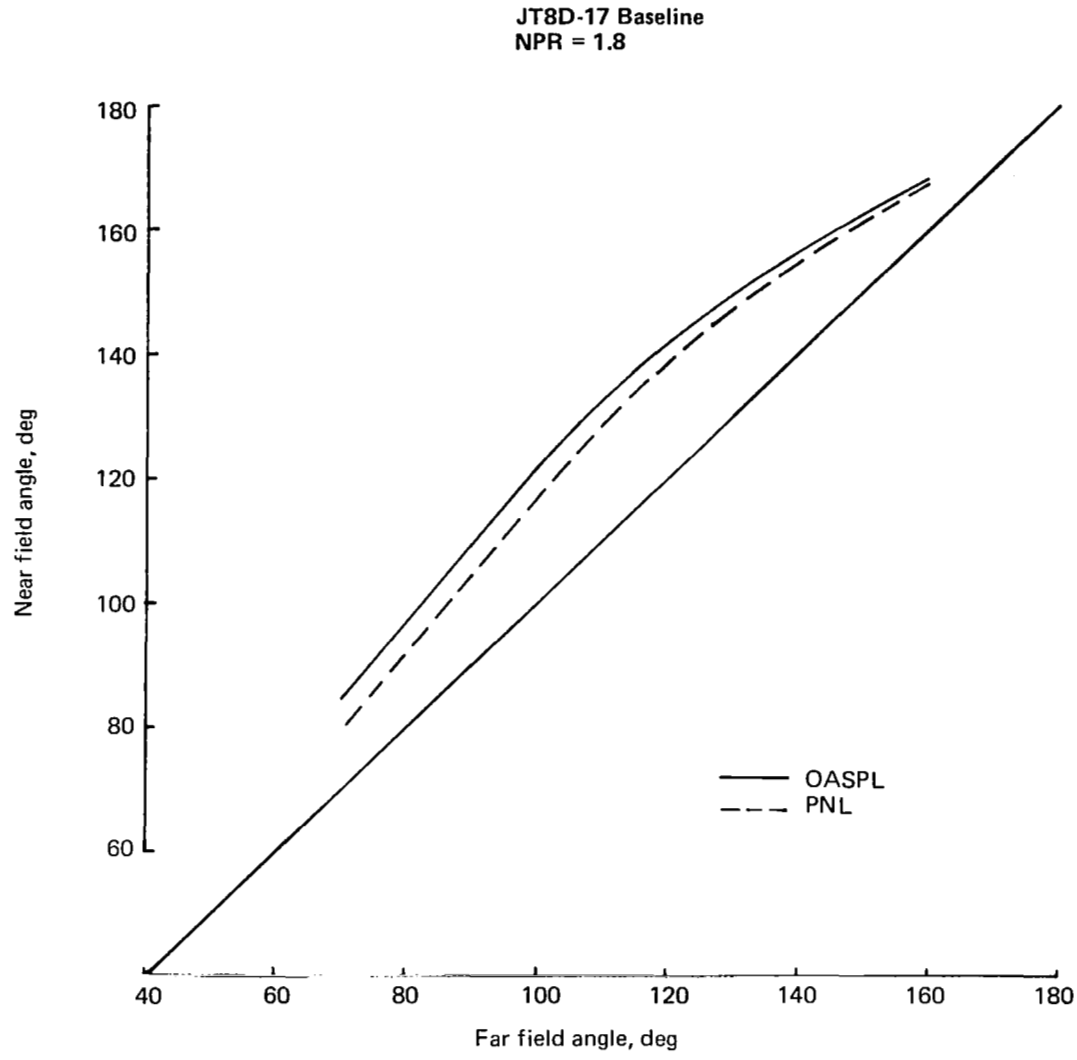

Figure 5.—Near/Far Field Correlation OASPL and PNL

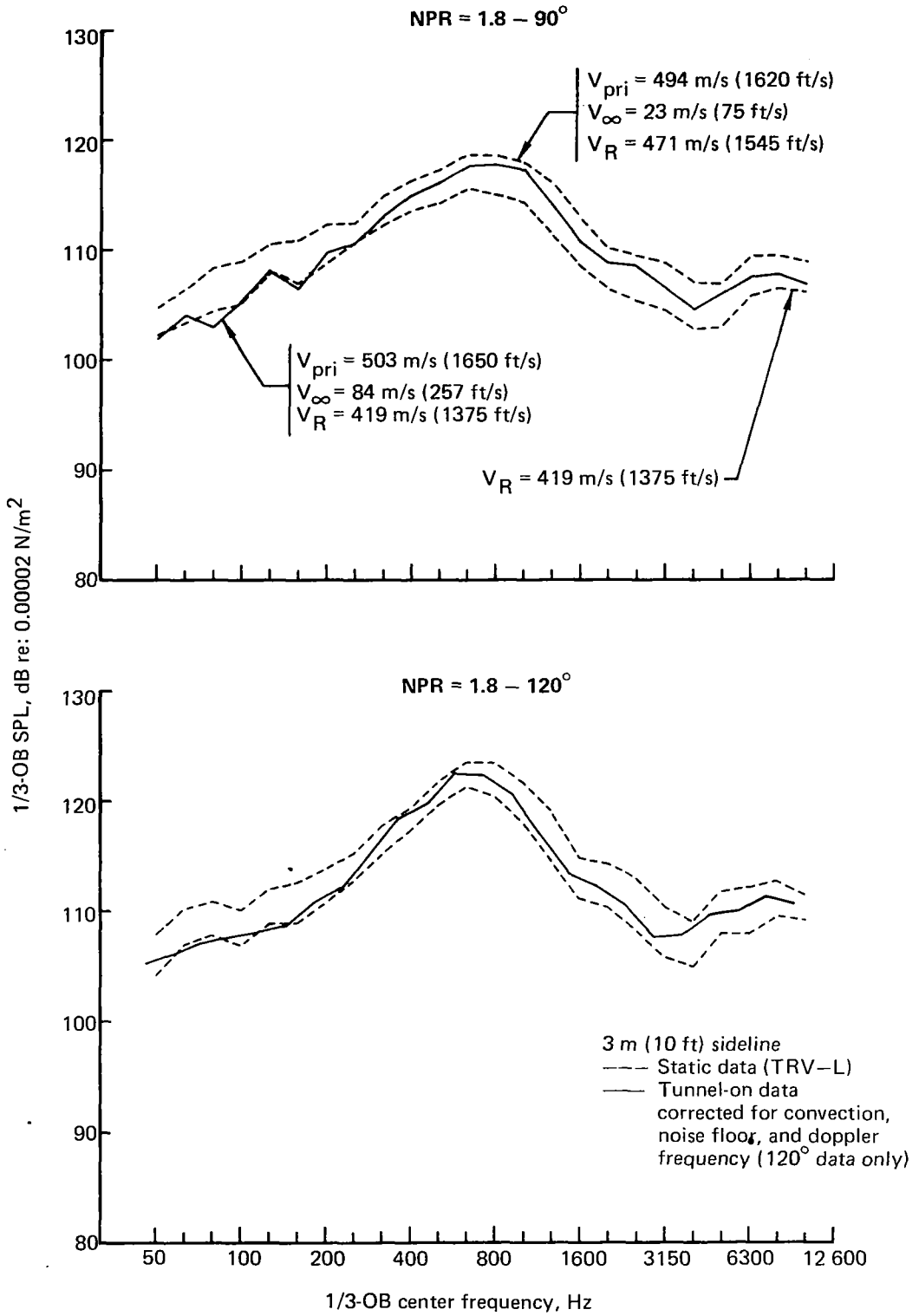

Figure 6.—NASA Ames 40 x 80 Wind Tunnel Test JT8D-17 Engine With 20-Lobe Ejector/ Suppressor—Static/Flight Spectra Comparison

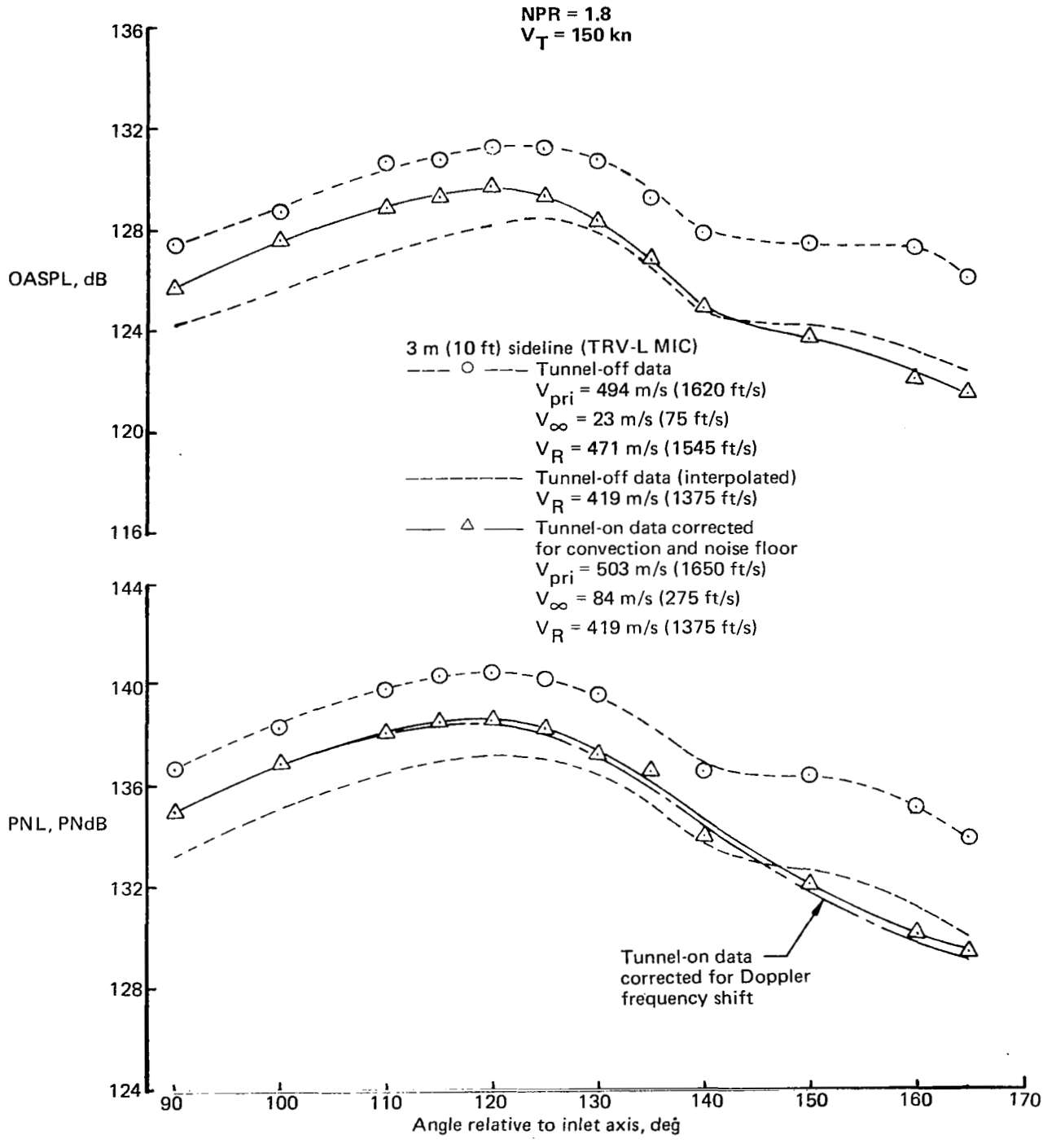

Figure 7.—NASA Ames 40 x 80 Wind Tunnel Test JT8D-17 Engine With 20-Lobe Ejector/ Suppressor—Static/Flight OASPL and PNL Directivity Comparison

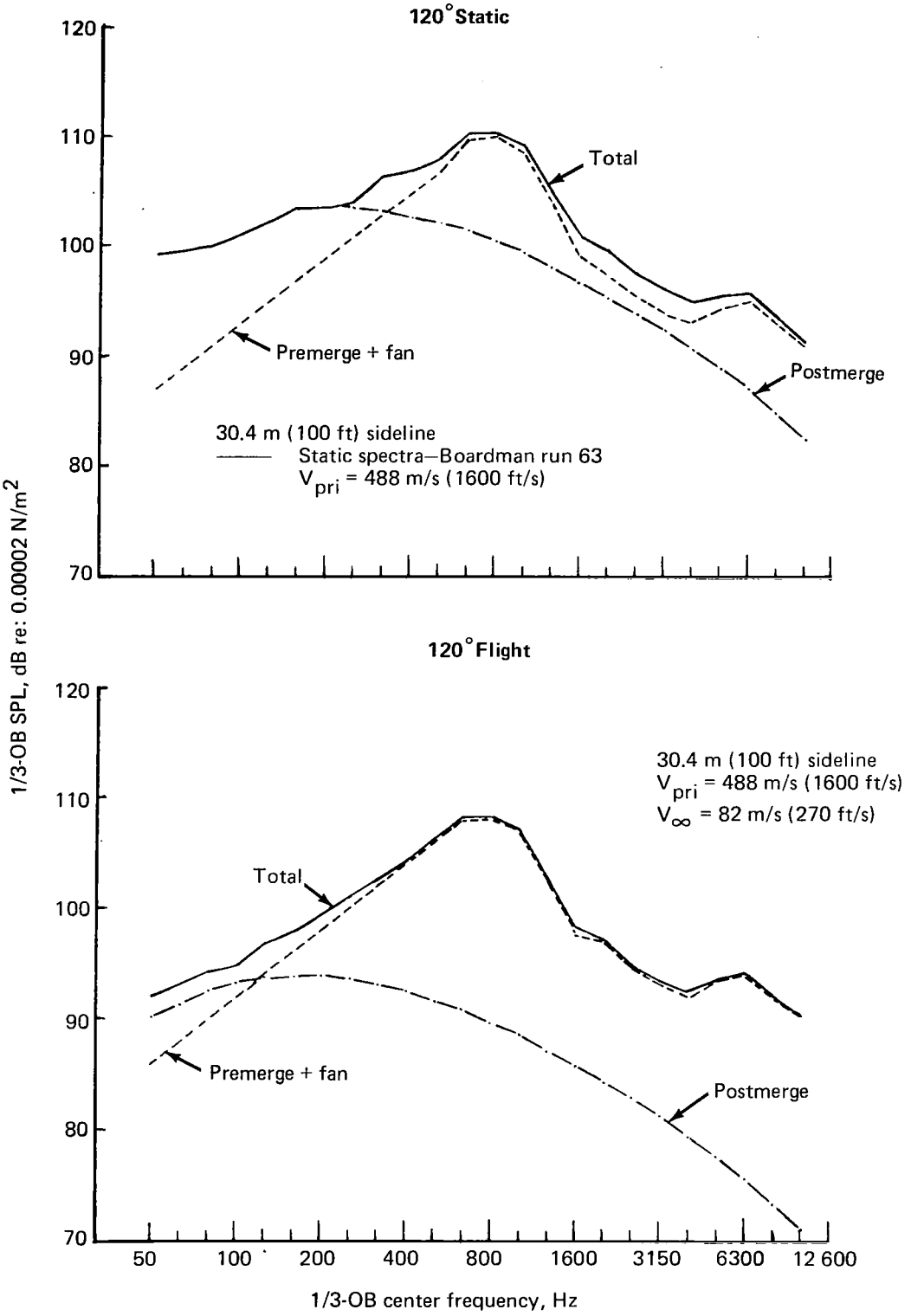

Figure 8.— NASA Ames 40 x 80 Wind Tunnel Test JT8D Engine With 20-Lobe Ejector/ Suppressor—Flight Spectra Estimate Using 40 x 80 Flight Effects

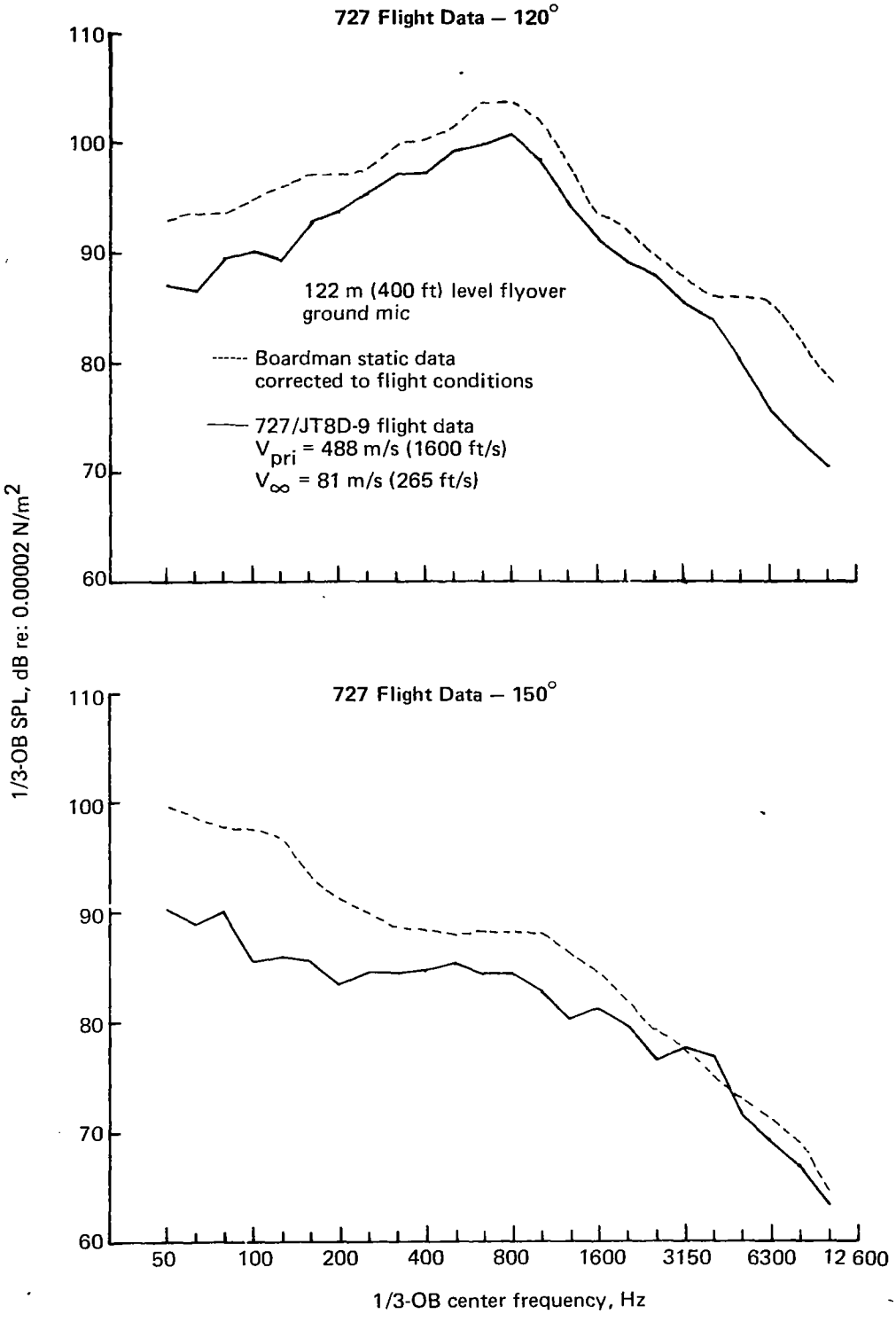

Figure 9.—NASA Ames 40 x 80 Wind Tunnel Test 727/JT8D-9 With 20-Lobe Ejector/ Suppressor—Static/Flight Spectra Comparison

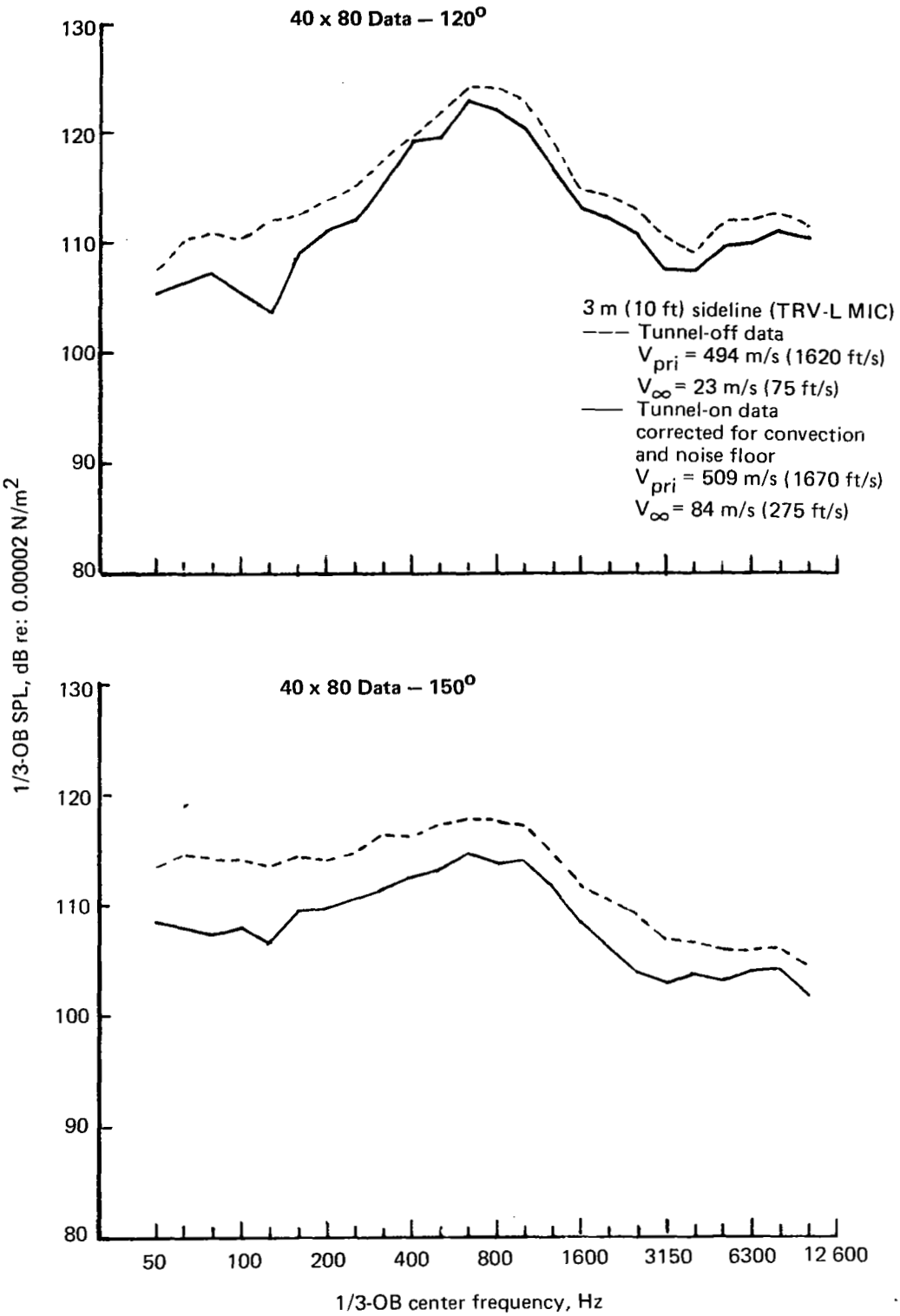

Figure 10.—NASA Ames 40 x 80 Wind Tunnel Test JT8D-17 Engine With 20-Lobe Ejector/ Suppressor—Measured Static/Flight Spectra Comparison

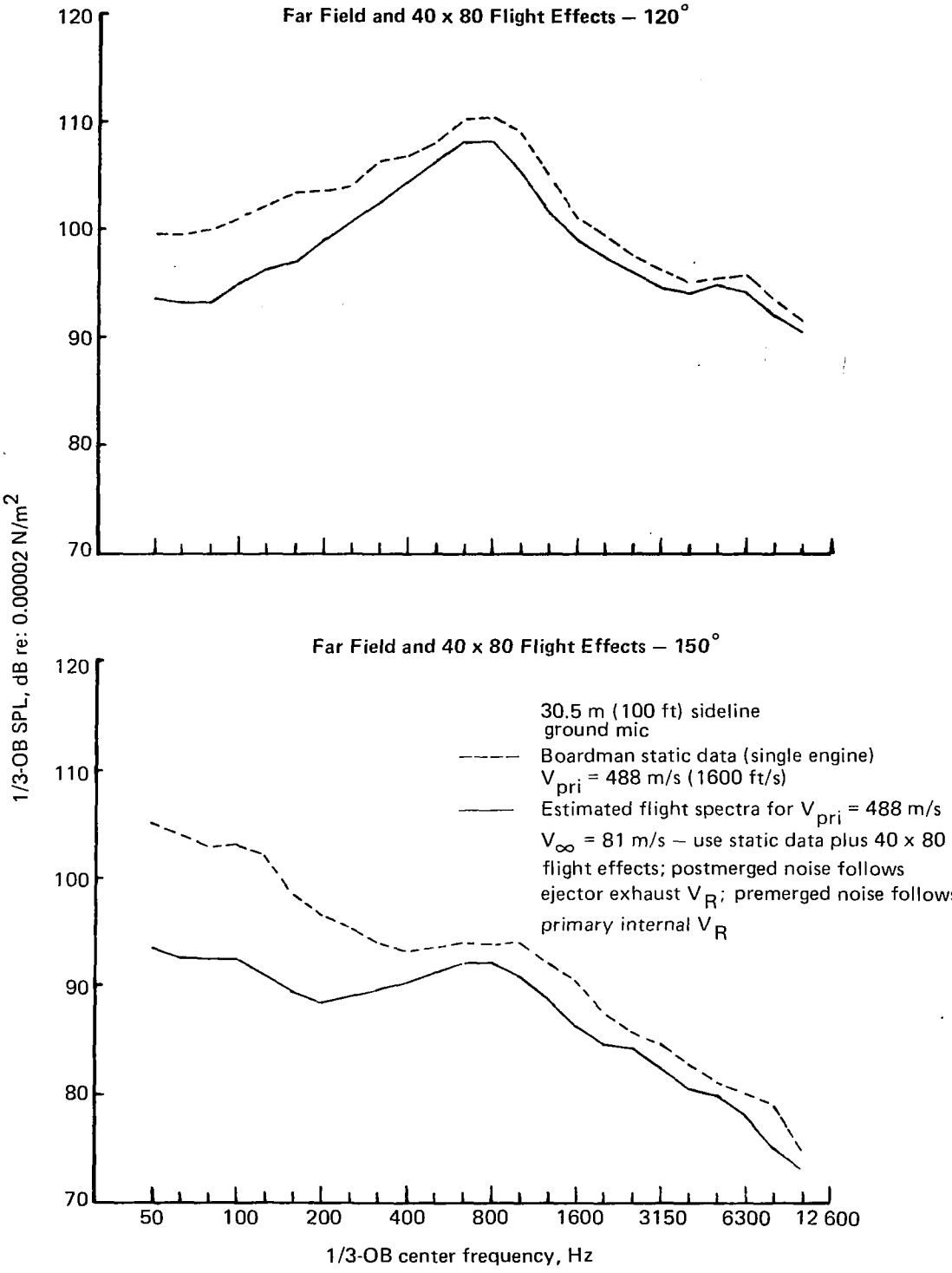

Figure 11.– NASA Ames 40 x 80 Wind Tunnel Test 20-Lobe Ejector/Suppressor–Static/ Flight Spectra–Far Field Data

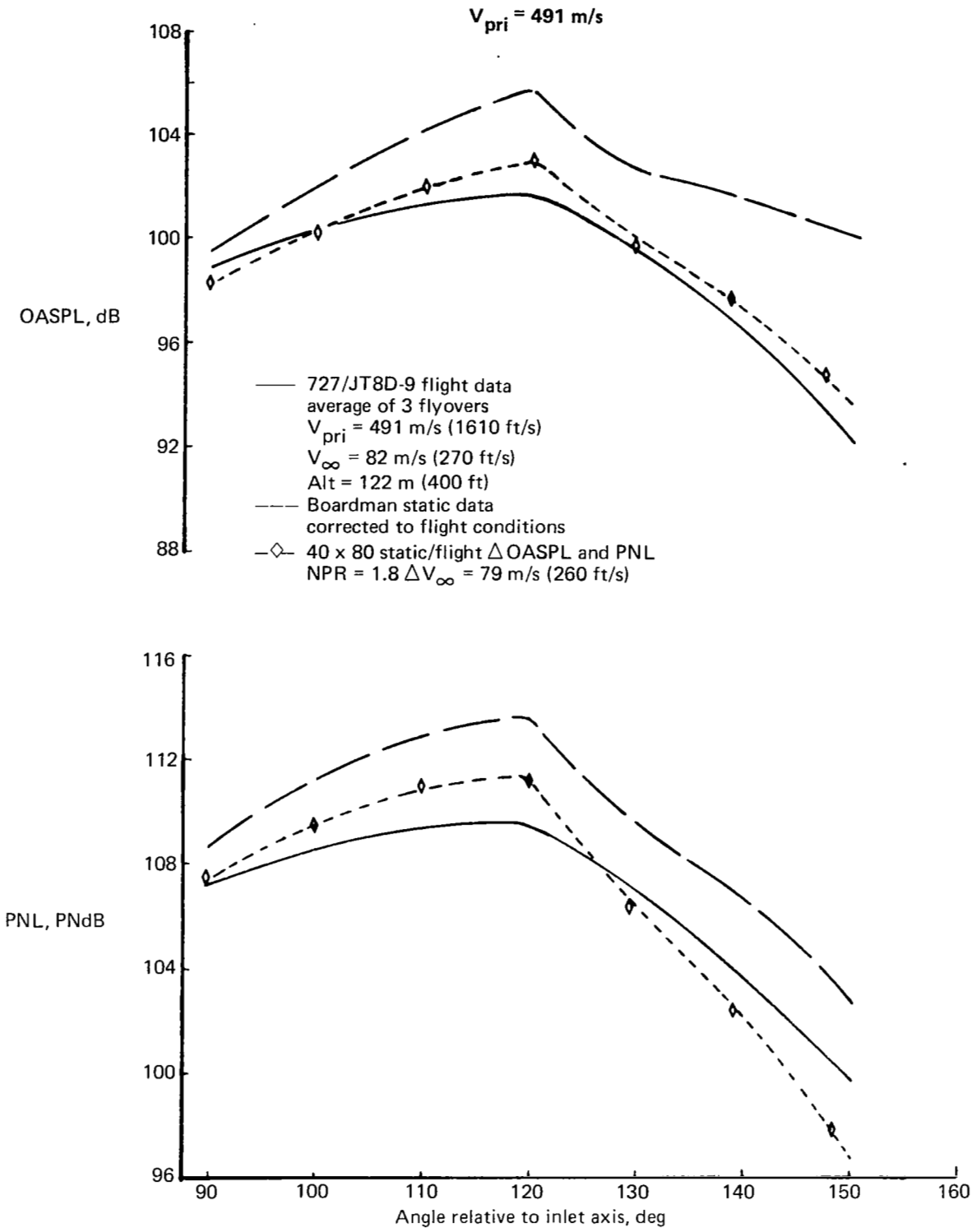

Figure 12.— NASA Ames 40 x 80 Wind Tunnel Test JT8D Engine With 20-Lobe Ejector/ Suppressor—Static/Flight OASPL and PNL Directivity—40 x 80 Versus 727 Flight Data

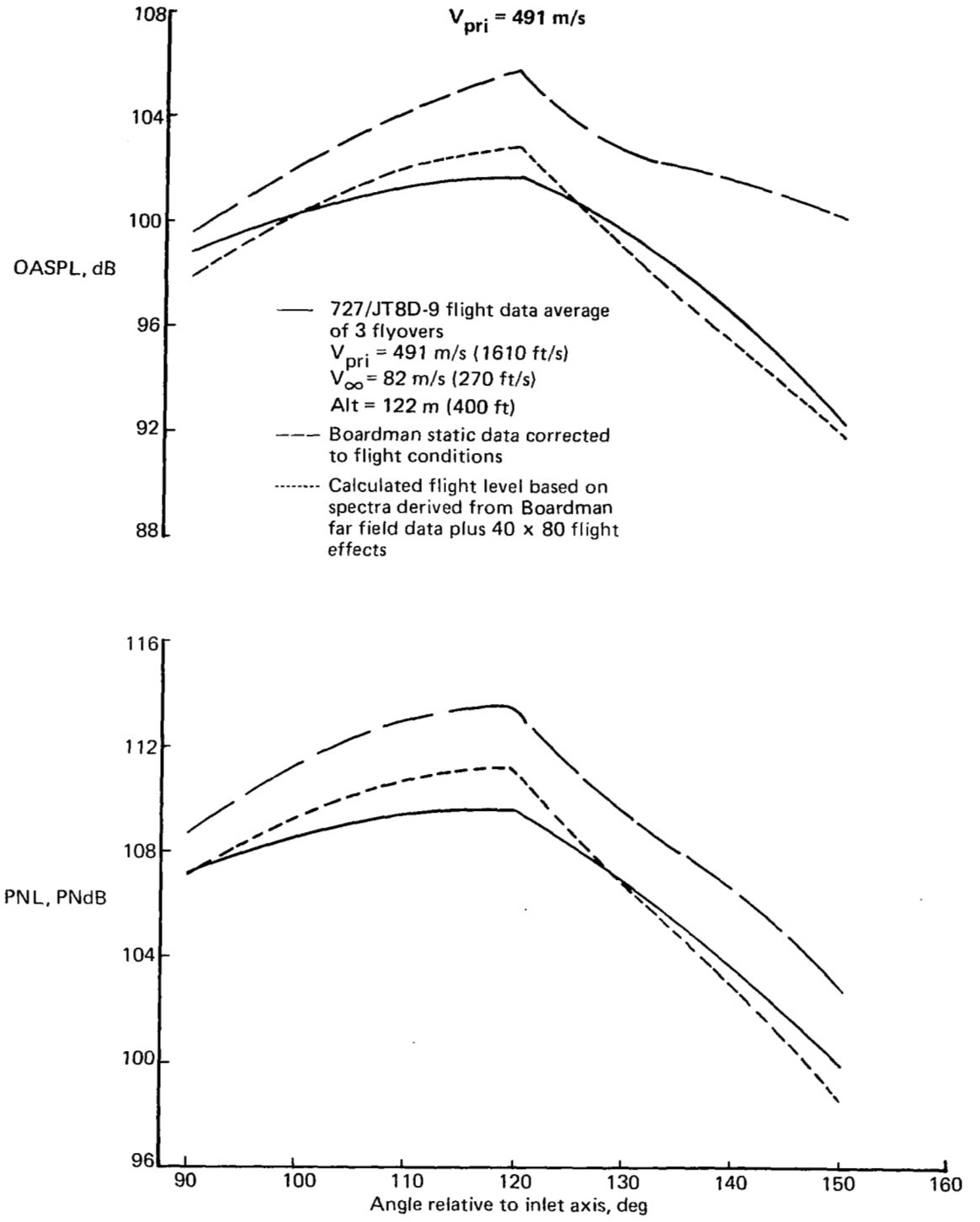

Figure 13.—NASA Ames 40 x 80 Wind Tunnel Test JT8D Engine With 20-Lobe Ejector/ Suppressor—Static/Flight OASPL and PNL Directivity—40 x 80 Versus 727 Flight Data

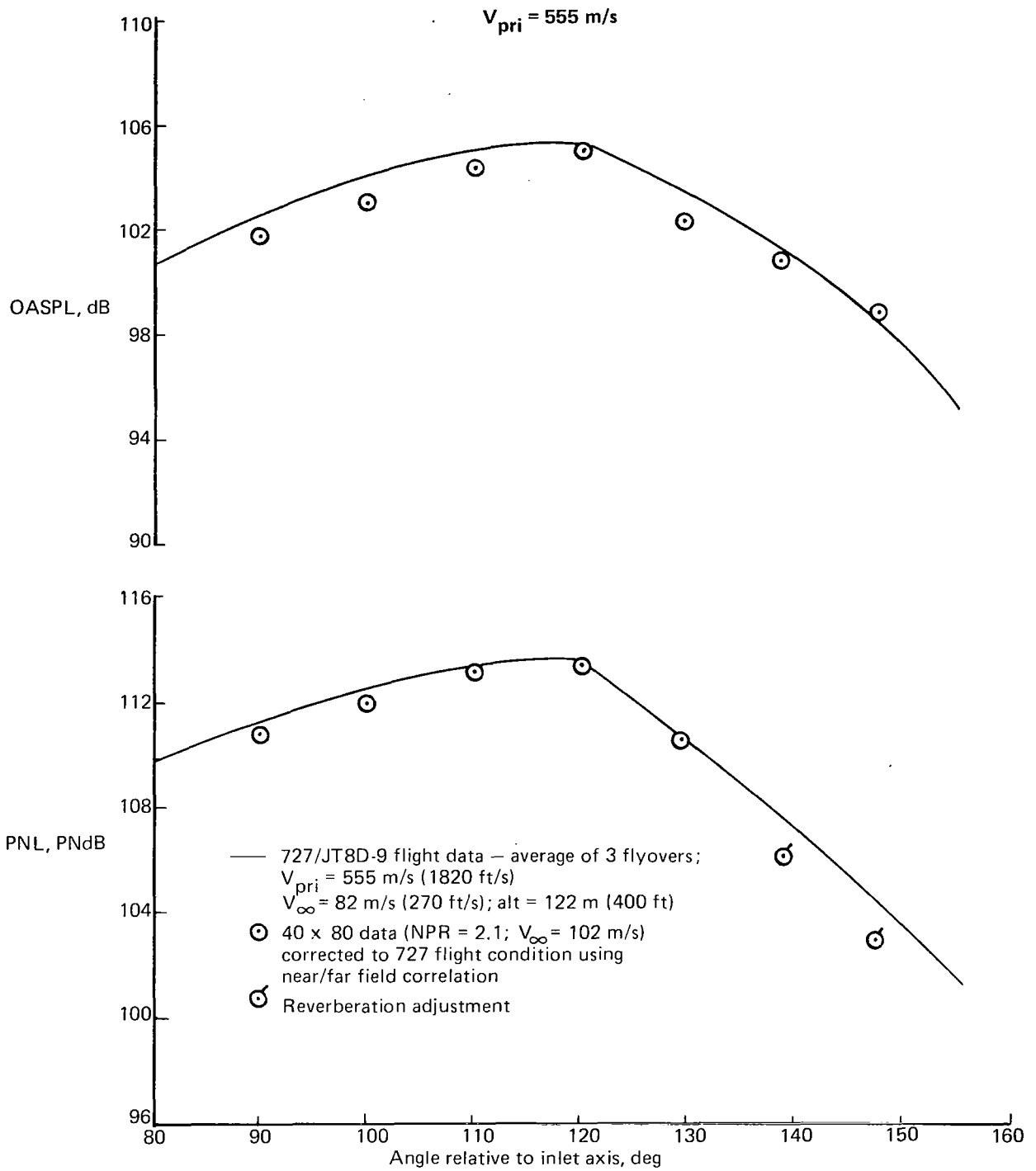

Figure 14.—NASA Ames 40 x 80 Wind Tunnel Test JT8D Engine With 20-Lobe Ejector/ Suppressor—Flight OASPL and PNL Directivity—40 x 80 Versus 727 Flight Data

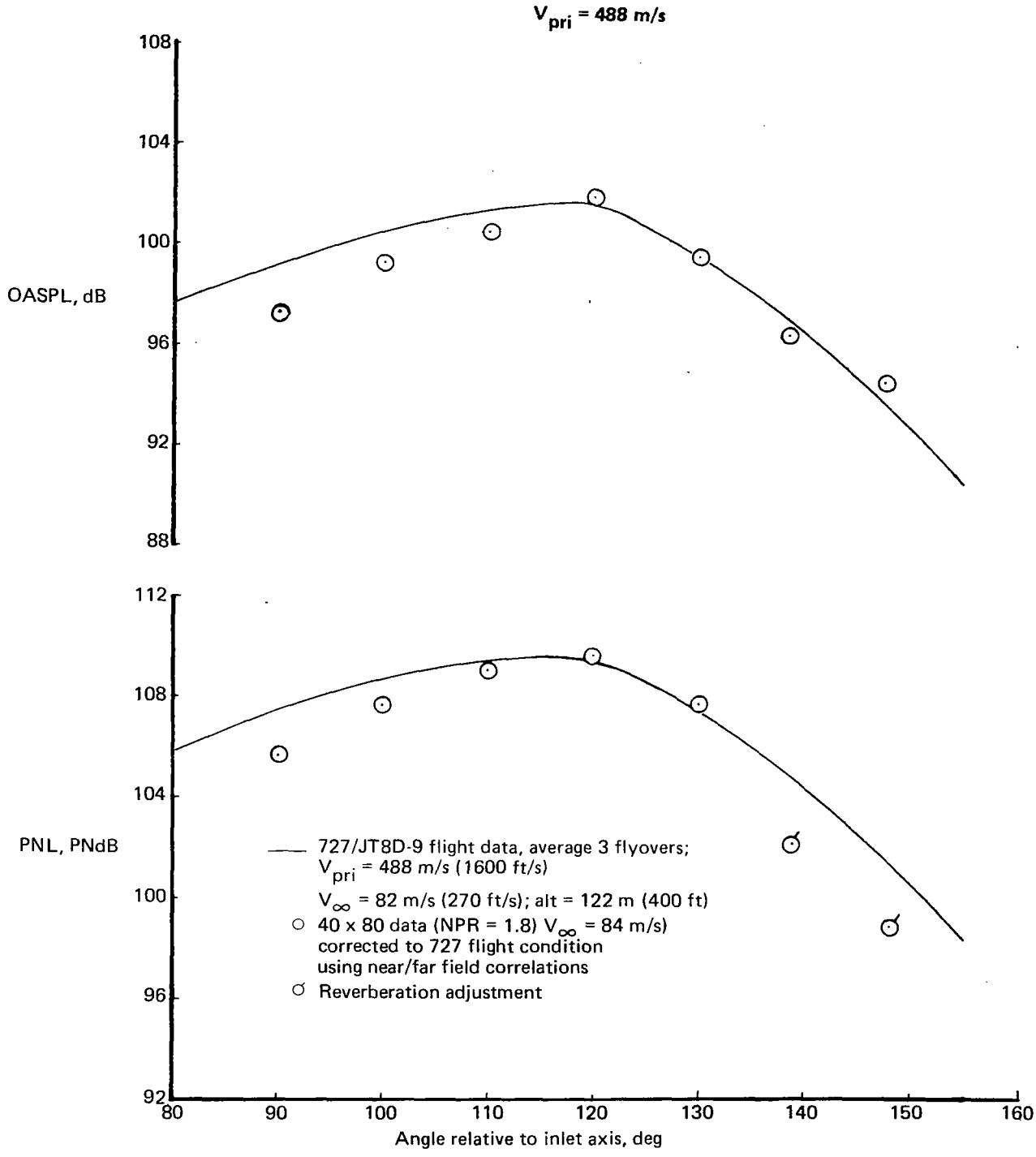

Figure 15.—NASA Ames 40 x 80 Wind Tunnel Test JT8D Engine With 20-Lobe Ejector/ Suppressor—Flight OASPL and PNL Directivity—40 x 80 Versus 727 Flight Data

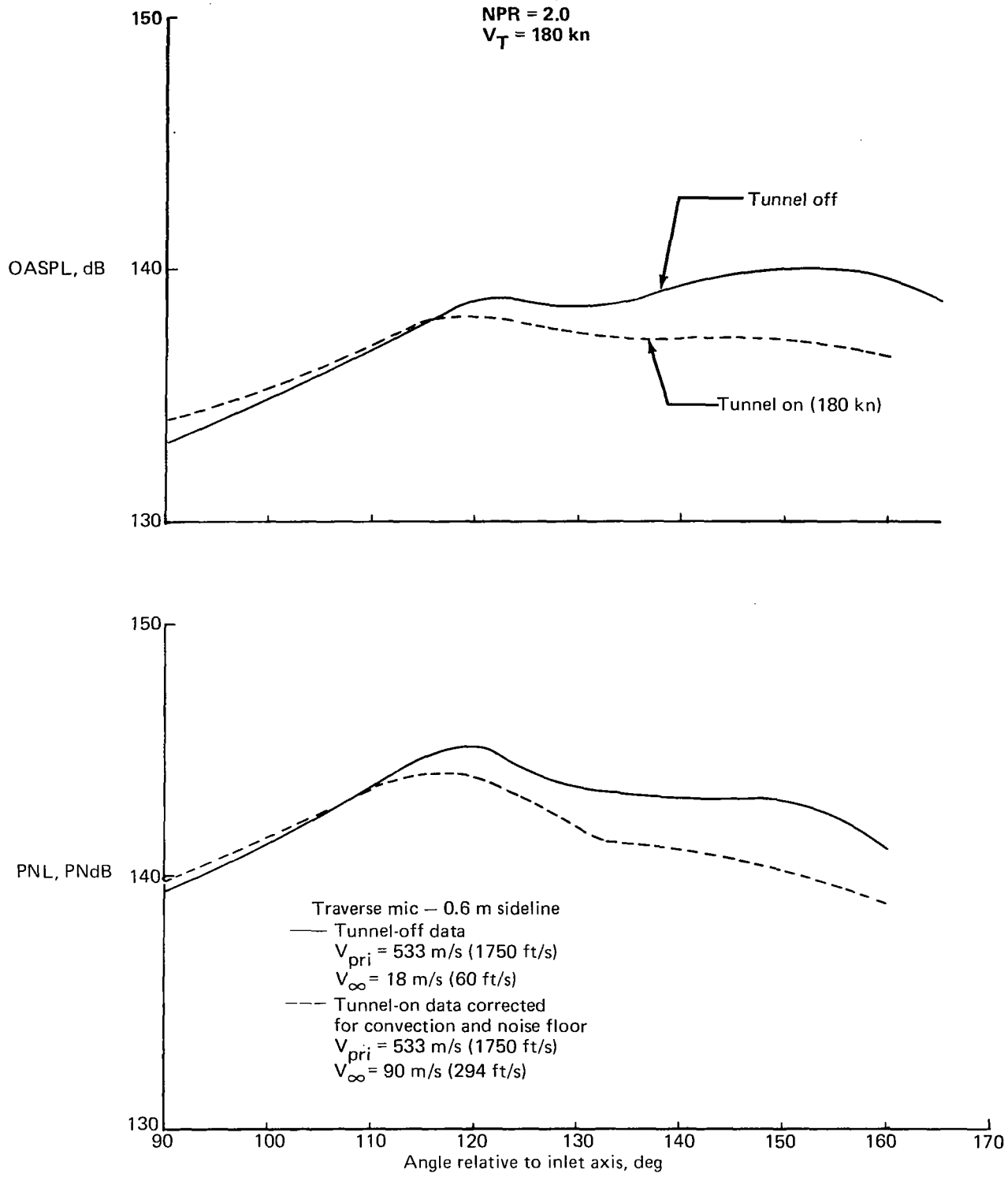

Figure 16.—Boeing 9 x 9 Wind Tunnel Test 20-Lobe Ejector/Suppressor-Lined Shroud—Static/Flight OASPL and PNL Directivity Comparison

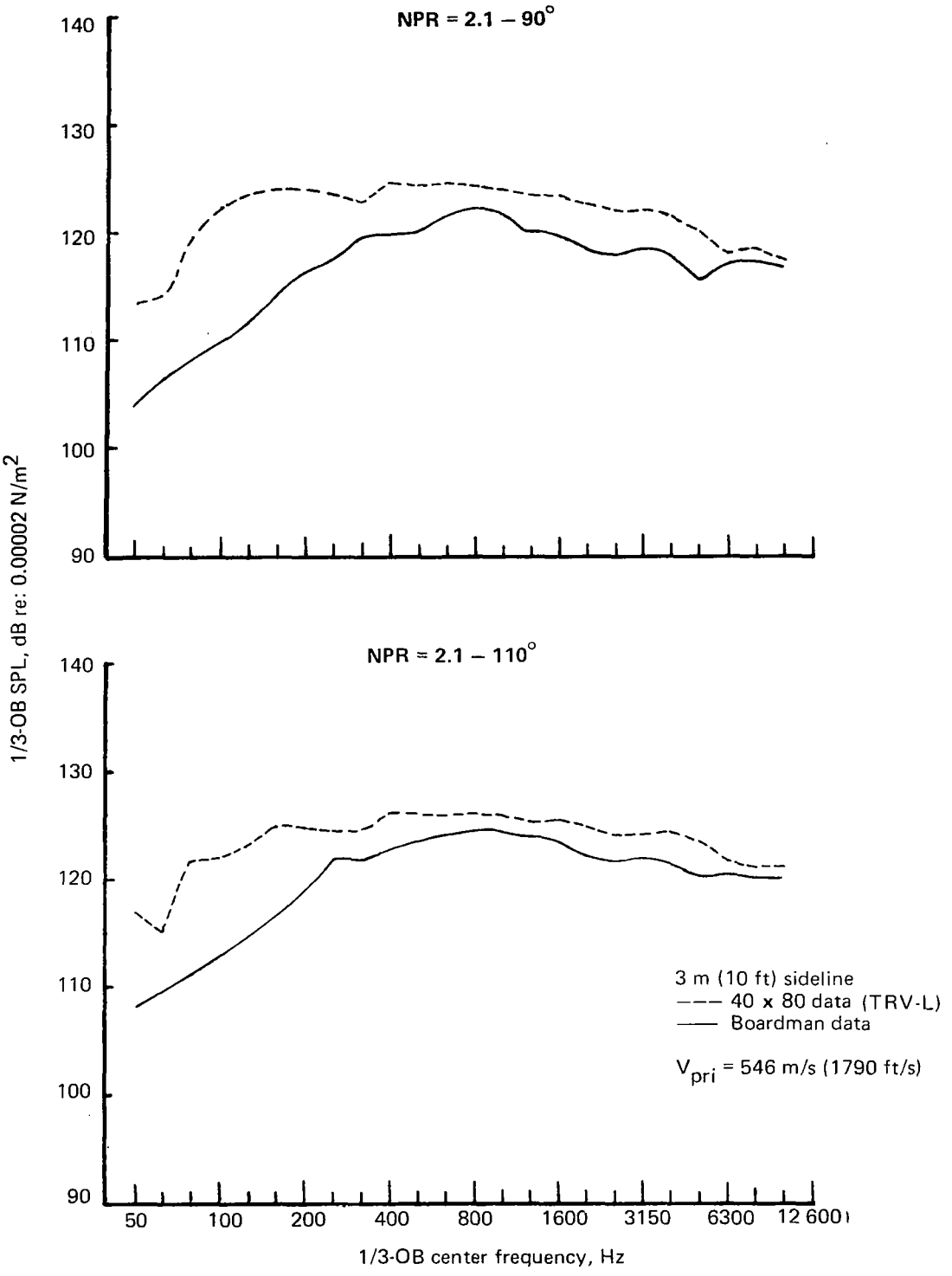

Figure 17.—NASA Ames 40 x 80 Wind Tunnel Test JT8D-17 Engine With Baseline Round Convergent Nozzle—Wind Tunnel and "Free Field" Spectra Comparison

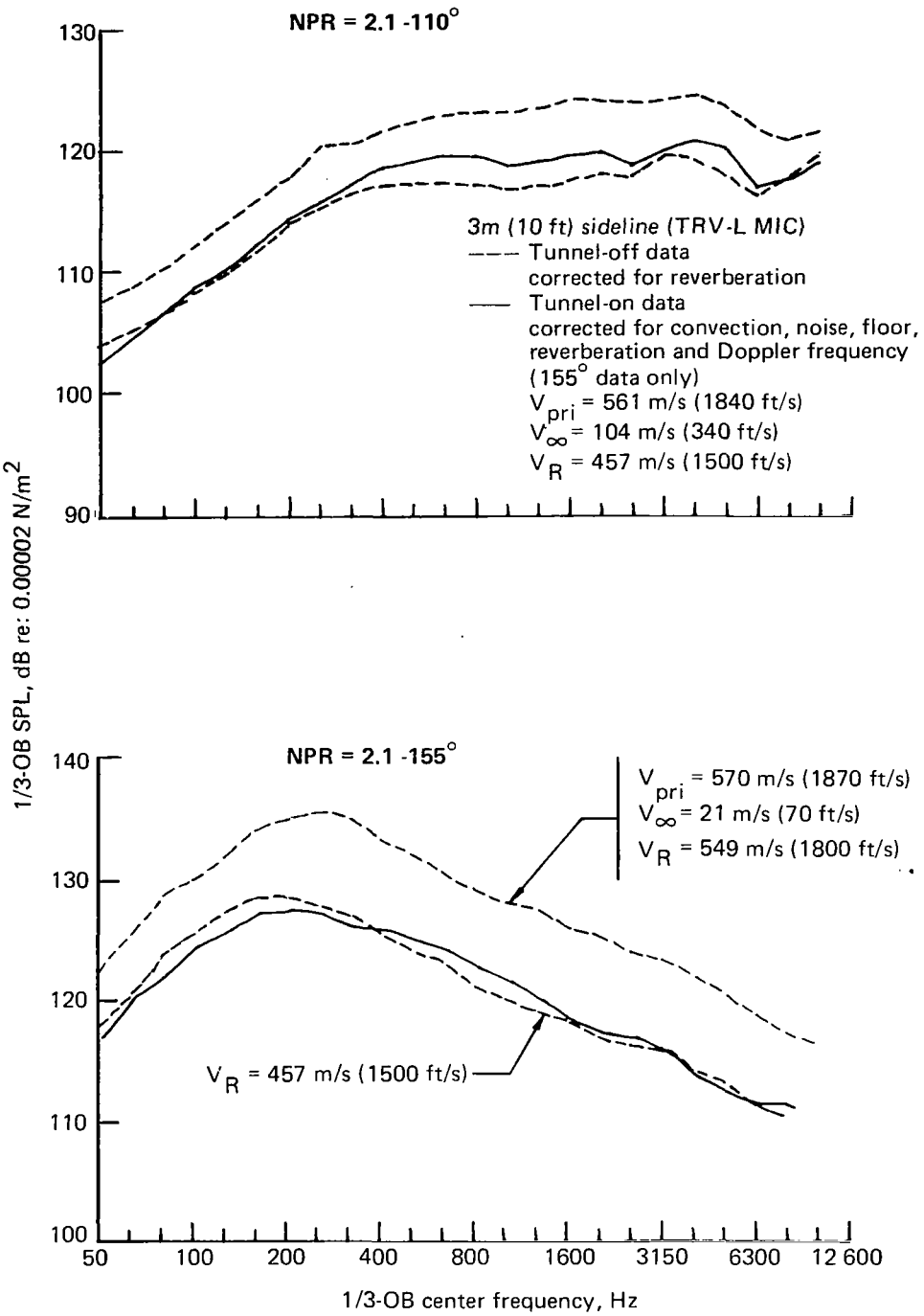

Figure 18.— NASA Ames 40 x 80 Wind Tunnel Test JT8D-17 Engine With Baseline Nozzle Static/Flight Spectra With Doppler

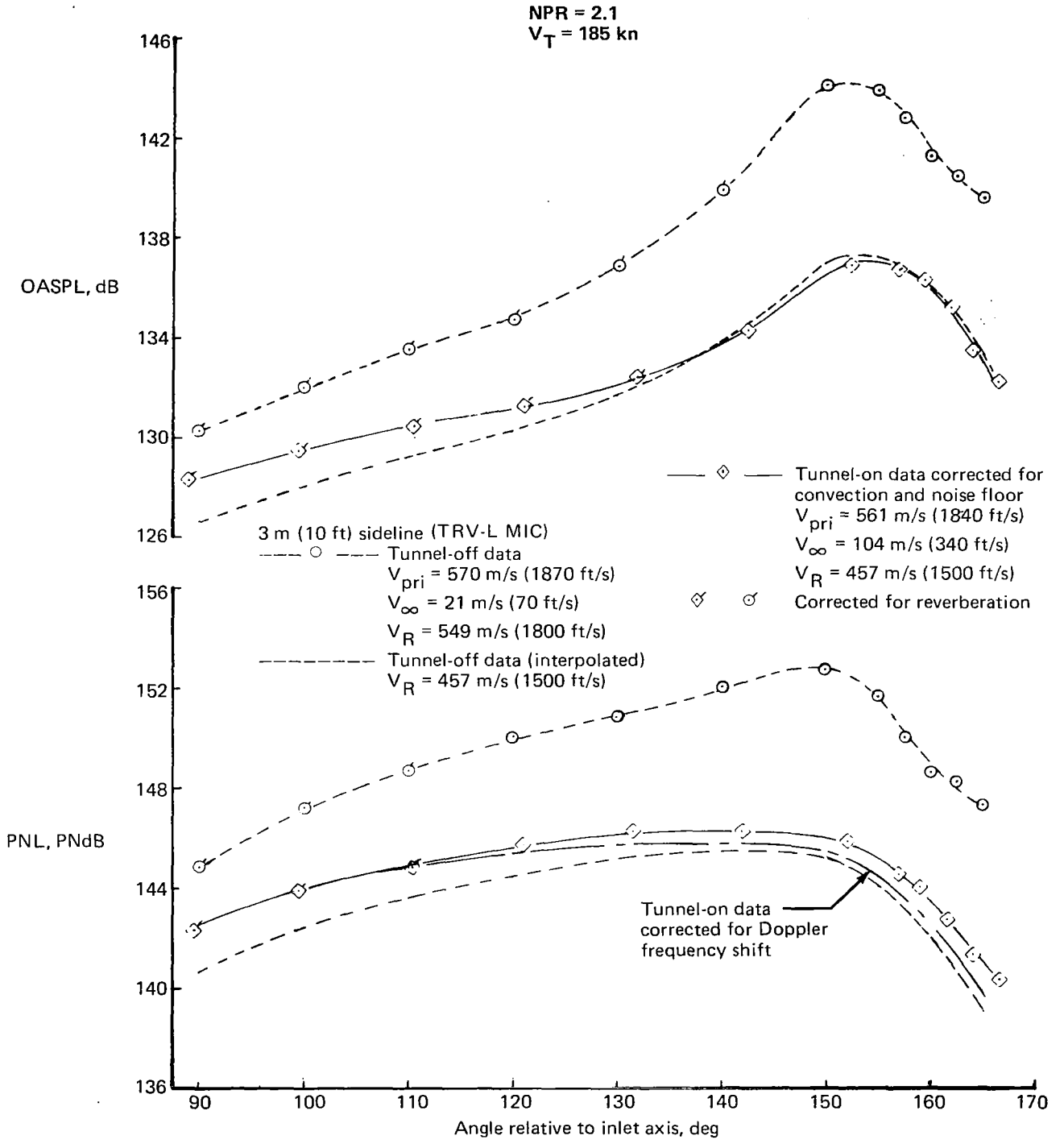

Figure 19.—NASA Ames 40 x 80 Wind Tunnel Test JT8D-17 Engine With Baseline Nozzle Static/Flight OASPL and PNL Directivity Comparison

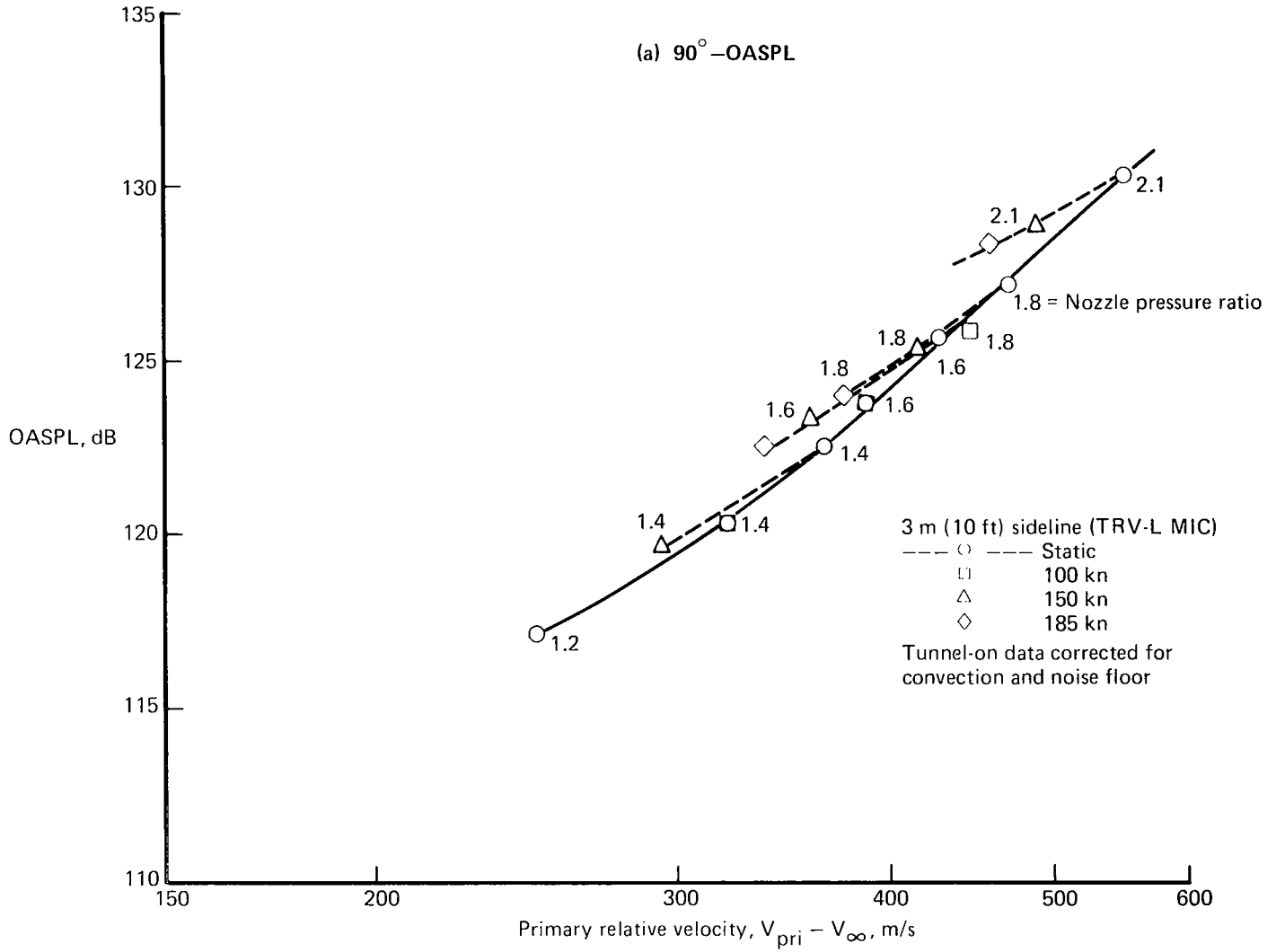

Figure 20.—NASA Ames 40 x 80 Wind Tunnel Test JT8D-17 Engine With Baseline Nozzle—OASPL Relative Velocity Correlation

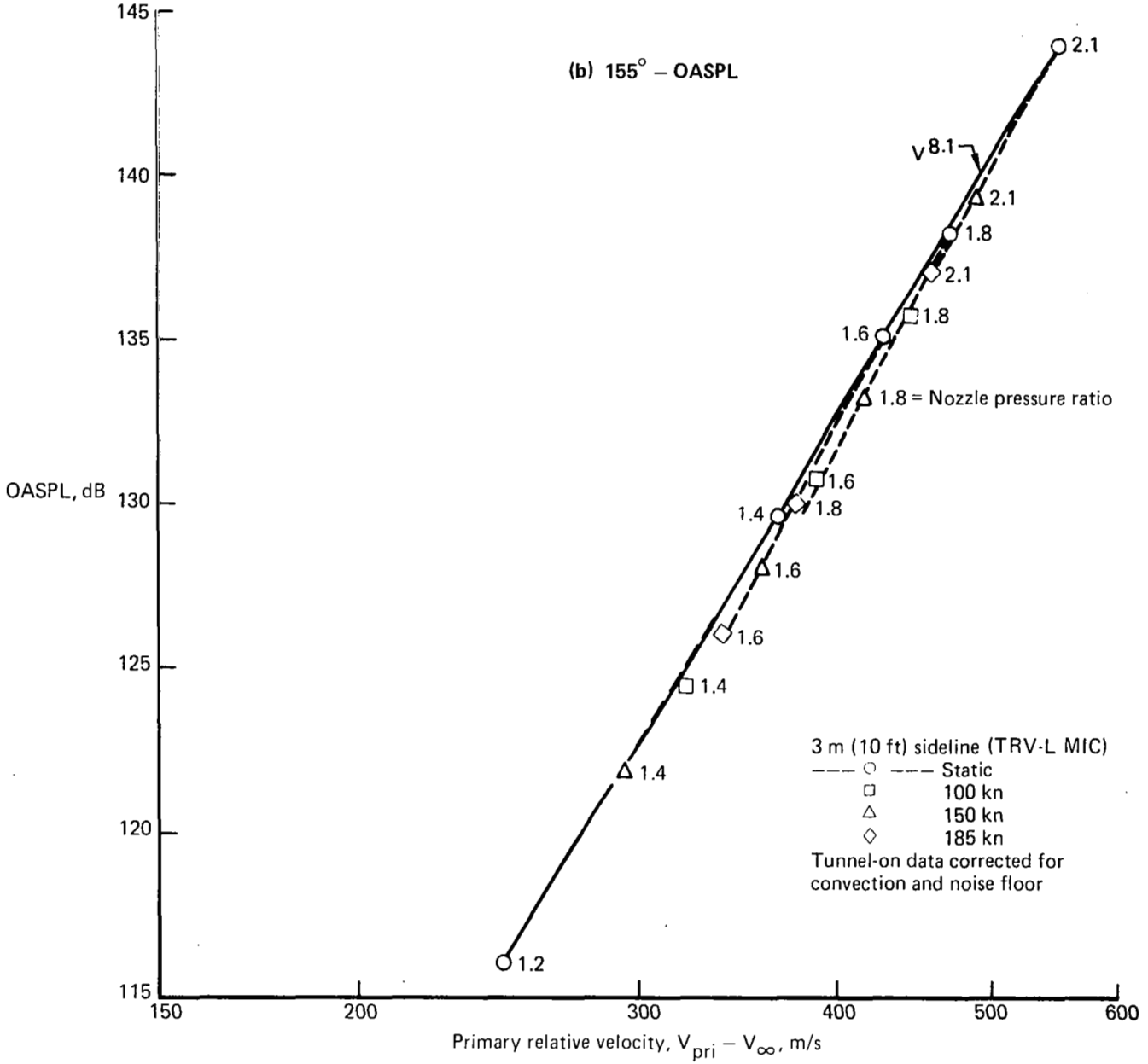

Figure 20.—(Concluded)

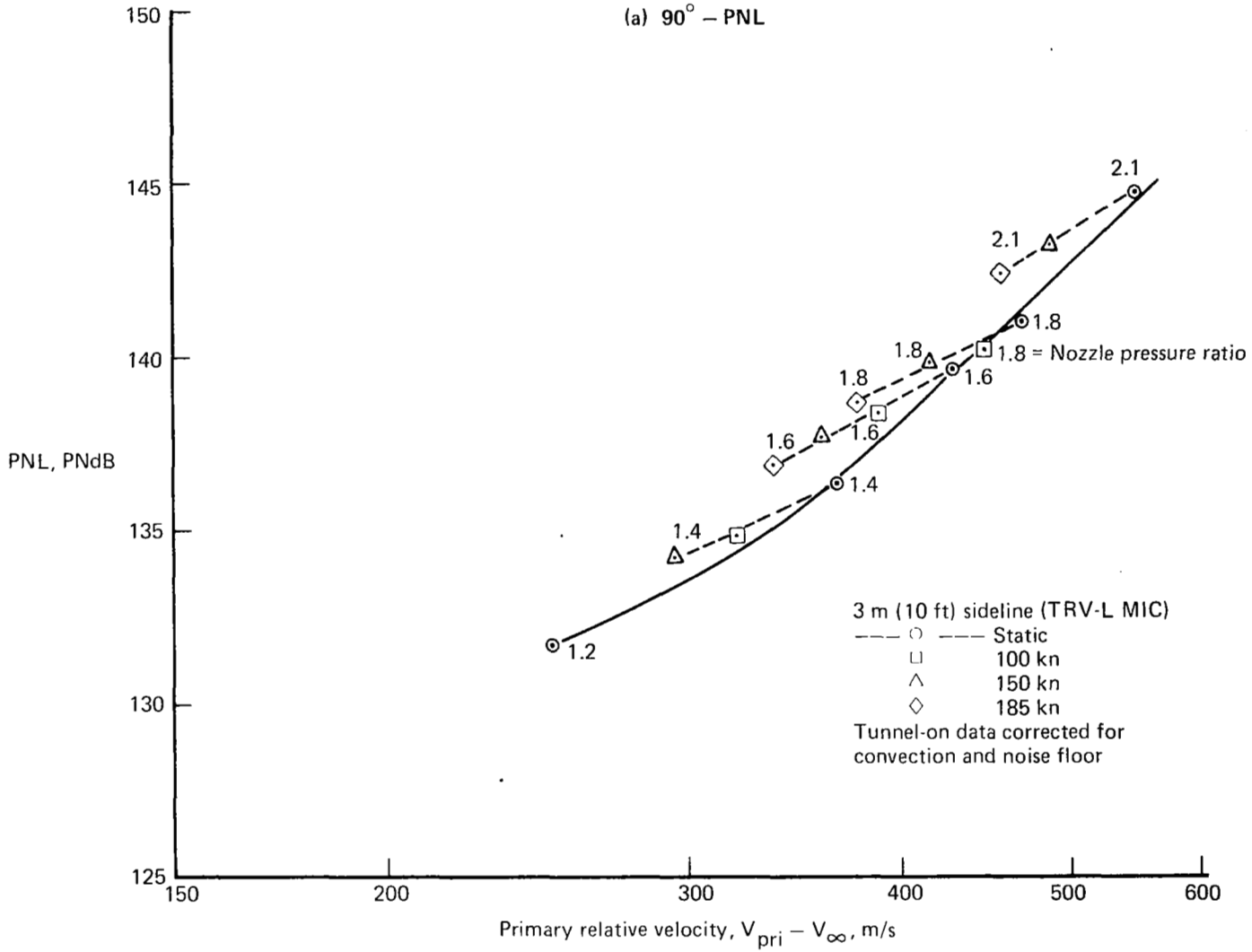

Figure 21.—NASA Ames 40 x 80 Wind Tunnel Test JT8D-17 Engine With Baseline Nozzle— PNL Relative Velocity Correlation

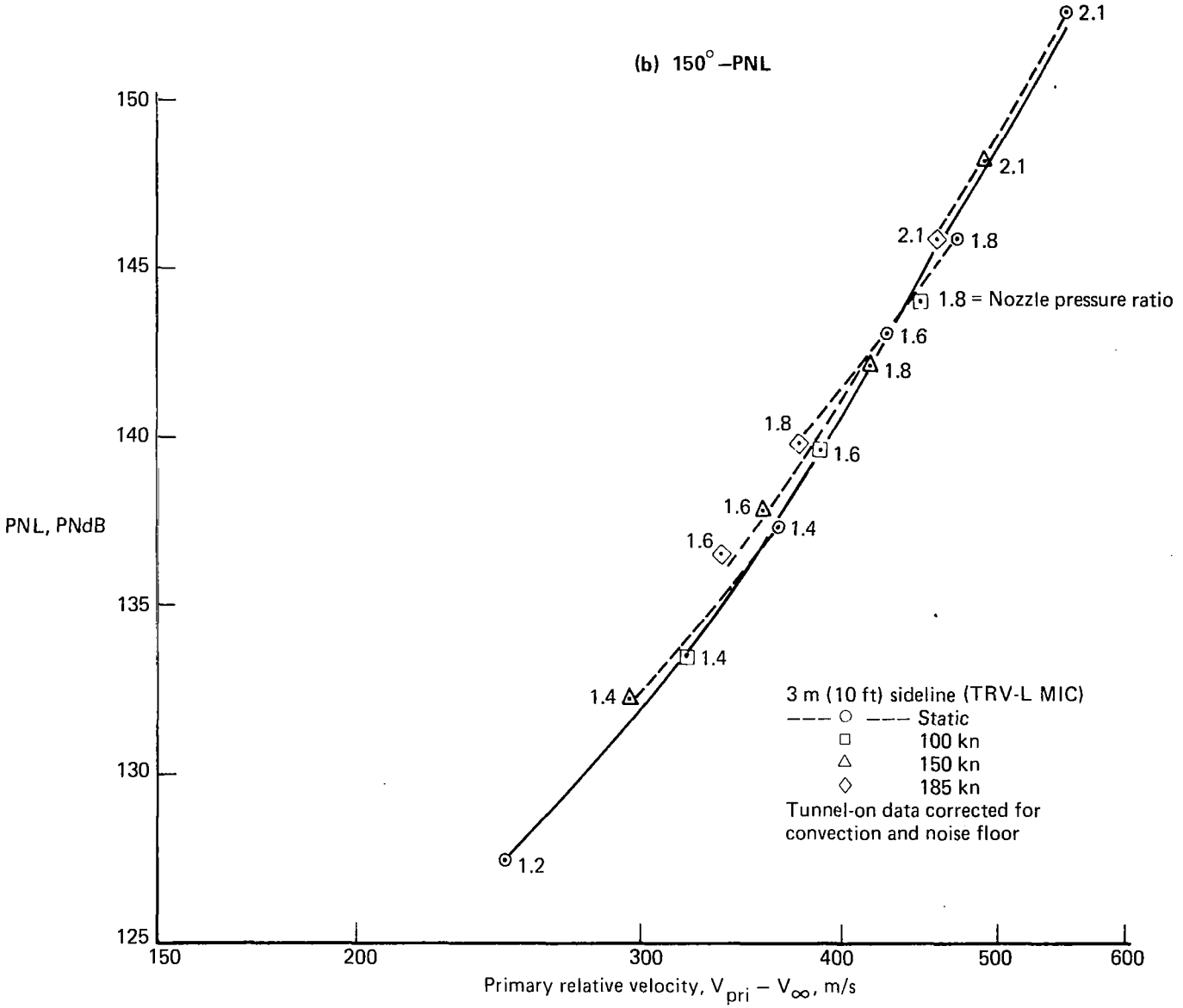

Figure 21.—(Concluded)

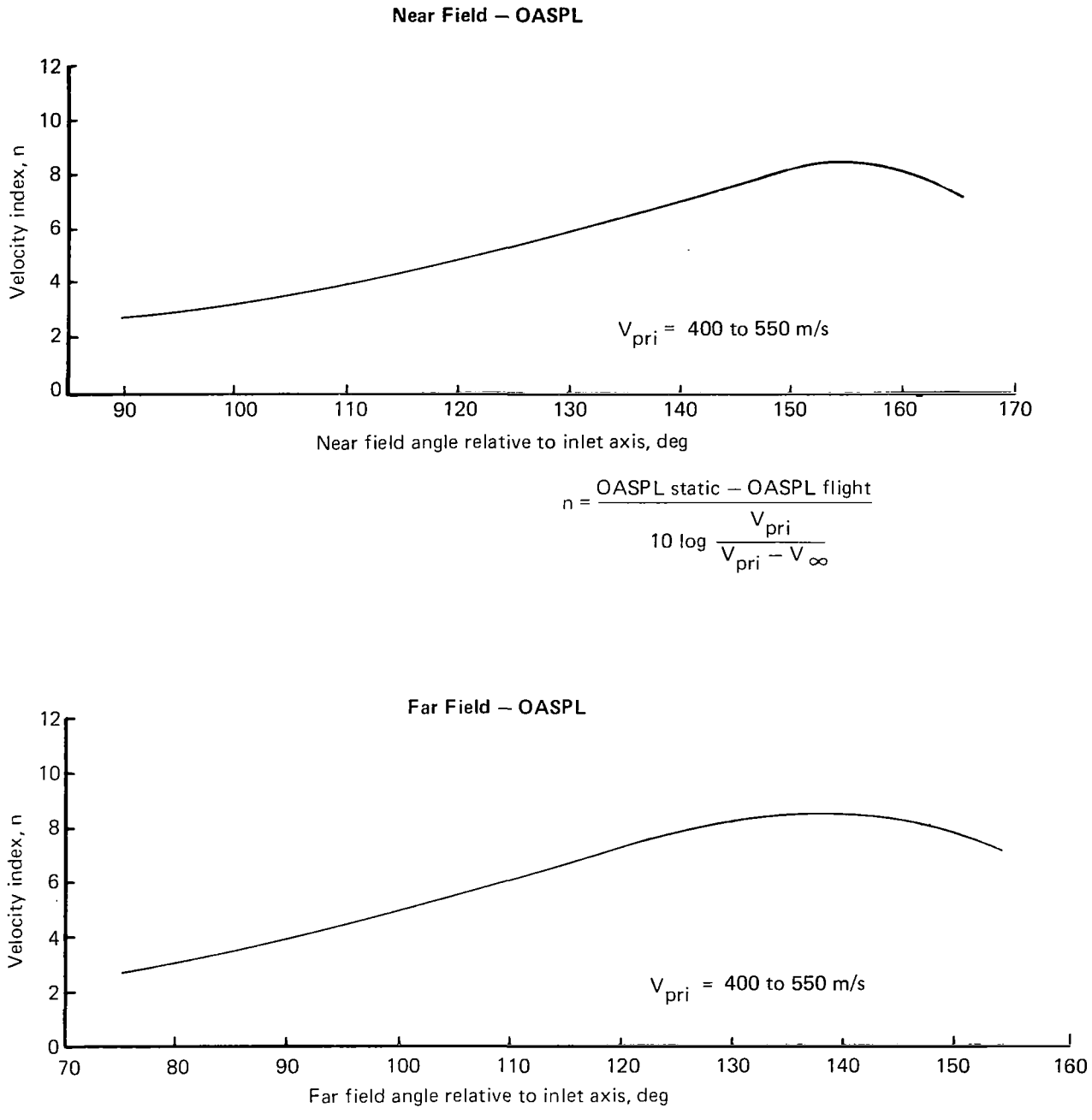

Figure 22.—NASA Ames 40 x 80 Wind Tunnel Test JT8D-17 Engine With Baseline Nozzle Relative Velocity Index for OASPL—Near and Far Field Angles

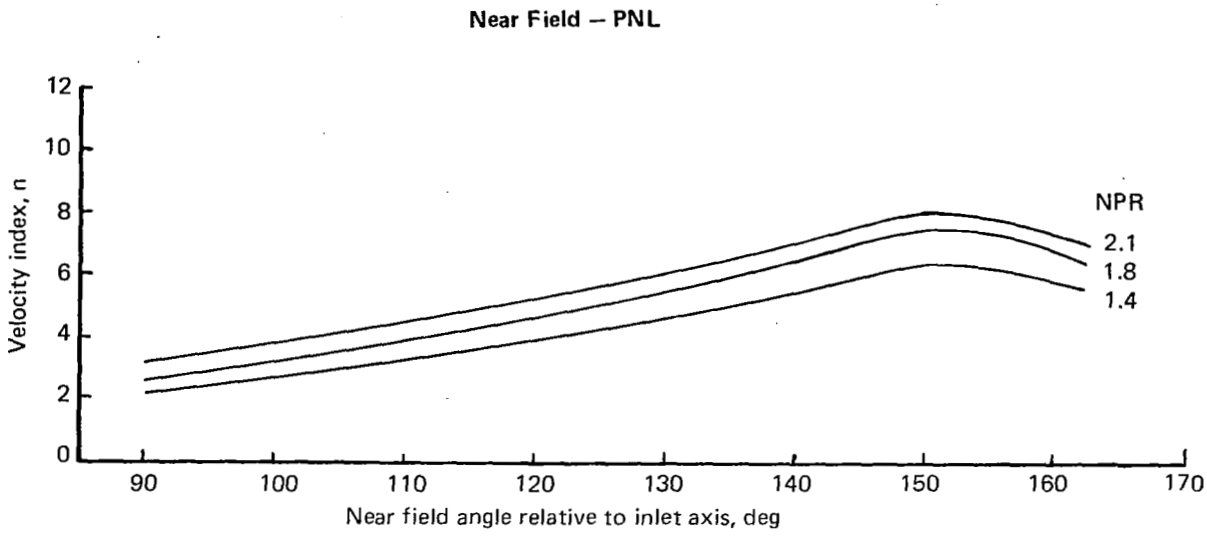

$$n = \frac{\text{PNL static} - \text{PNL flight}}{10 \log \dfrac{V_{pri}}{V_{pri} - V_{\infty}}}$$

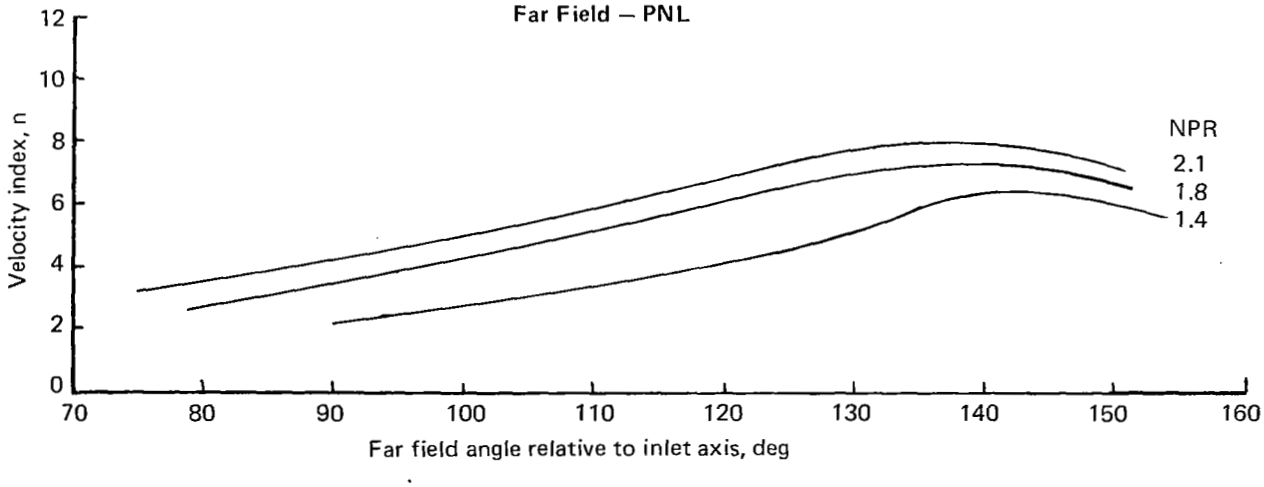

Figure 23.—NASA Ames 40 x 80 Wind Tunnel Test JT8D-17 Engine With Baseline Nozzle Relative Velocity Index for PNL—Near and Far Field Angles

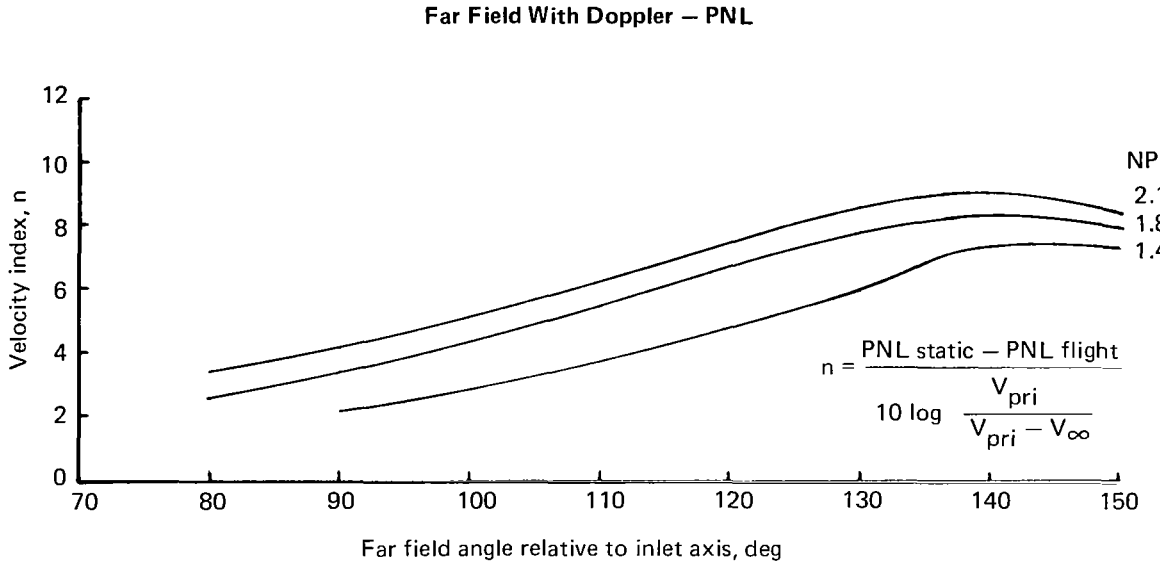

Figure 24.– NASA Ames 40 x 80 Wind Tunnel Test JT8D-17 Engine With Baseline Nozzle Relative Velocity Index for PNL–Far Field Angle With Doppler Effect

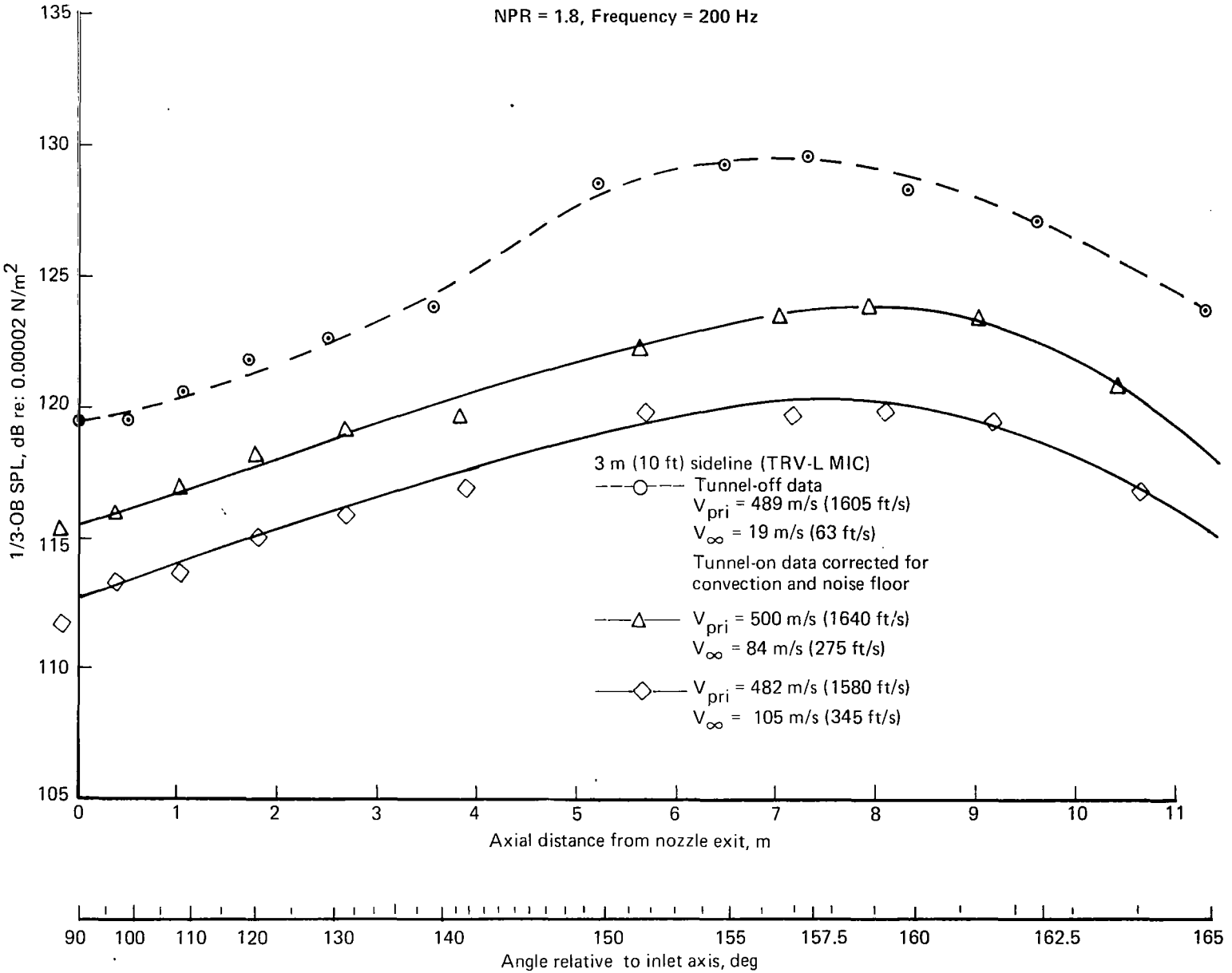

Figure 25.—NASA Ames 40 x 80 Wind Tunnel Test JT8D-17 Engine With Baseline Nozzle Static/Flight SPL Directivity

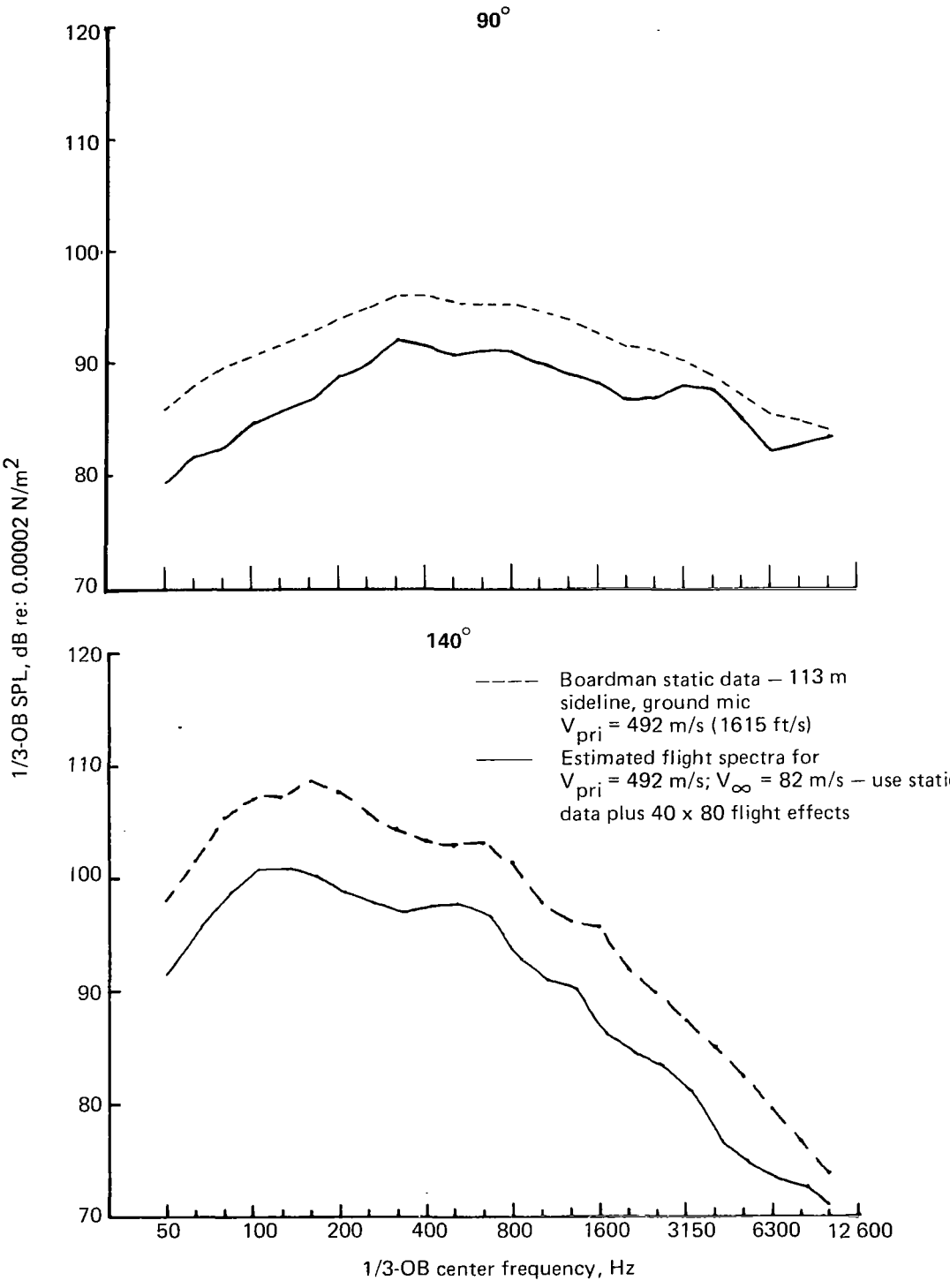

Figure 26.—NASA Ames 40 x 80 Wind Tunnel Test JT8D-17 Engine With Baseline Nozzle Comparison of Far-Field Static/Flight Spectra

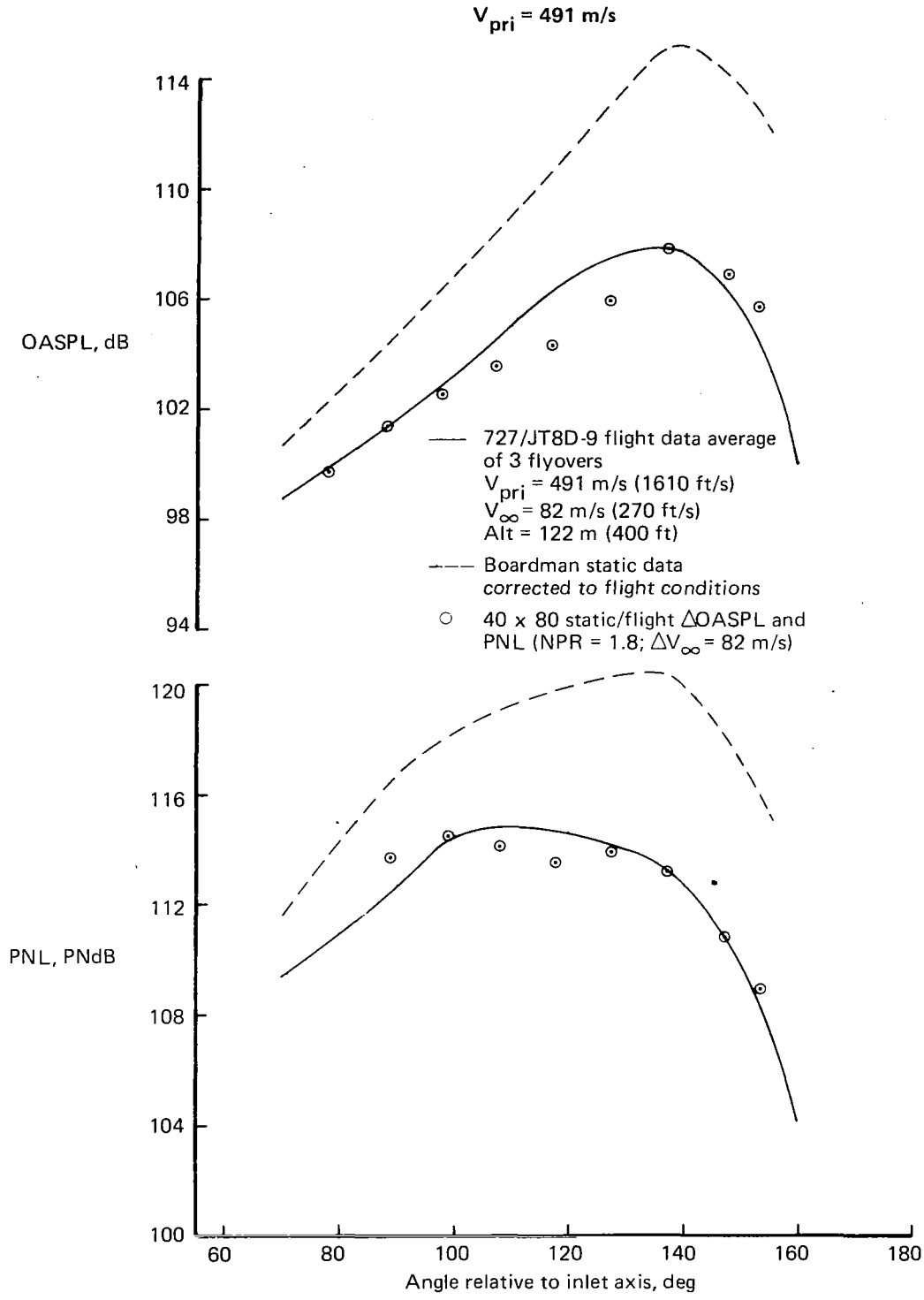

Figure 27.— NASA Ames 40 x 80 Wind Tunnel Test JT8D Engine With Baseline Nozzle Static/Flight OASPL and PNL Directivity 40 x 80 Versus 727 Flight Data

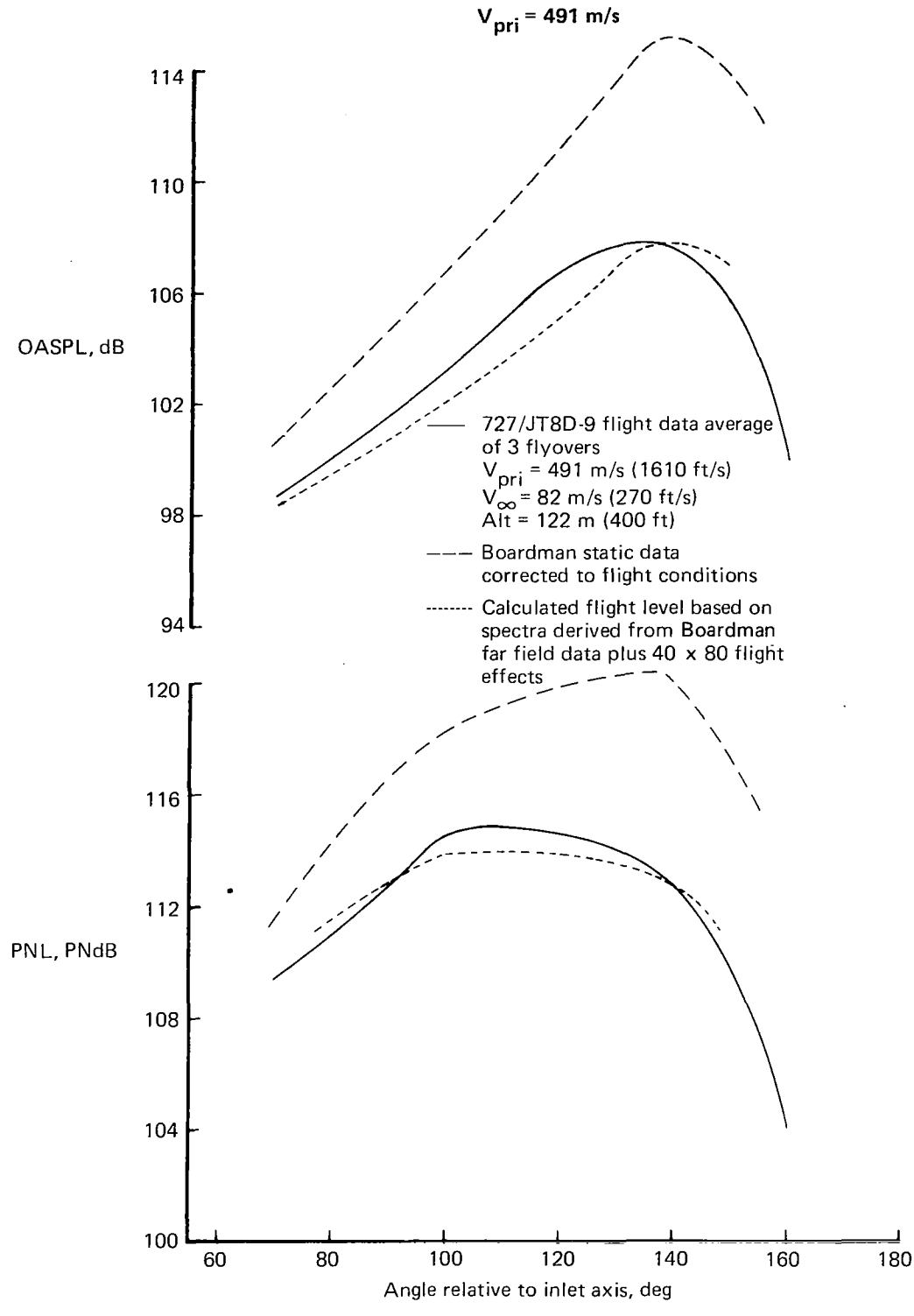

Figure 28.—NASA Ames 40 x 80 Wind Tunnel Test JT8D Engine With Baseline Nozzle Static/Flight OASPL and PNL Directivity 40 x 80 Versus 727 Flight Data

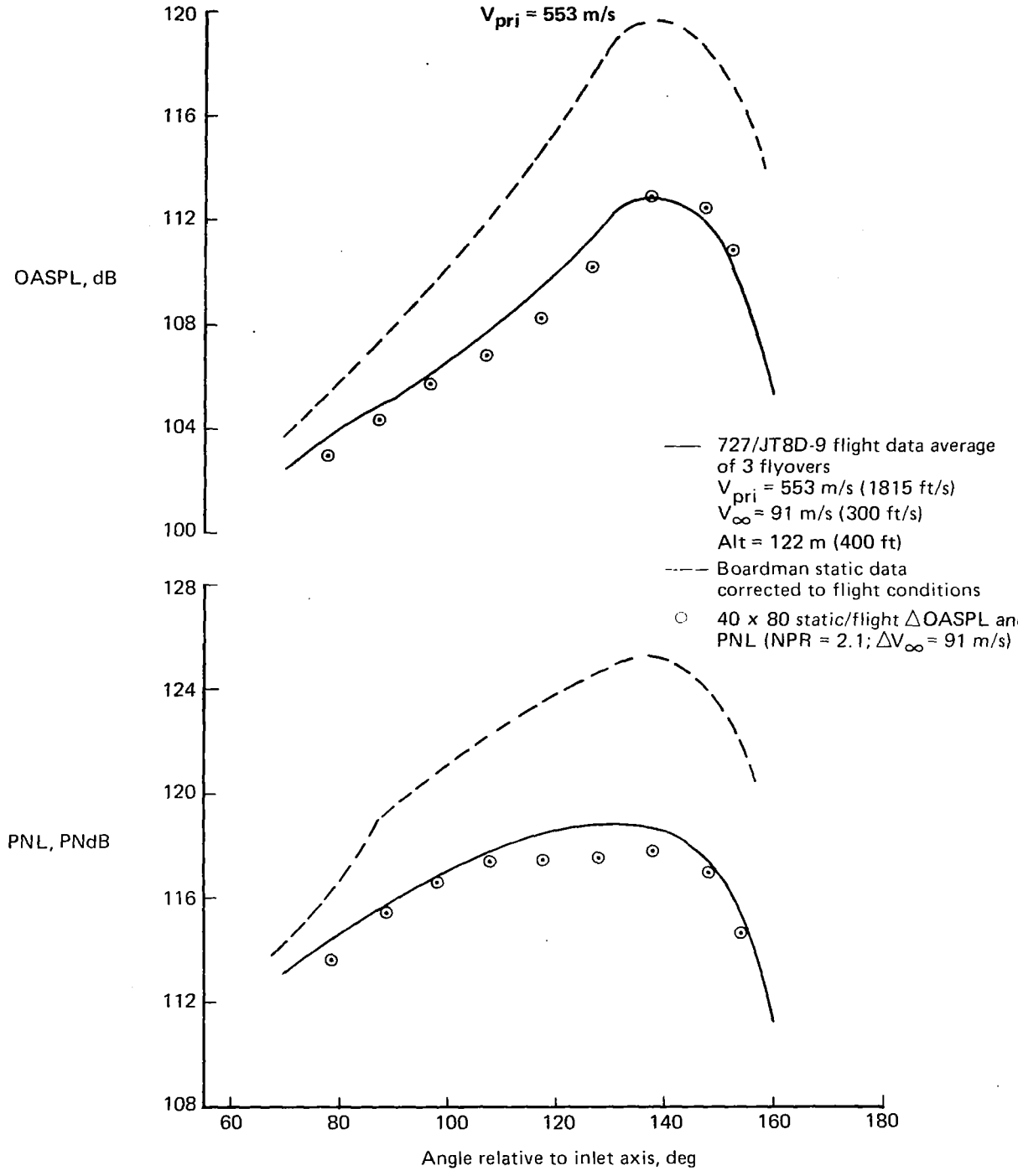

Figure 29.— NASA Ames 40 x 80 Wind Tunnel Test JT8D Engine With Baseline Nozzle Static/Flight OASPL and PNL Directivity 40 x 80 Versus 727 Flight Data

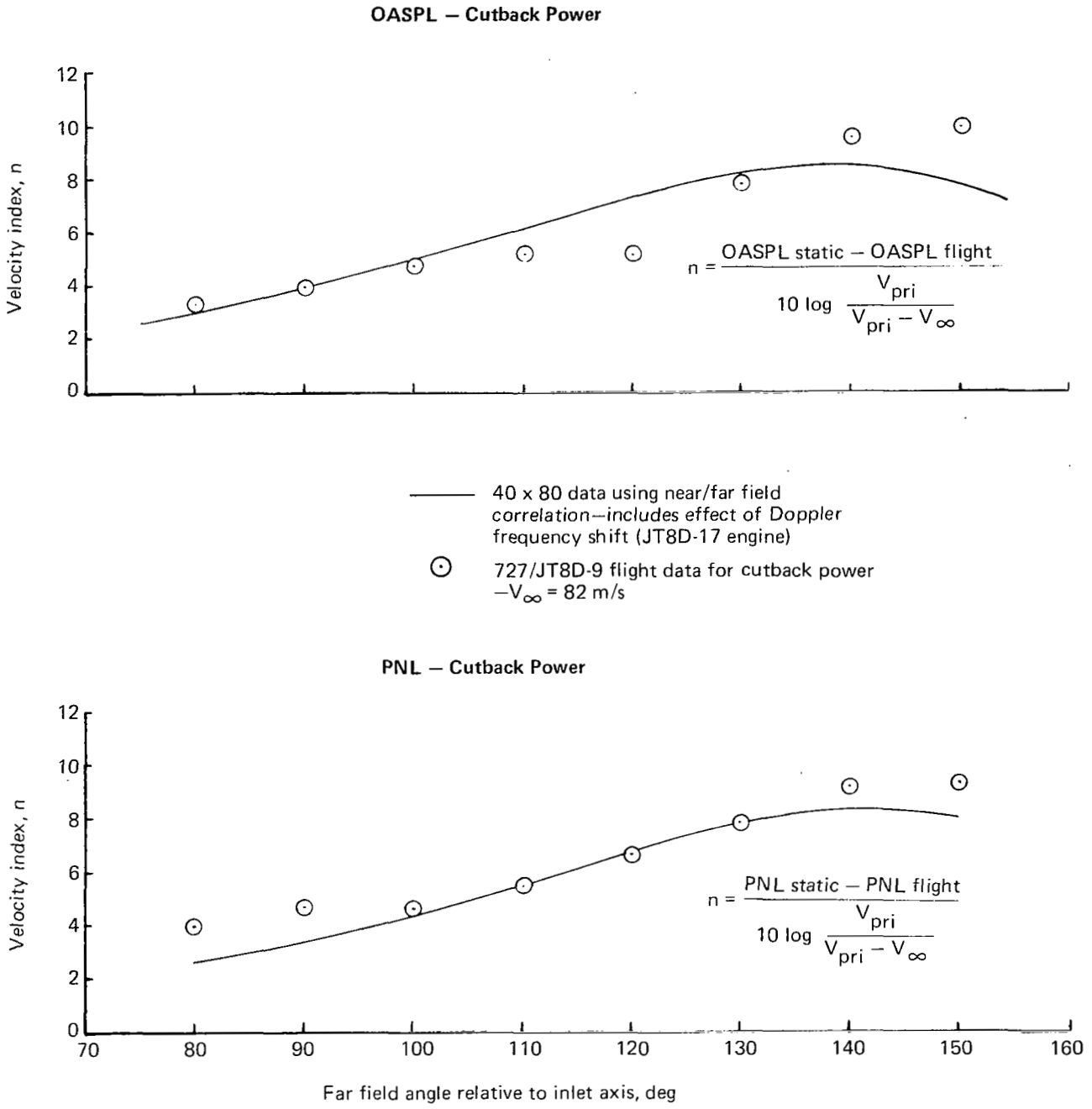

Figure 30.–NASA Ames 40 x 80 Wind Tunnel Test JT8D-17 Engine With Baseline Nozzle Relative Velocity Index Comparison–40 x 80 Versus 727 Flight Data

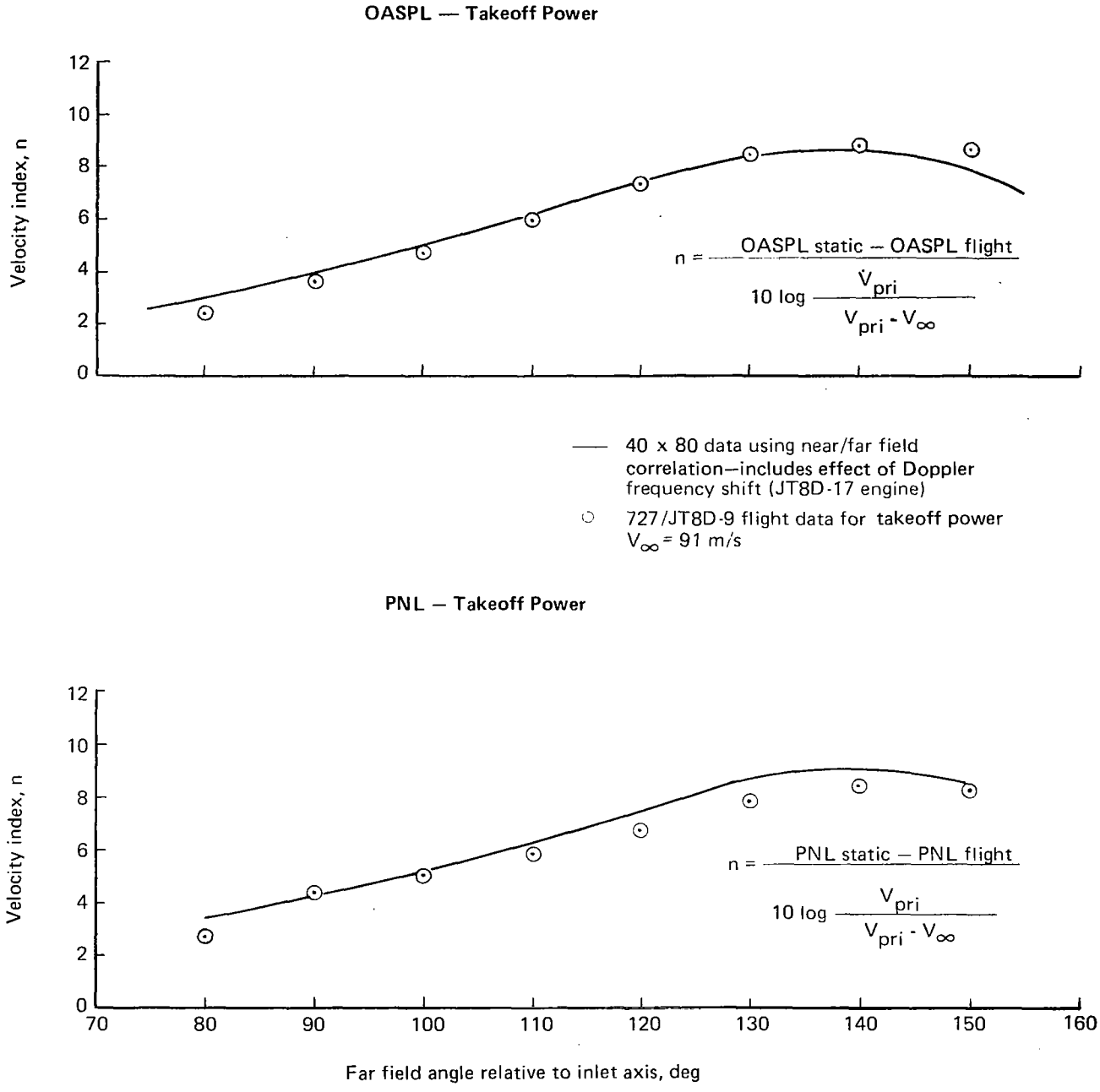

Figure 31.—NASA Ames 40 x 80 Wind Tunnel Test JT8D Engine With Baseline Nozzle Relative Velocity Index Comparison—40 x 80 Versus 727 Flight Data

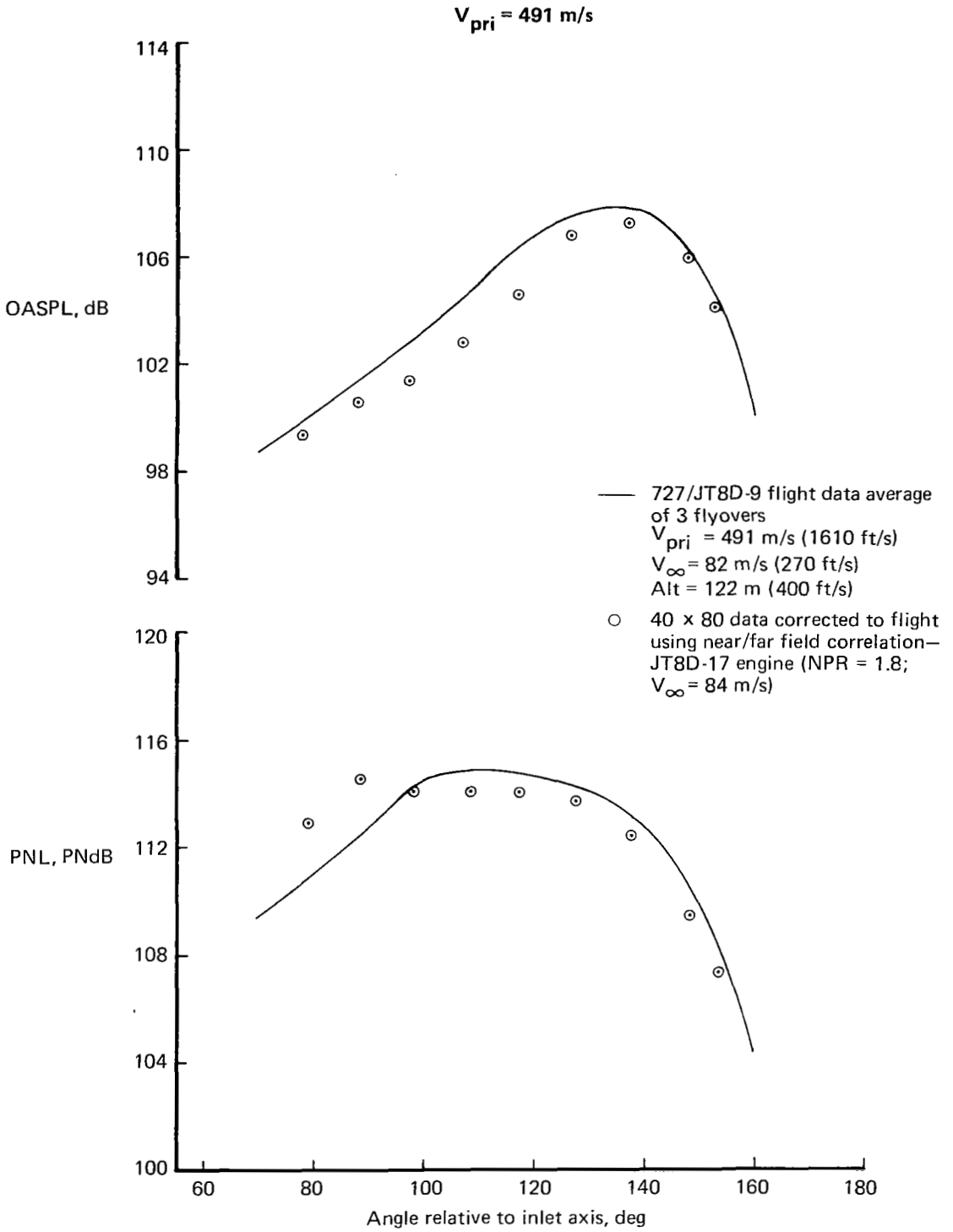

Figure 32.– NASA Ames 40 x 80 Wind Tunnel Test JT8D Engine With Baseline Nozzle– Flight OASPL and PNL Directivity–40 x 80 Versus 727 Flight Data

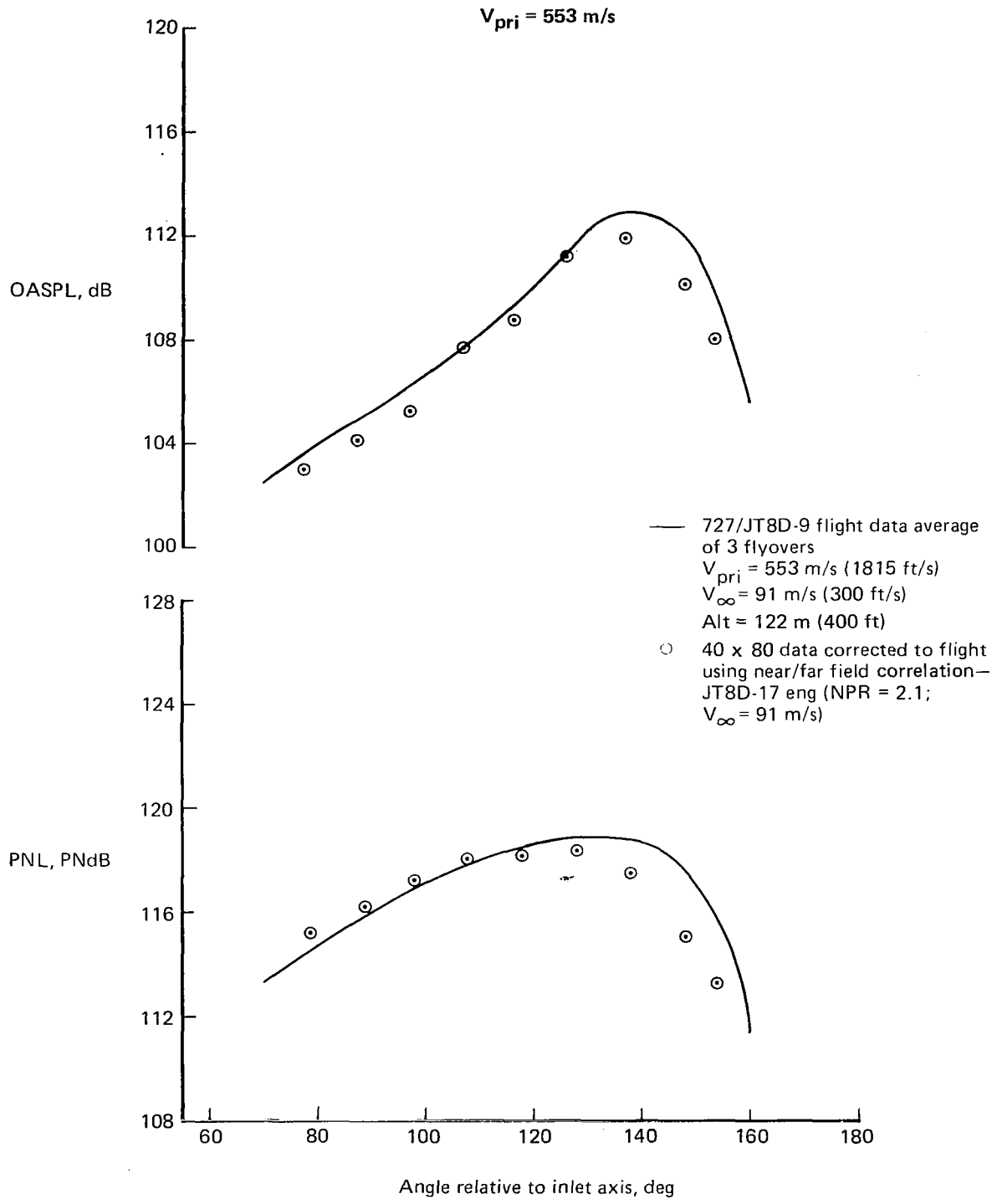

Figure 33.—NASA Ames 40 x 80 Wind Tunnel Test JT8D Engine With Baseline Nozzle—Flight OASPL and PNL Directivity—40 x 80 Versus 727 Flight Data

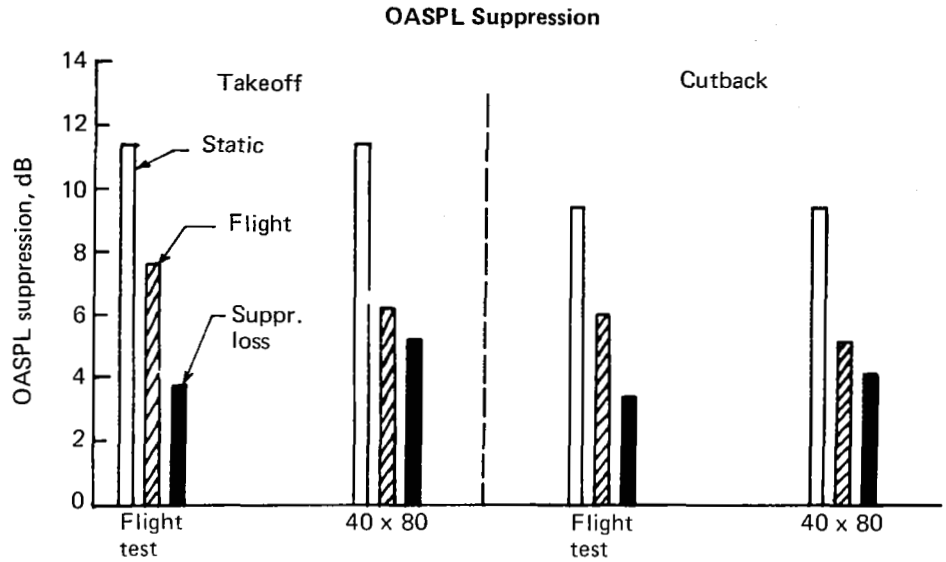

Note: Suppression is peak to peak delta noise of JT8D baseline and 20-lobe ejector/suppressor

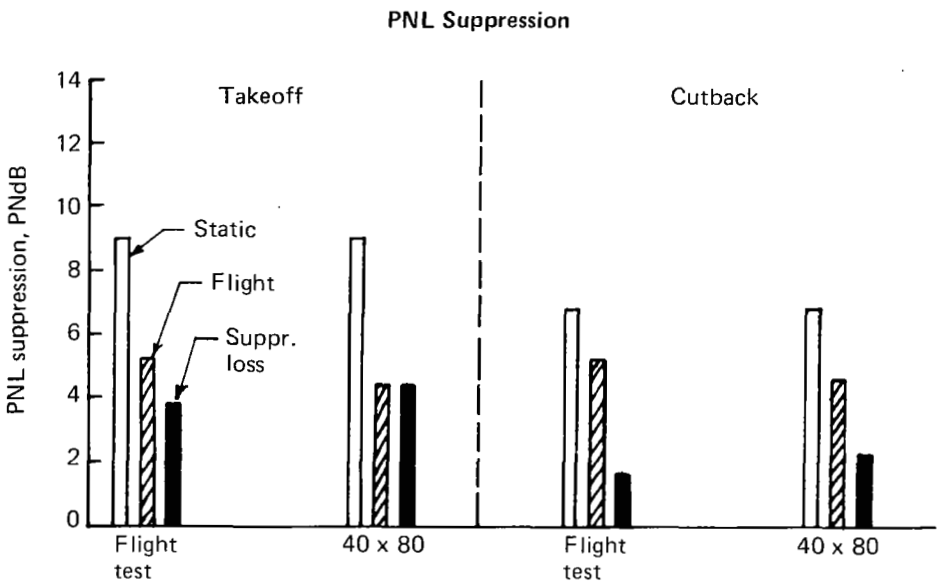

Figure 34.—NASA Ames 40 x 80 Wind Tunnel Test Comparison of 20-Lobe Ejector/ Suppressor—Static and Flight Suppression

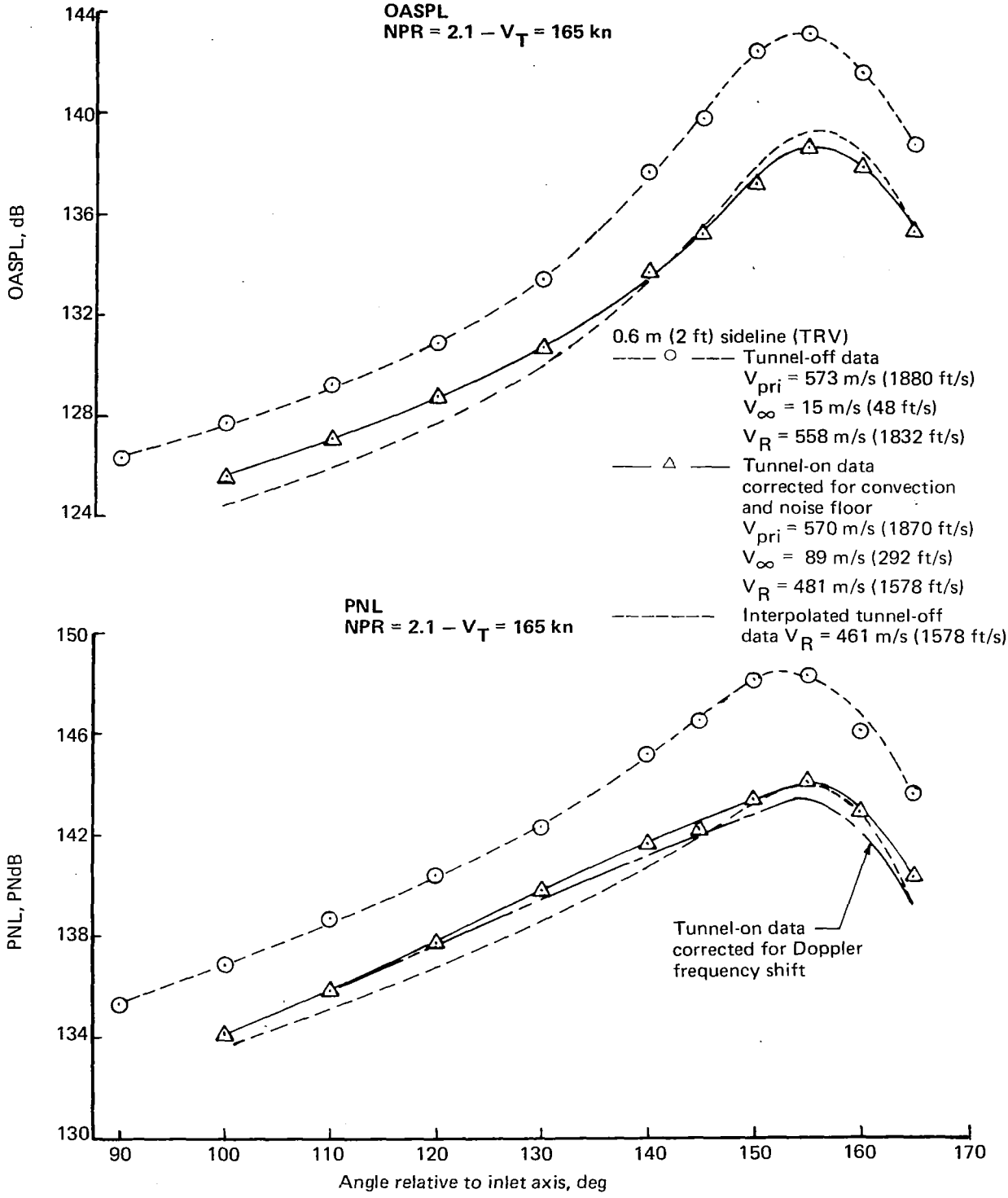

Figure 35.—Boeing 9 x 9 Wind Tunnel Test JT8D Baseline Model Nozzle Static/Flight OASPL and PNL Directivity Comparison

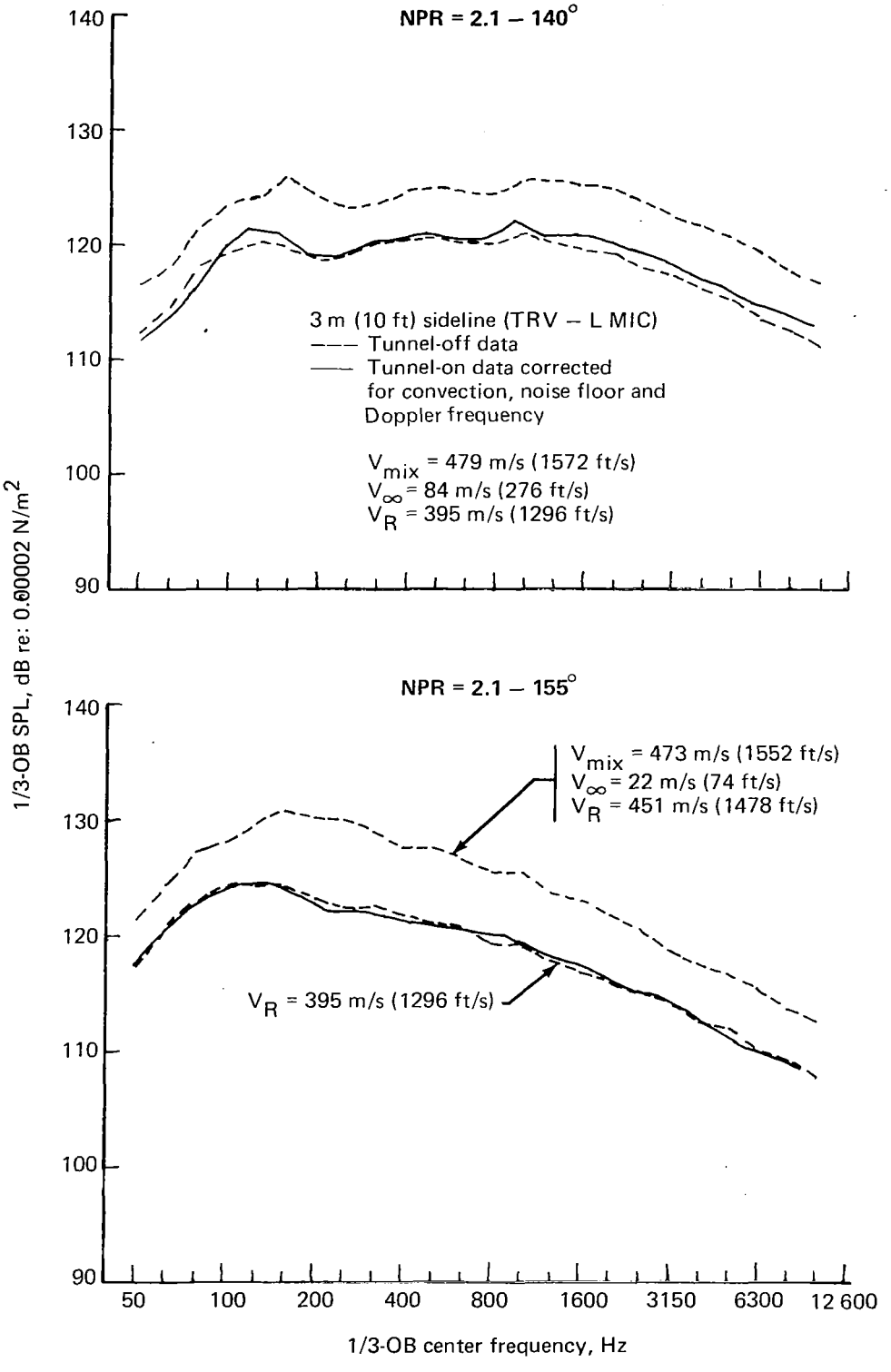

Figure 36.– NASA Ames 40 x 80 Wind Tunnel Test JT8D-17 Engine With Lined Internal Mixer–Static/Flight Spectra With Doppler

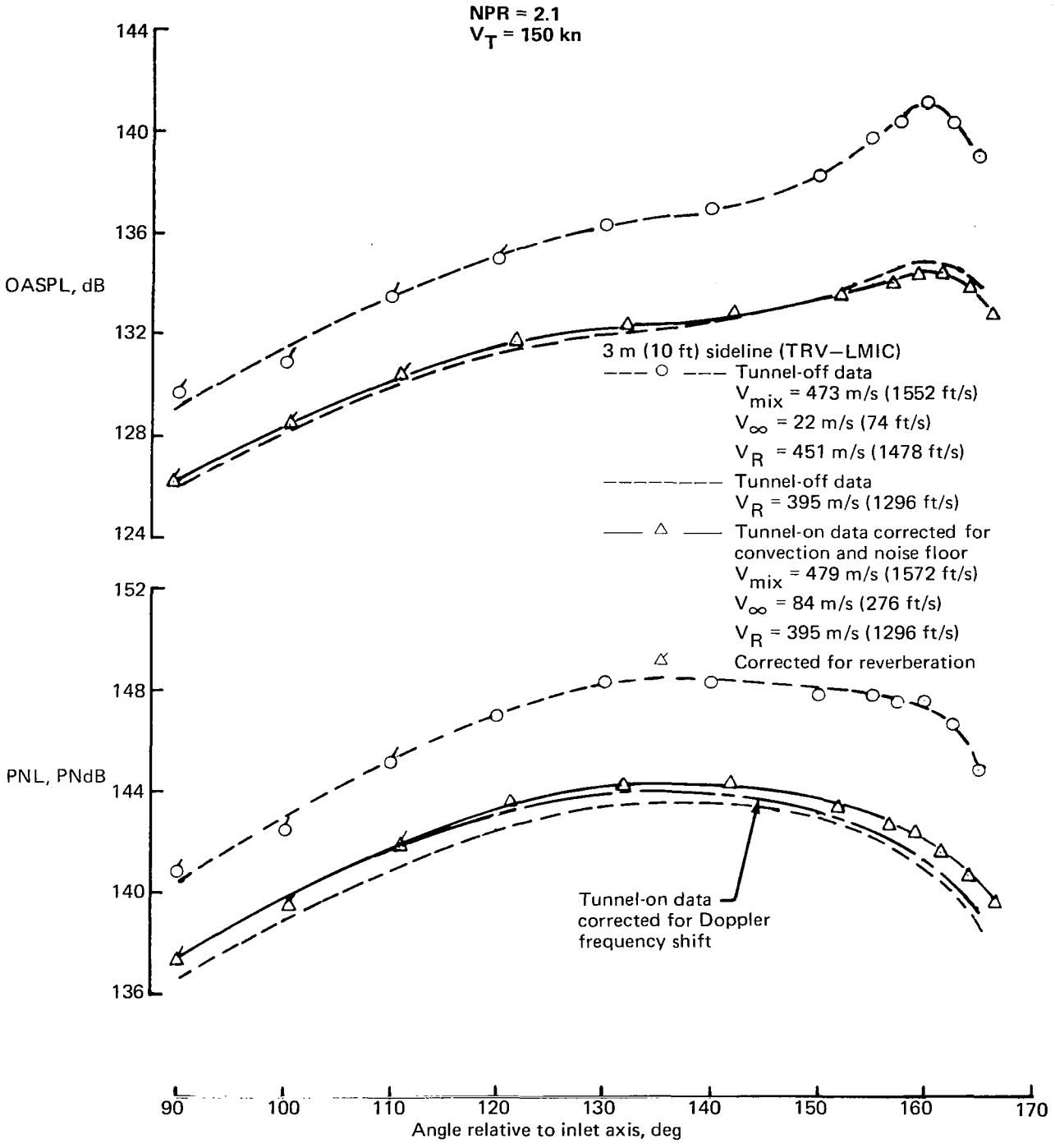

Figure 37.– NASA Ames 40 x 80 Wind Tunnel Test JT8D-17 Engine With Lined Internal Mixer–Static/Flight OASPL and PNL Directivity Comparison

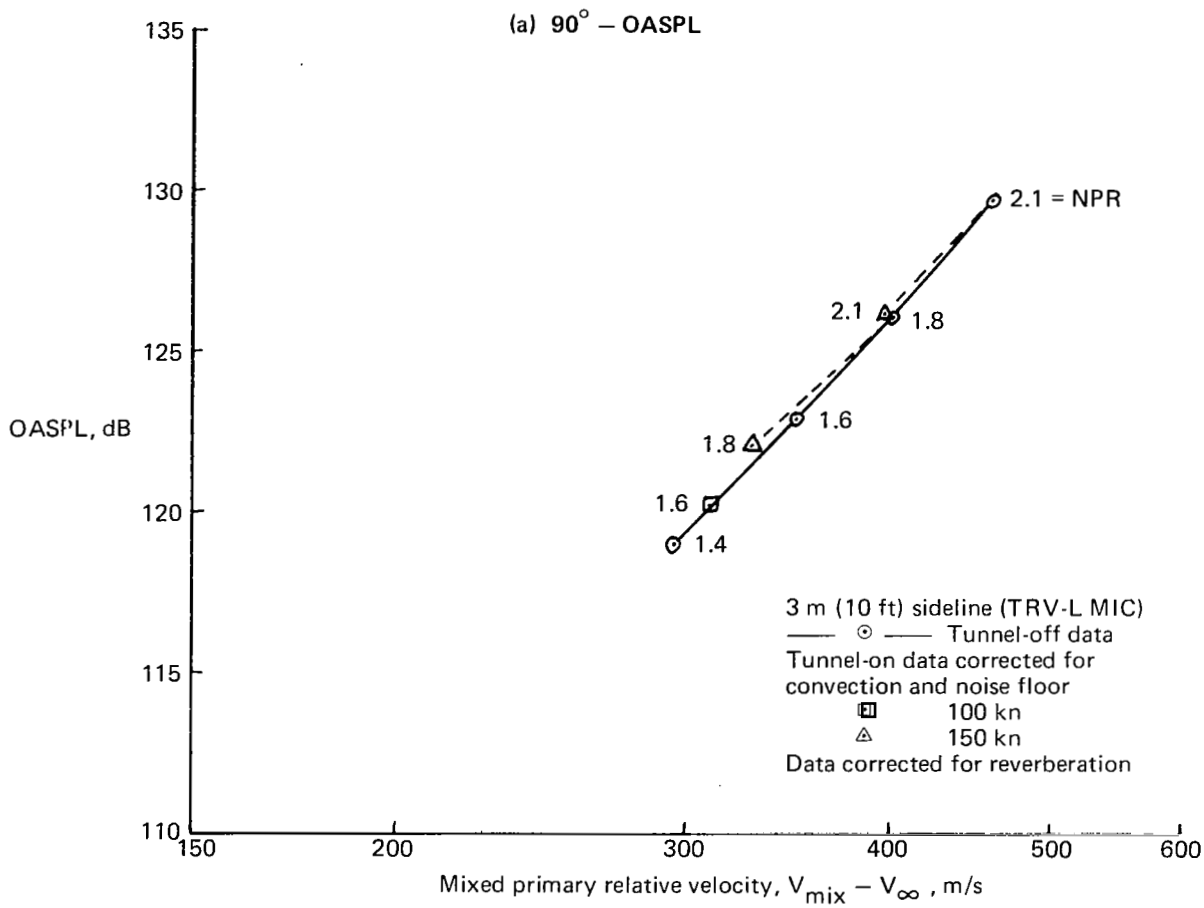

Figure 38.—NASA Ames 40 x 80 Wind Tunnel Test JT8D-17 Engine With Lined Internal Mixer—OASPL Relative Velocity Correlation

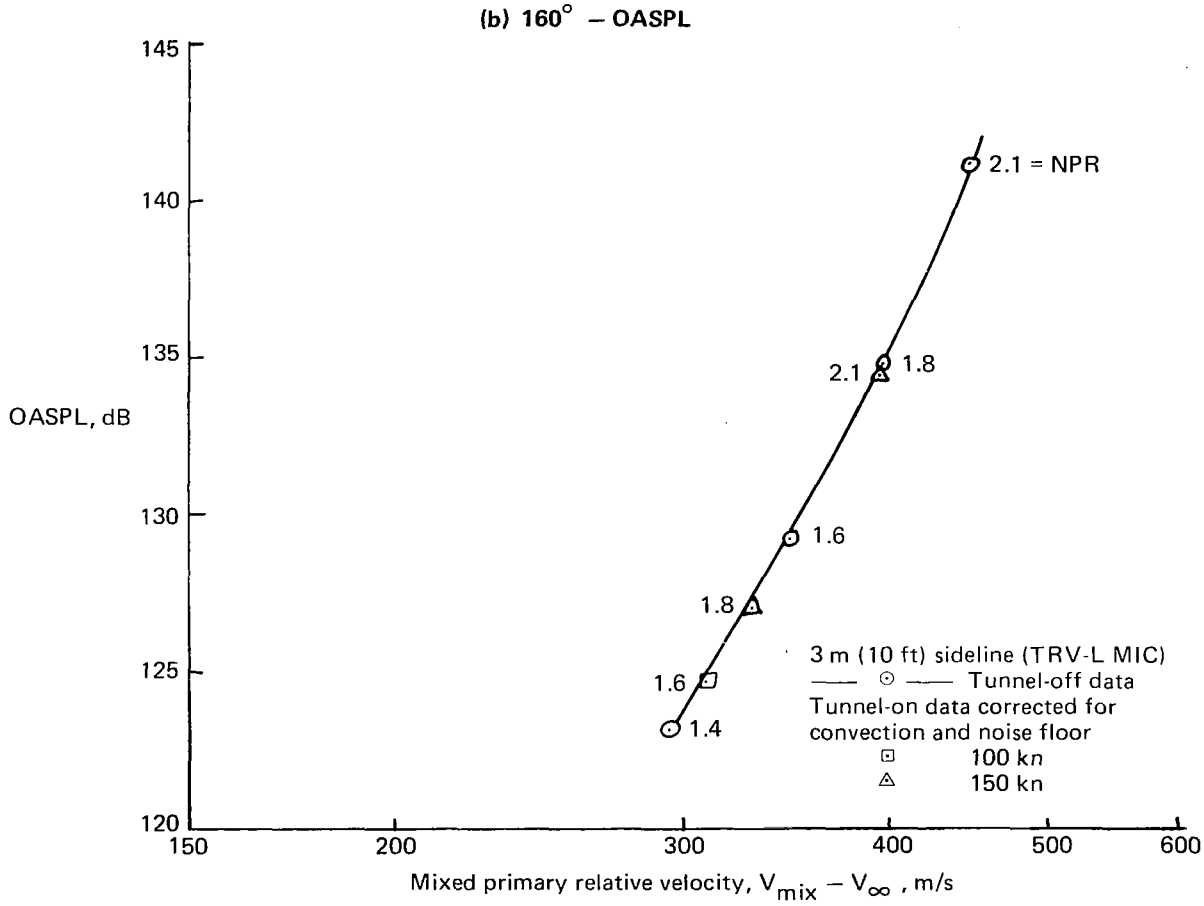

Figure 38.—(Concluded)

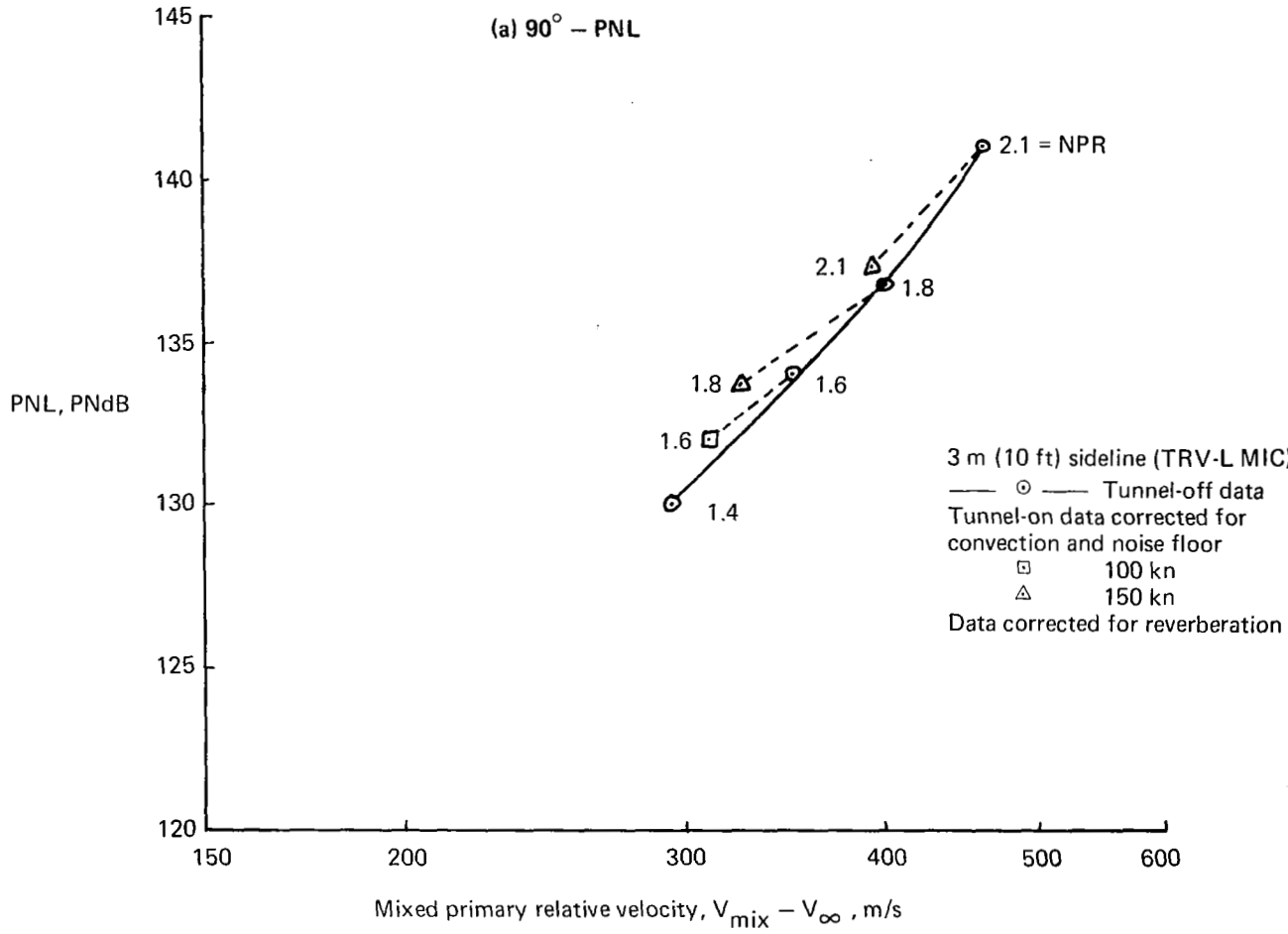

Figure 39.– NASA Ames 40 x 80 Wind Tunnel Test JT8D-17 Engine With Lined Internal Mixer–PNL Relative Velocity Correlation

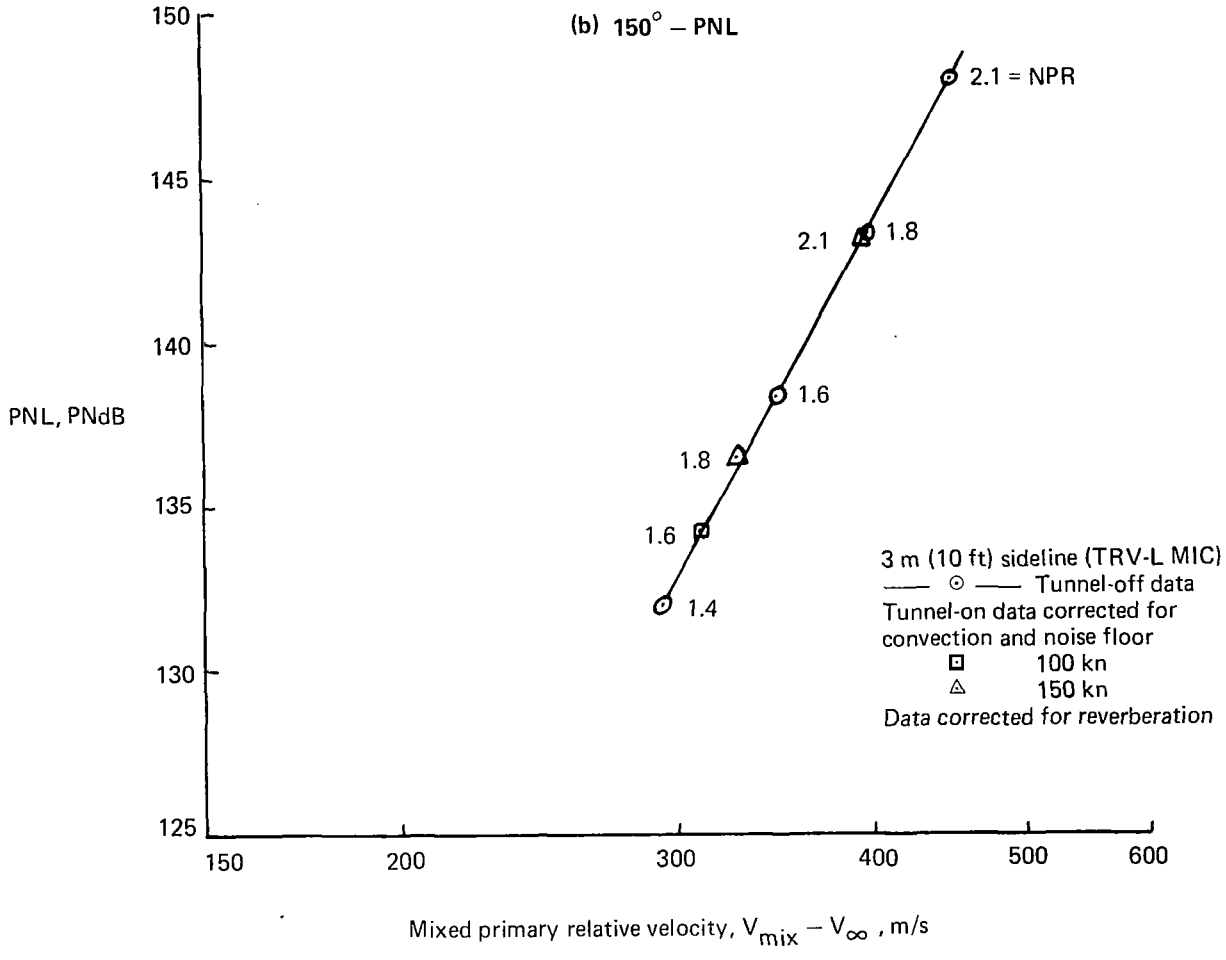

Figure 39.—(Concluded)

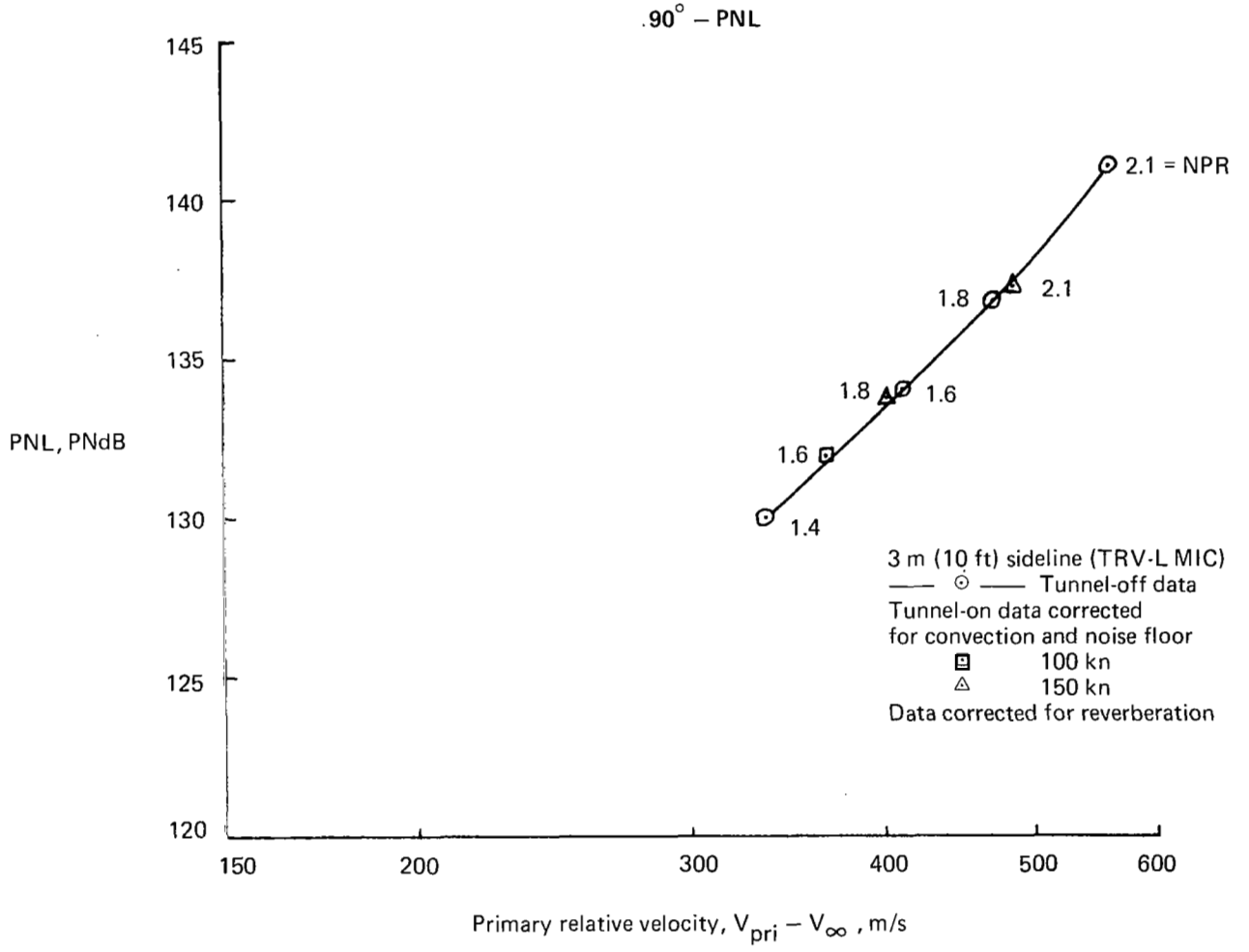

Figure 40.—NASA Ames 40 x 80 Wind Tunnel Test JT8D-17 Engine With Lined Internal Mixer—PNL Relative Velocity Correlation

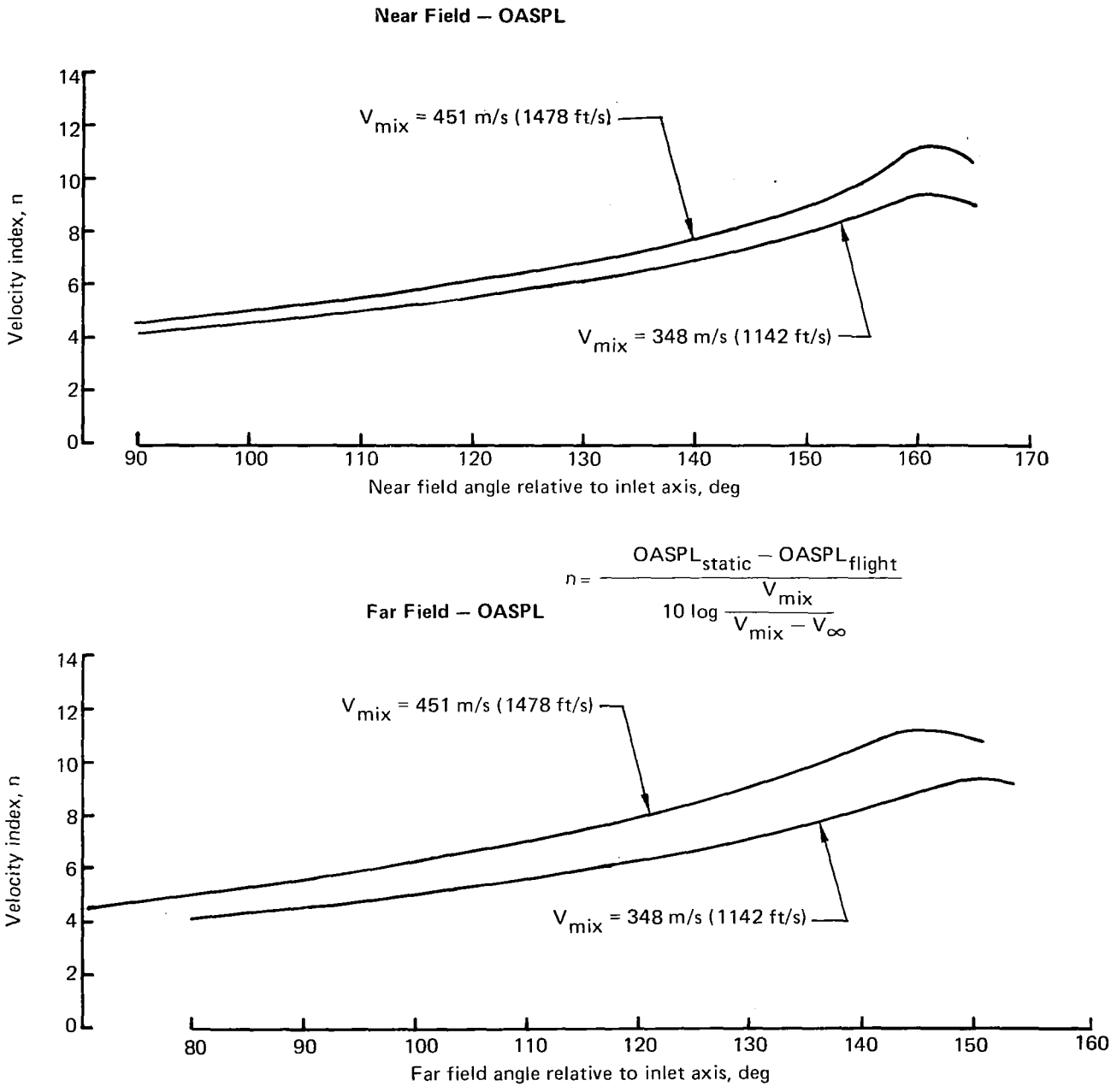

Figure 41.—NASA Ames 40 x 80 Wind Tunnel Test JT8D-17 Engine With Lined Internal Mixer—Relative Velocity Index for OASPL

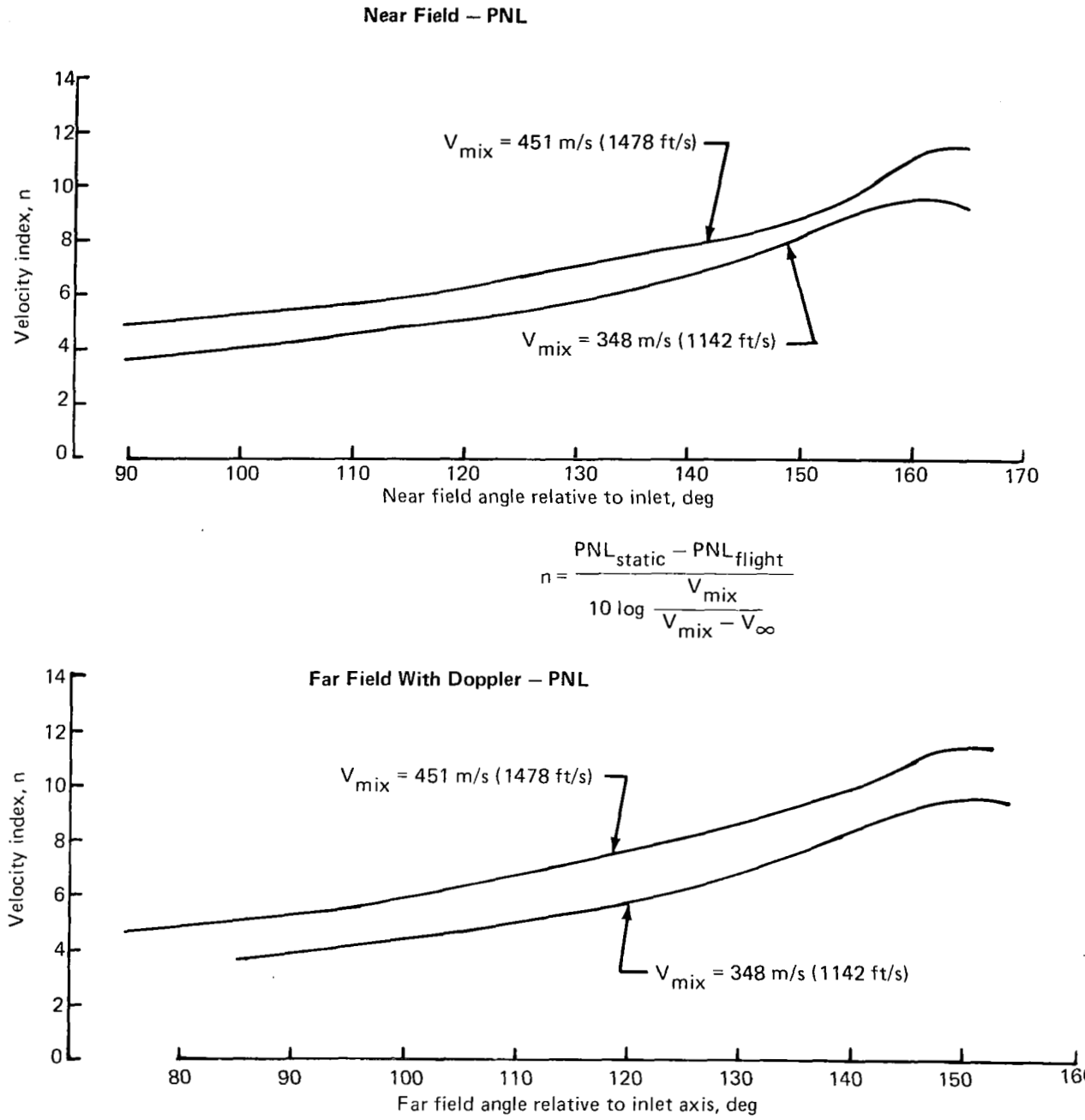

Figure 42.—NASA Ames 40 x 80 Wind Tunnel Test JT8D-17 Engine With Lined Internal Mixer—Relative Velocity Index for PNL

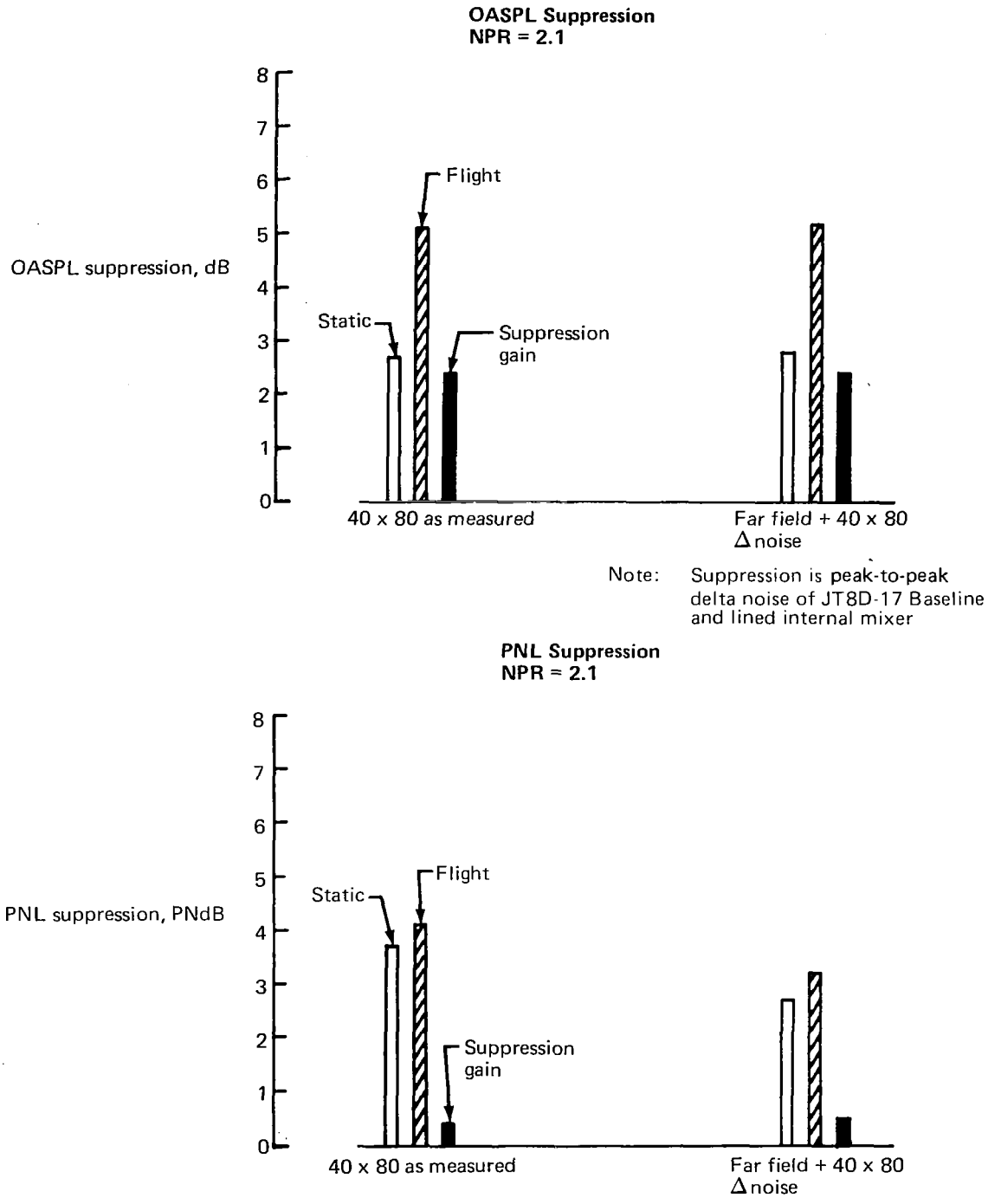

Figure 43.— NASA Ames 40 x 80 Wind Tunnel Test Comparison of Internal Mixer Static/ Flight Suppression

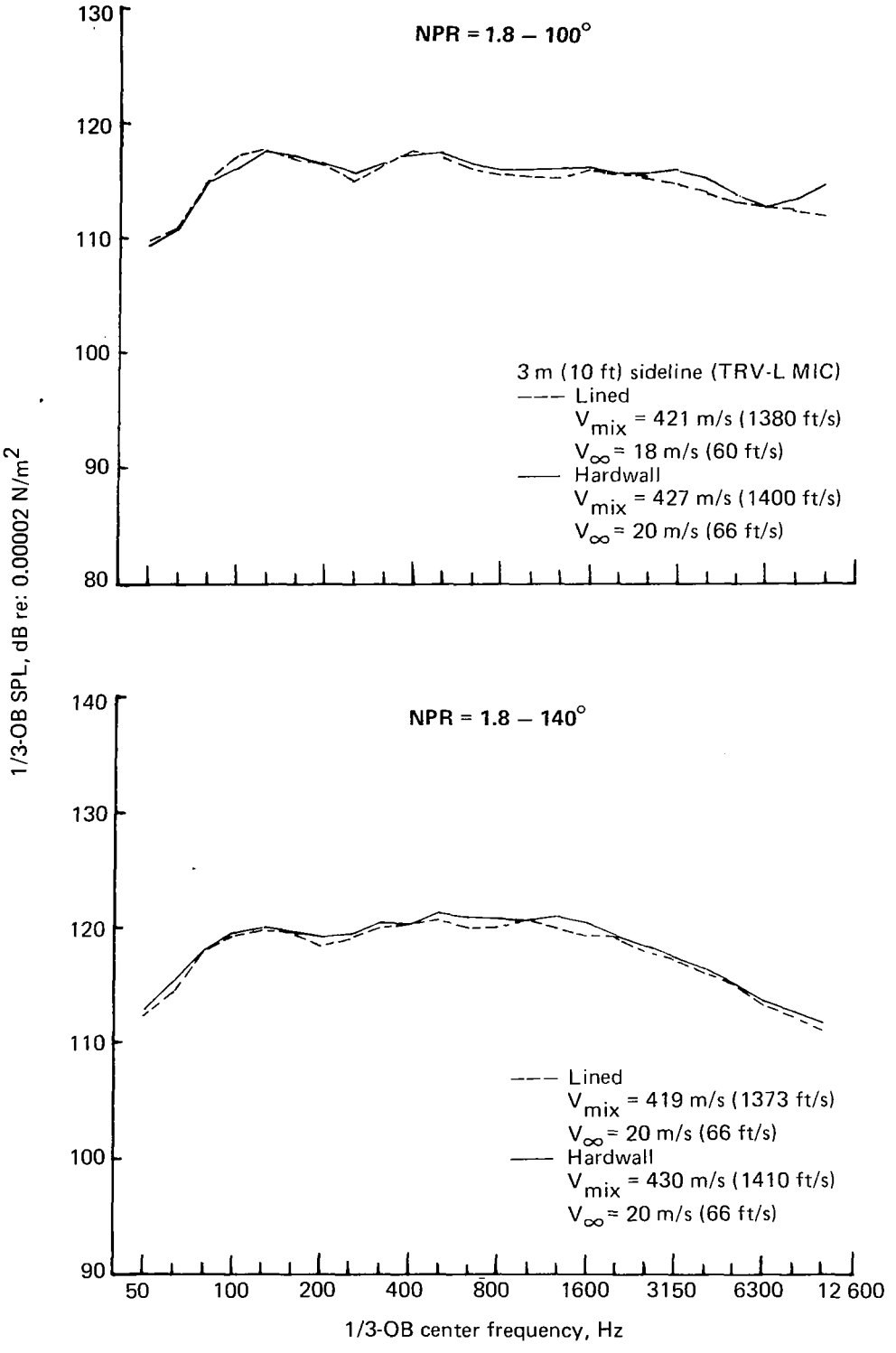

Figure 44.– NASA Ames 40 x 80 Wind Tunnel Test JT8D-17 Engine With Internal Mixer– Comparison of Lined and Hardwall Spectra–Tunnel-Off

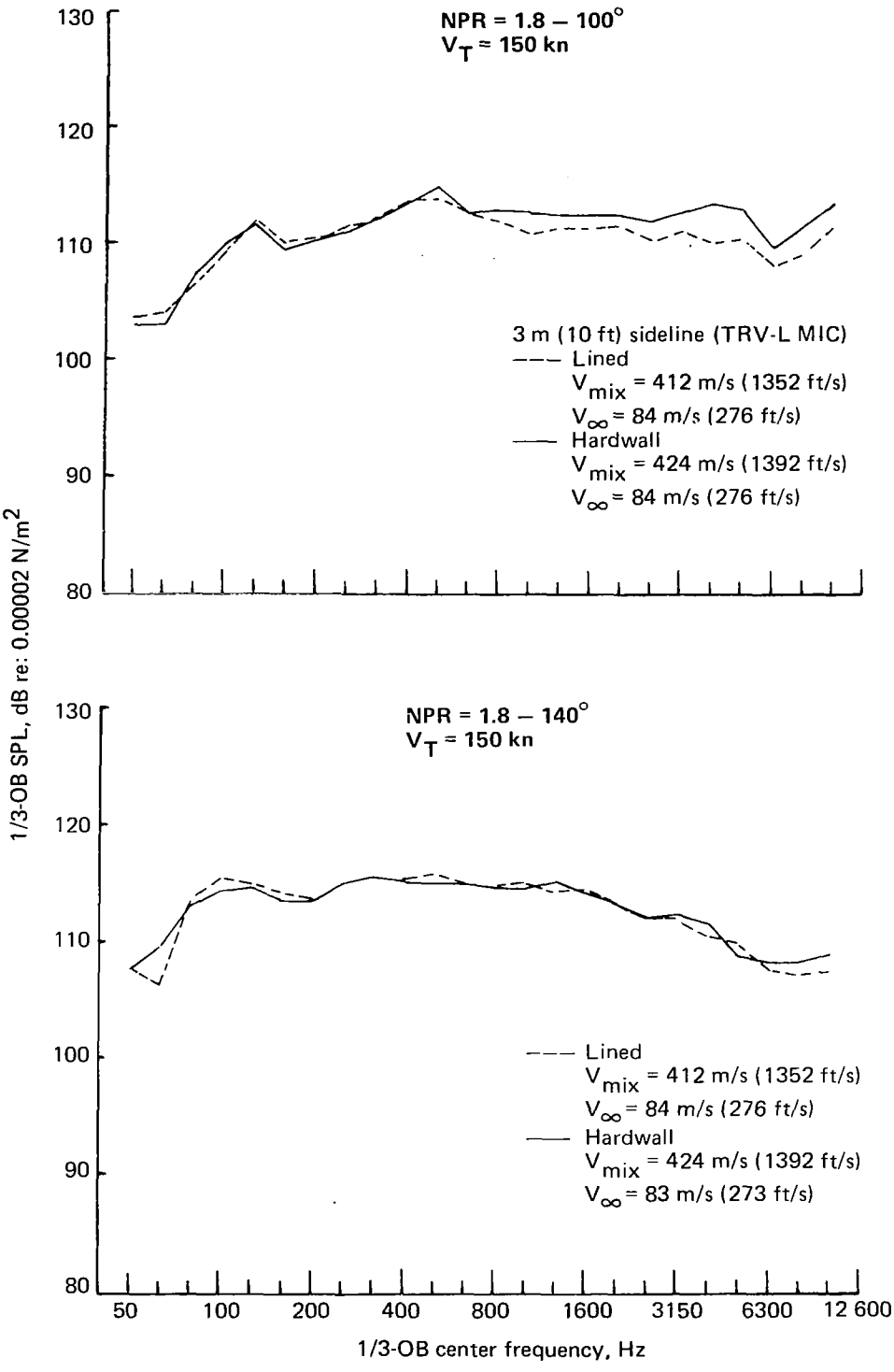

Figure 45.– NASA Ames 40 x 80 Wind Tunnel Test JT8D-17 Engine With Internal Mixer– Comparison of Lined and Hardwall Spectra–Tunnel-On

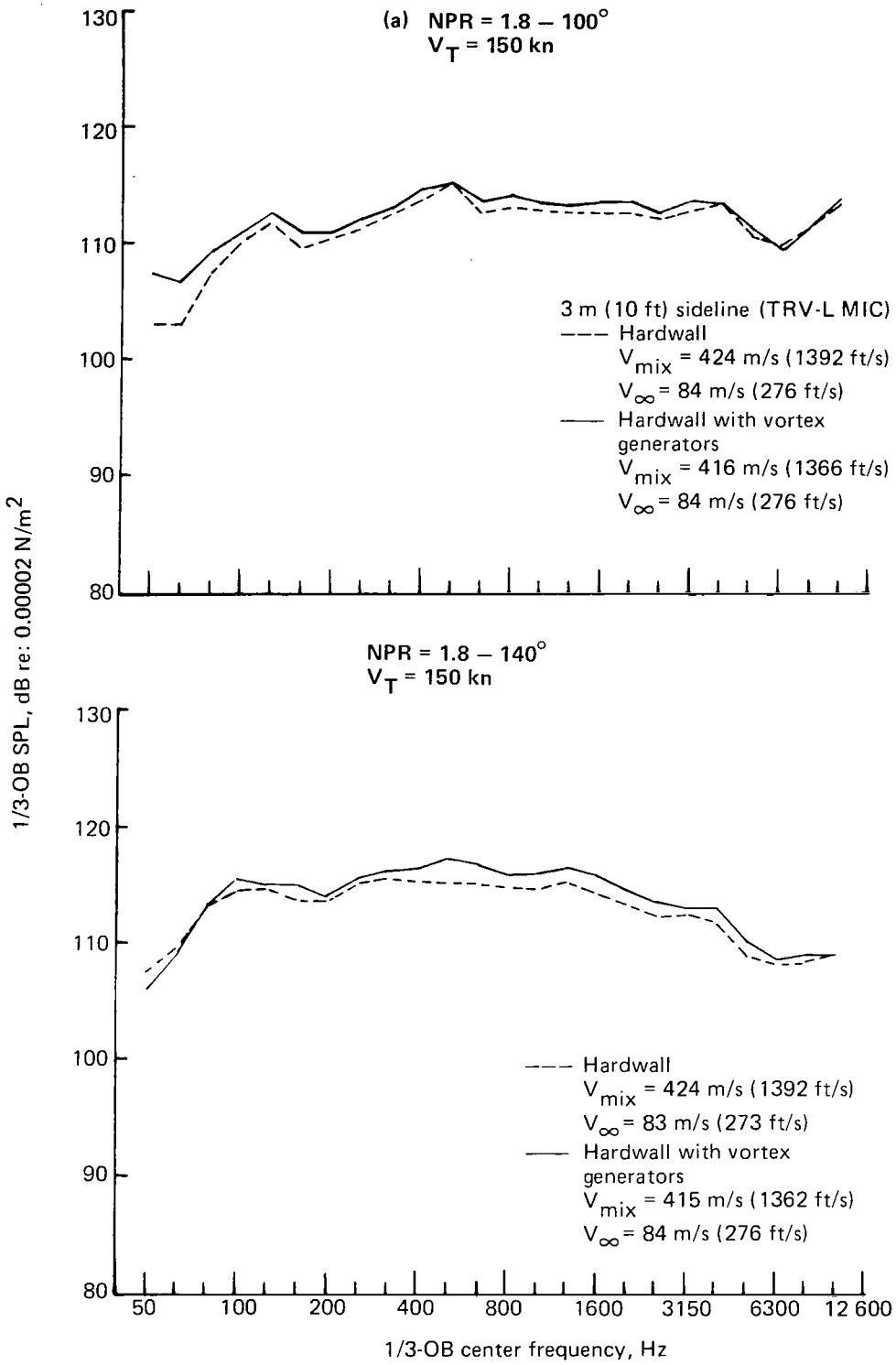

Figure 46.—NASA Ames 40 x 80 Wind Tunnel Test JT8D-17 Engine With Internal Mixer—Influence of Vortex Generators on Hardwall Spectra

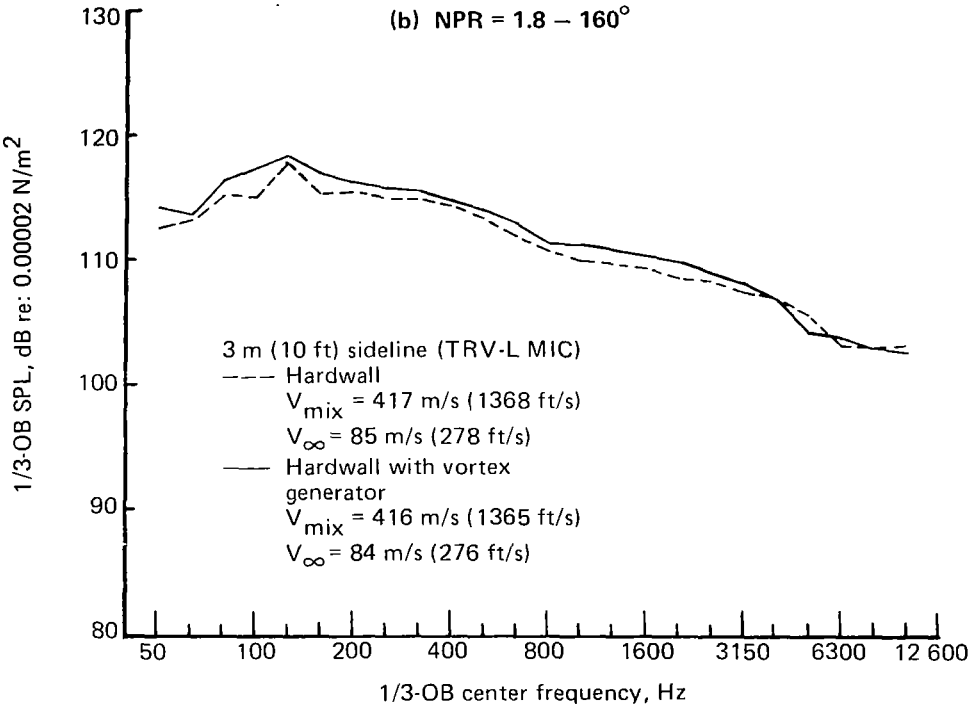

Figure 46.—(Concluded)

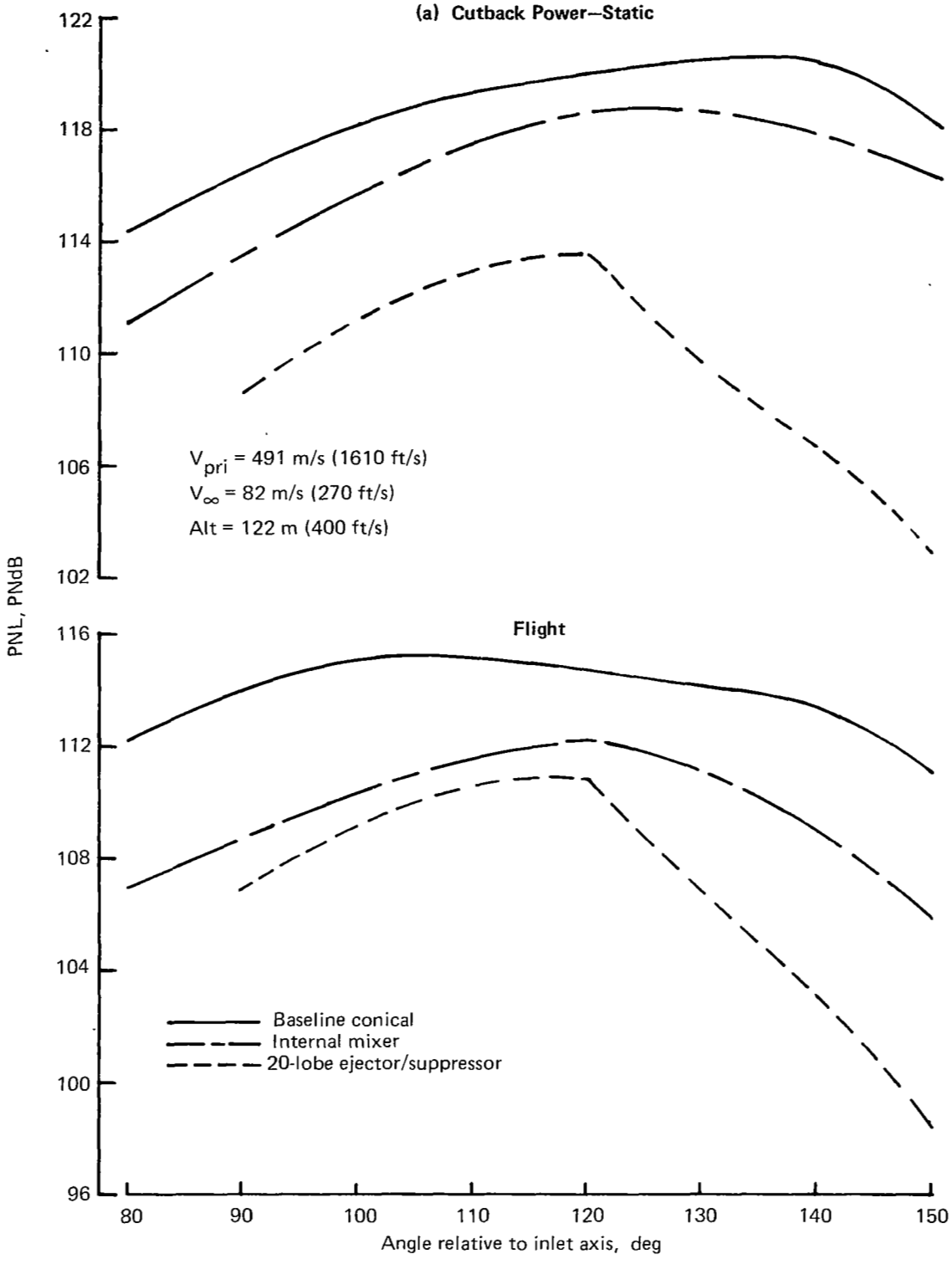

Figure 47.—NASA Ames 40 x 80 Wind Tunnel Test JT8D Engine—Static/Flight PNL Directivity Comparison

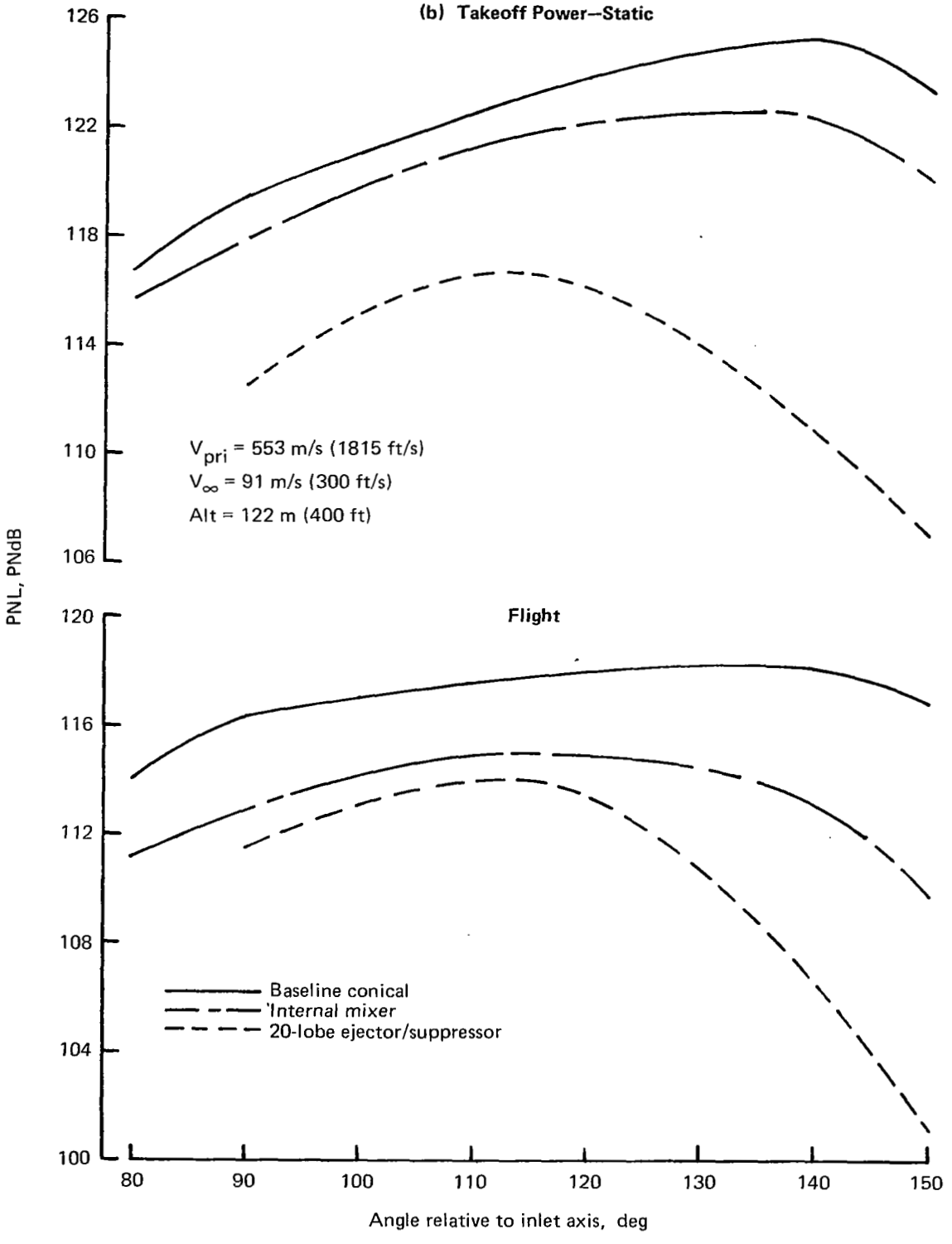

Figure 47.—(Concluded)

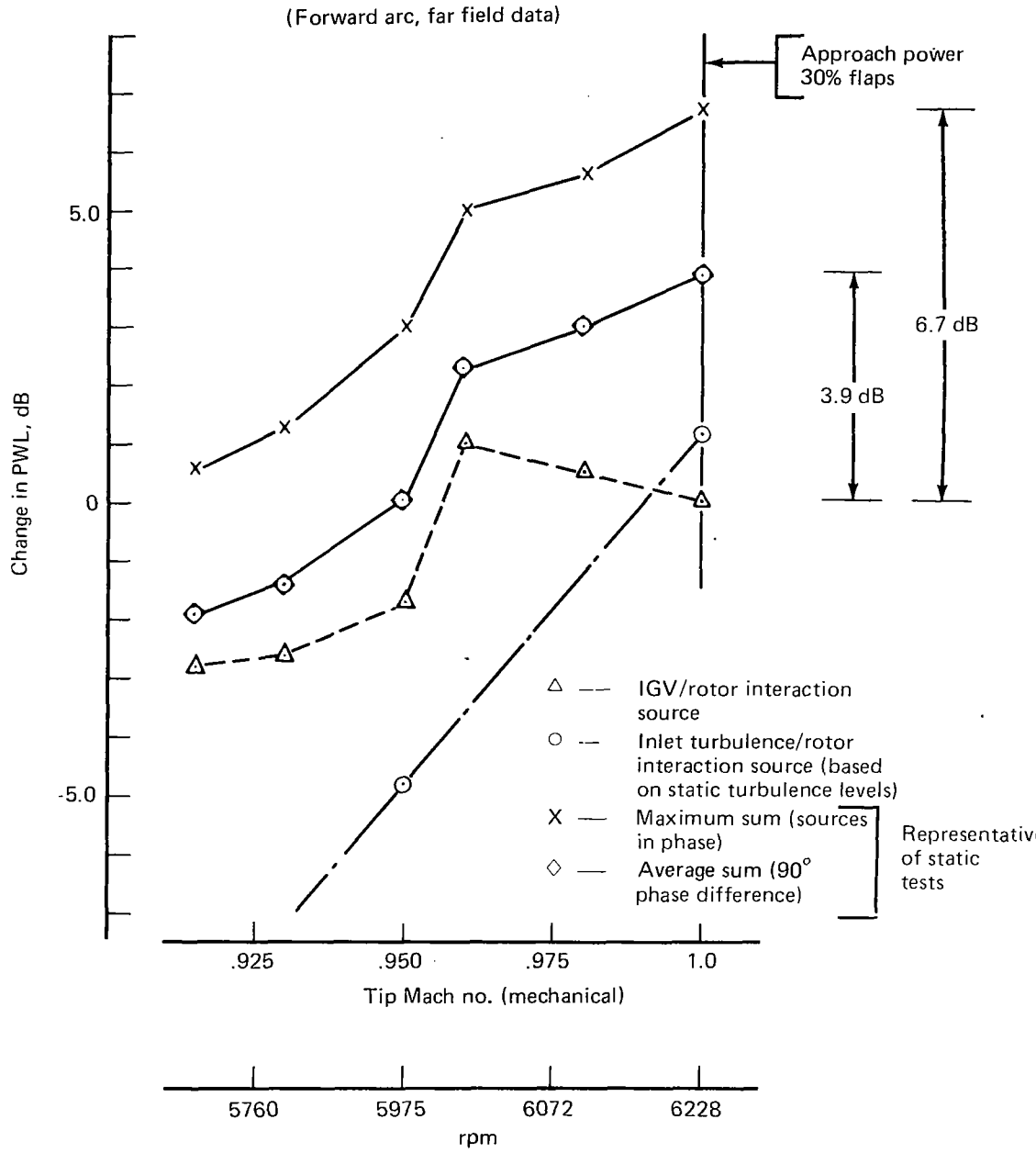

Figure 48.— Comparison of Analytical Predictions for Noise Due to IGV's and Inlet Turbulence at Blade Passage Frequency for the First Rotor Stage of the JT8D Engine

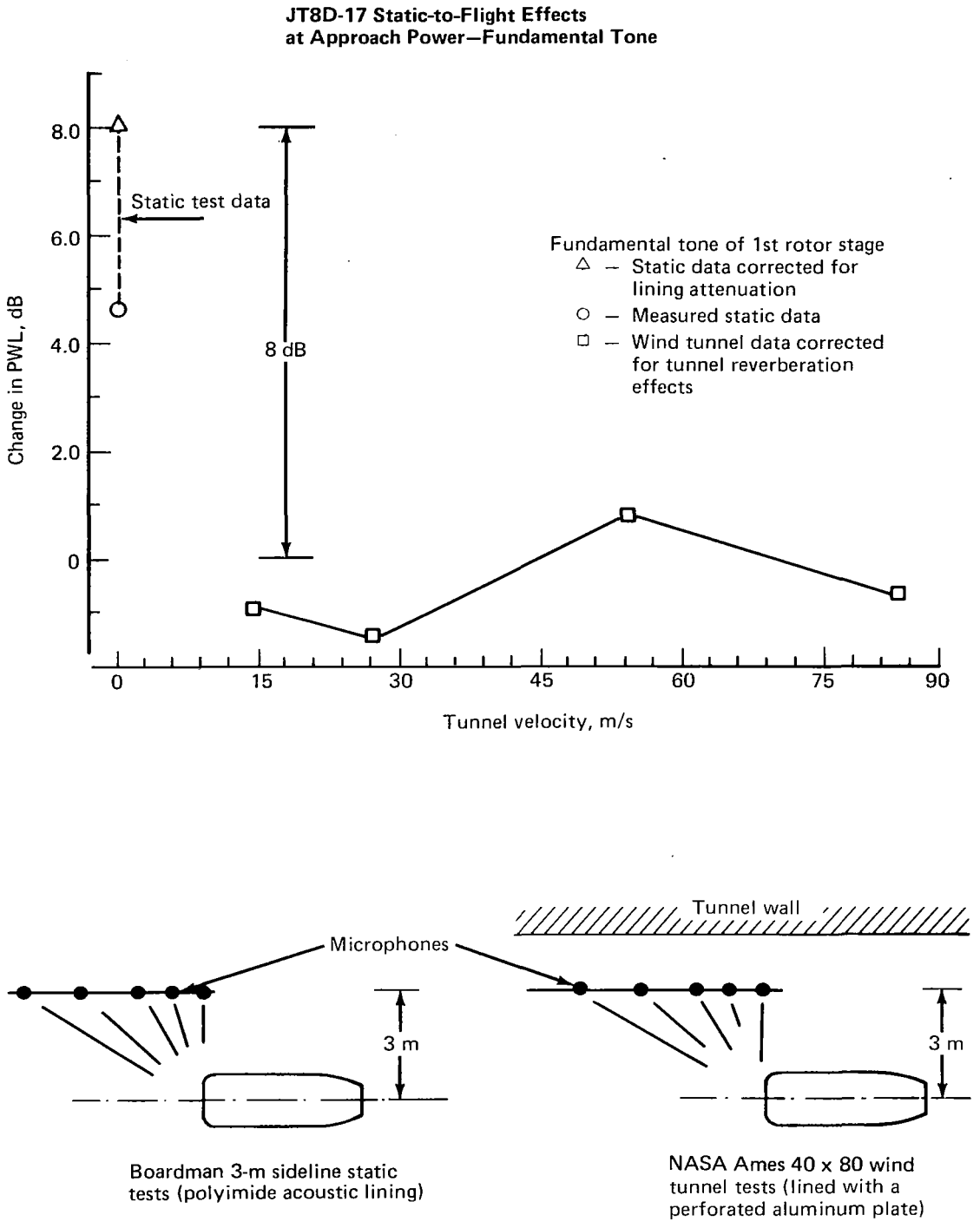

Figure 49.— Static-to-Flight Effects Approach Power

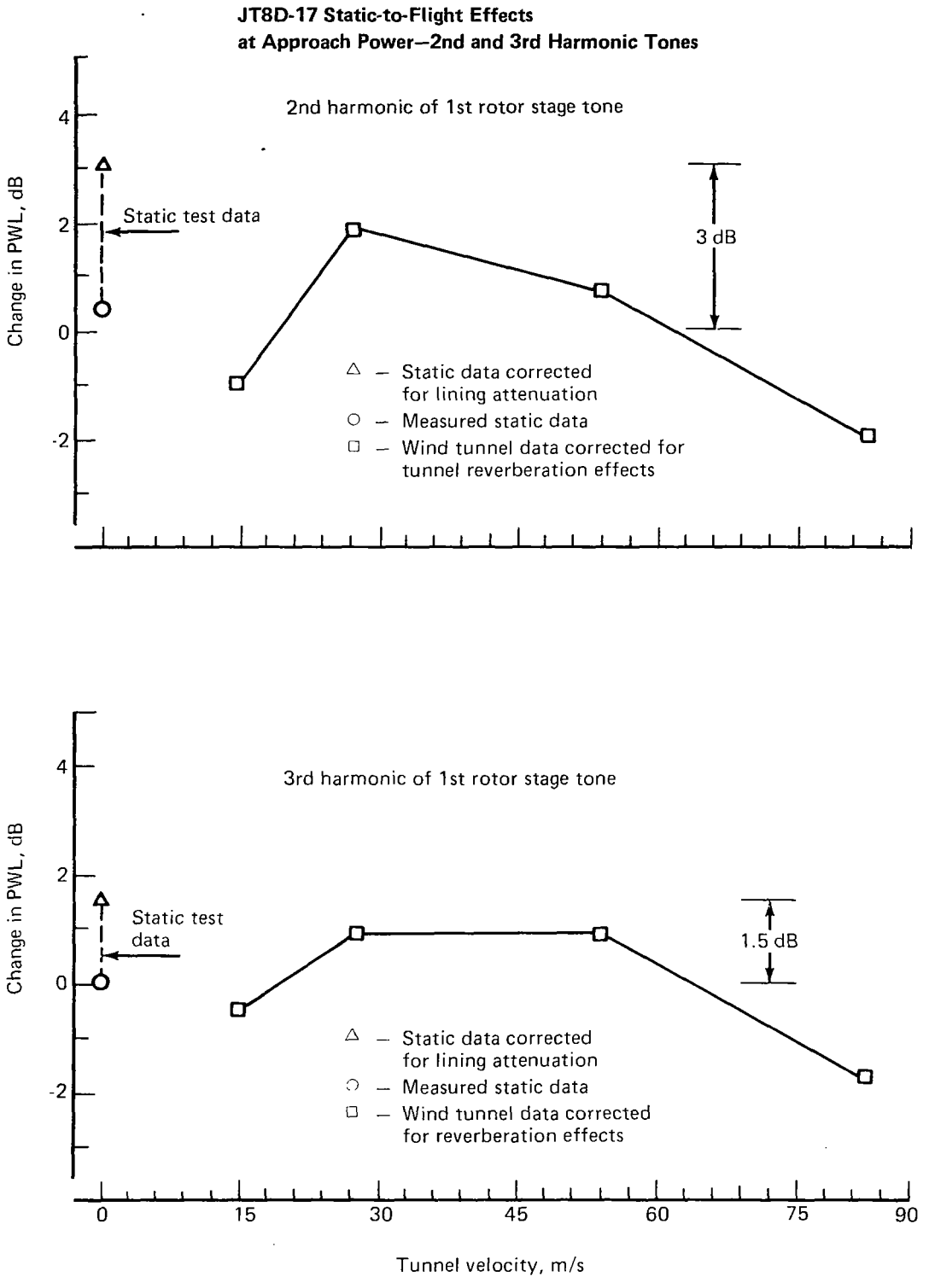

Figure 50.— Static-to-Flight Effects Approach Power

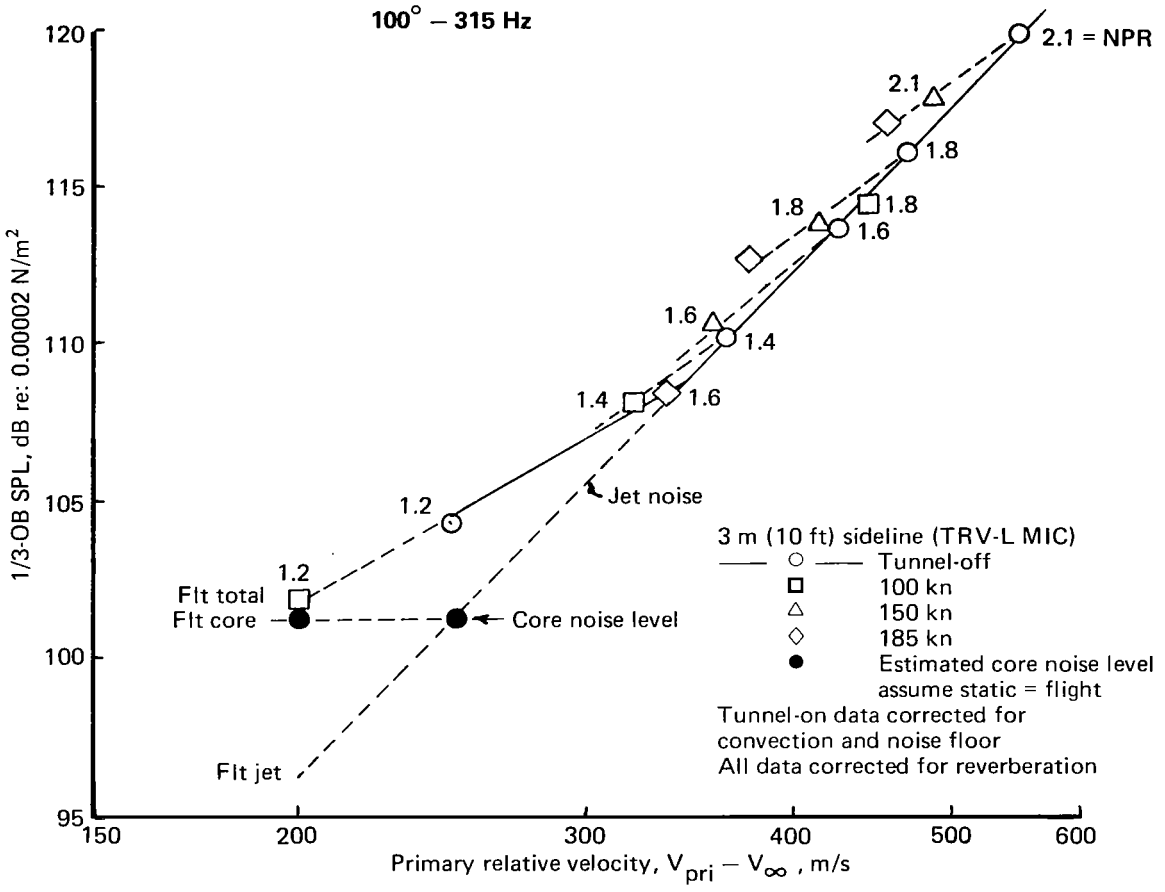

Figure 51.— NASA Ames 40 x 80 Wind Tunnel Test JT8D-17 Engine With Baseline Nozzle— Effect of Core Noise on Engine Noise Flight Effect

REFERENCES

1. Strout, F. G.: *Flight Effects on Noise Generated by the JT8D-17 Engine in a Quiet Nacelle and a Conventional Nacelle as Measured in the NASA Ames 40 x 80 Foot Wind Tunnel.* NASA CR-137797, January 1976.

2. Shain, W. M.: *Test Data Report, Noise Measurement in the NASA Ames Research Center 40 x 80 Foot Wind Tunnel of a JT8D-17 Engine With Several Exhaust Nozzle Systems.* Boeing document T6-5971, July 1975

3. Jaeck, C. L.; and Hollatz, F. W.: *Empirical Jet Noise Prediction Procedures–Vol. I–Single Flow Clean Jet.* Boeing document D6-42367TN-1, February 1976.

4. Anon: *Definitions and Procedures for Computing the Perceived Noise Level of Aircraft Noise.* SAE ARP 865, August 1969.

5. Roundhill, J. P.; and Schaut, L. A.: *Model and Full-Scale Test Results Relating to Fan Noise In-Flight Effects.* AIAA paper 75-465, AIAA 2nd Aeroacoustics Conference, Hampton, Virginia, March 24-26, 1975.

6. Clark, T. L., et al: *Analytic Models of Ducted Turbomachinery Tone Noise Sources.* NASA CR-132443, May 1974.

7. Amiet, R. K.: *Transmission and Reflection of Sound by a Blade Row.* AIAA paper 71-181, January 25-27, 1971.